

Intensity-modulated radiotherapy for breast and head-and-neck cancer

Bram van Asselen

Colofon:

This text was set using the freely available $\text{\LaTeX} 2_{\epsilon}$ typesetting and text formatting system. The line drawings were made using the freely available Xfig program.

ISBN: 90-393-3503-6

Druk:

PrintPartners Ipskamp B.V., Enschede

Copyright:

Chapter 2 and 4 copyright Elsevier Science Ireland Ltd.

Chapter 6 copyright Elsevier Science Inc.

Intensity-modulated radiotherapy for breast and head-and-neck cancer

Intensiteitsgemoduleerde radiotherapie voor borst en hoofd & hals
kanker
(met een samenvatting in het Nederlands)

Proefschrift ter verkrijging van de graad van doctor aan de
Universiteit Utrecht
op gezag van de Rector Magnificus, Prof. dr. W.H. Gispen
ingevolge het besluit van het College voor Promoties
in het openbaar te verdedigen
op dinsdag 4 november 2003 des middags te 2:30 uur

door
Bram van Asselen
geboren op 4 mei 1975 te Vinkeveen

promotor: Prof. dr. ir. J.J.W. Lagendijk
Faculteit der Geneeskunde, Universiteit Utrecht
co-promotoren: Dr. C.P.J. Raaijmakers
Faculteit der Geneeskunde, Universiteit Utrecht
Dr. C.H.J. Terhaard
Faculteit der Geneeskunde, Universiteit Utrecht



Het beschreven werk werd verricht op de afdeling Radiotherapie van het Universitair Medisch Centrum Utrecht, participierend in het Image Sciences Institute en de onderzoekschool voor biomedische beeldwetenschappen, ImagO, in een door de Nederlandse Kankerbestrijding/KWF gefinancierd project (UU 99-1863). Deze uitgave is tot stand gekomen met financiële steun de Nederlandse Kankerbestrijding/KWF en Nucletron B.V.

Voor Otto en Corrie.

Contents

1	General introduction	1
1.1	Image-guided radiotherapy	1
1.2	IMRT delivery	2
1.3	Geometric uncertainties in radiotherapy	3
1.4	Management of geometric uncertainties	4
1.4.1	Position verification using and EPID	4
1.4.2	PTV-CTV margin	6
1.5	Clinical applications of IMRT	6
1.5.1	IMRT for breast cancer	6
1.5.2	IMRT for Head & Neck cancer	7
1.6	Outline of this thesis	9
2	An improved breast irradiation technique using three-dimensional geometrical information and intensity modulation	11
2.1	Introduction	12
2.2	Methods and Materials	13
2.2.1	MLC field shaping	13
2.2.2	Volumes of interest	14
2.2.3	Conventional technique	14
2.2.4	IMRT technique	15
2.2.5	Analysis	18
2.3	Results	18
2.3.1	Equivalent path length maps	18
2.3.2	Dose analysis	21
2.4	Discussion	22
2.4.1	Conclusion	25
3	Segmental IMRT for oropharyngeal cancer in a clinical setting	27
3.1	Introduction	28
3.2	Method	30
3.2.1	Patients	30

3.2.2	Dose prescription	31
3.2.3	Inverse planning	32
3.2.4	Analysis of the dose distribution	33
3.3	Results	35
3.3.1	Primary tumor	35
3.3.2	Lymph nodes	37
3.3.3	Spinal cord and brain	40
3.3.4	Body	40
3.3.5	Parotid glands	40
3.3.6	Segments	40
3.4	Discussion	41
3.5	Conclusion	44
4	The dose to the parotid glands with IMRT for oropharyngeal tumors: the effect of reduction of positioning margins	47
4.1	Introduction	48
4.2	Materials and method	49
4.2.1	Patients	49
4.2.2	Intensity modulated radiotherapy planning	49
4.2.3	Analysis	52
4.3	Results	53
4.3.1	Target volumes	53
4.3.2	Spinal cord and brain	55
4.3.3	Parotid gland	55
4.4	Discussion	57
4.5	Conclusion	60
5	Implanted gold markers for position verification during irradiation of head-and-neck cancers: a feasibility study	61
5.1	Introduction	62
5.2	Methods and materials	63
5.2.1	Patients	63
5.2.2	Marker implantation	63
5.2.3	Toxicity	64
5.2.4	Portal imaging	65
5.2.5	Marker migration	65
5.2.6	Rotations	65
5.2.7	Interfraction motion	66
5.3	Results	66
5.3.1	Marker detection	66
5.3.2	Toxicity	67
5.3.3	Marker migration	67

5.3.4	Rotation	69
5.3.5	Interfraction motion	69
5.4	Discussion	70
5.5	Conclusion	73
6	Intrafraction motions of the larynx during radiotherapy	75
6.1	Introduction	76
6.2	Methods and materials	77
6.2.1	Patients	77
6.2.2	Flat-panel imager	77
6.2.3	Analysis of larynx motions	78
6.3	Results	79
6.4	Discussion	82
6.5	Conclusion	85
7	General discussion	87
7.1	Introduction	87
7.2	Image-guided IMRT	87
7.3	Breast cancer	89
7.4	Head-and-neck cancer	92
7.5	Conclusion	96
	Summary	97
	Samenvatting	101
	References	105
	Publications	115
	Dankwoord	117
	Curriculum vitae	119

Chapter 1

General introduction

1.1 Image-guided radiotherapy

Radiotherapy is a treatment modality for cancer using high-energy ionizing radiation. The deposition of ionizing radiation causes damage to the cells in the treated area. This damage can result in cell death (Rubin, 2001). The most common form of radiotherapy is external beam irradiation with high-energy photons. Radiotherapy aims to deliver high doses to the area containing malignant cells, while sparing the normal tissue adjacent to this area. Models based on simple biophysical assumptions have been developed to predict the tumor control probability (TCP) (Brenner, 1993; Webb, 1993). Depending on the radiosensitivity and the volume of clonogenic cells with a certain cell density, the TCP can be predicted for an inhomogeneous dose distribution. These models indicate that, for the same biological effect, higher doses are needed when more clonogenic cells are present in the target volume and when the tumor cells are relatively insensitive to radiation. Ideally, when tumor specific data are available, this should result in dose painting, i.e. creating a heterogeneous dose distribution within the target based on tumor characteristics, such as radiosensitivity, clonogenic cell density and tumor hypoxia (Ling *et al.*, 2000).

In order to perform dose painting, radiotherapy should be image guided. Images should provide anatomical and biological data. The advent of computed tomography (CT) and magnetic resonance imaging (MRI) made it possible to visualize the human anatomy. Using this anatomical information three-dimensional conformal radiotherapy (3D-CRT) (Webb, 1997) could be developed. 3D-CRT is used to avoid as much as possible irradiation of the surrounding tissue and at the same time deliver the prescribed dose to the target. Sharper dose gradients and a better homogeneity of the dose within the target can be achieved when intensity-modulated radiotherapy (IMRT; Webb (2001)) is applied, which is an advanced form of 3D-CRT. Instead of using a uniform beam intensity, IMRT uses non-uniform beam

intensities to provide more degrees of freedom for dose shaping. IMRT can also be used for dose painting within the target volume. Positron emission tomography (PET), nuclear magnetic resonance imaging (MRI) and spectroscopy (MRS) are beginning to provide physical and functional information about the tumor and its surroundings (Ling *et al.*, 2000). The use of these imaging techniques for radiotherapy is, however, still under development, and full dose painting is not yet possible. For conventional radiotherapy the prescribed tumor dose is usually limited by the dose to the surrounding critical organs. The first attempt to dose painting using IMRT is, therefore, to escalate the dose within the gross tumor volume (GTV) (Nederveen *et al.*, 2001b; Mohan *et al.*, 2000; Zelefsky *et al.*, 2000).

Due to the sharp dose gradient between critical organs and the tumor, special attention should be paid to the localization of the tumor when using IMRT. The position of the tumor during the imaging process needed for the IMRT planning, should be the same as during the actual treatment, to assure that the dose is delivered to the right spot. Misalignment of the patient, or organ motion, may result in underdosage to the tumor sites and overdosage to critical organs. It is therefore important to determine and manage geometrical uncertainties (Langen and Jones, 2001; Jaffray *et al.*, 1999) for IMRT treatments. Ideally, the position of the target should be visualized during the treatment.

1.2 IMRT delivery

There are several methods to delivered intensity-modulated beams. The main clinically available methods use compensator filters, multi-leaf collimators (MLCs), or tomotherapy (Webb, 1997; IMRT Collaborative Working Group, 2001). Like at many other institutes, most linear accelerators at our department are nowadays equipped with a MLC. The MLC consists of a set of thin blades, which can be individually positioned, and therefore create irregularly shaped beams. There are two approaches of IMRT delivery using MLC: the dynamic and segmental MLC approach. Using a dynamic MLC (DMLC) technique, each pair of MLC leaves moves during irradiation. By changing the setting of the leaf pair opening and the speed of the leaves, it is possible to create intensity-modulated beams. The segmental approach uses a series of multiple segmental fields (Fig. 1.1). The method is also called step-and-shoot, because the beam is off when the leaves move to the next position. By adding the individual shaped segmental fields, an intensity-modulated beam is created. To obtain these segments, the optimized intensity profile is divided in a discrete number of intensity levels.

The advantage of the DMLC technique is that the delivered intensity profile closely matches the intended profile. When using segmental IMRT the intended profile is approximated by a discrete number of segments. The conversion of the optimized

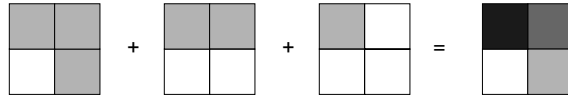


Figure 1.1: Schematic view of segmental IMRT. Adding three individual shaped segments with the same intensity results in an intensity-modulated field. A high gray value corresponds with a high intensity.

intensity profile to the deliverable intensity profile is consequently important. The quality assurance of segmental IMRT is, however, less complicated since only the leaf positions need to be checked, whereas in DMLC both leaf position and the speed need to be controlled (Chui *et al.*, 2001).

1.3 Geometric uncertainties in radiotherapy

The location of the tumor is not exactly at the same position during the course of the radiotherapy, due to geometric uncertainties, such as patient positioning errors, patient movement and organ motion. Differences between the actual position and the position during the planning, lead to misalignment between the treatment fields and the tumor. To avoid possible reduction in TCP, the field size has to be extended. In other words, an extra margin is added to the target volume, resulting in a planning target volume (section 1.4.2), to ensure the that target is irradiated with the prescribed dose (Fig. 1.2). This leads to an extra dose to the normal tissue adjacent to the target, which can result in an increased normal tissue complication probability (NTCP). The prescribed dose to the tumor is consequently often limited by the dose to the surrounding normal tissue.

The geometric uncertainties can result in a change of the position of the target relative to other fractions (interfraction motion), and within a single fraction (intrafraction motion). Interfraction motion can, for example, occur due to positioning errors or changes in patient anatomy such as weight loss. Organ motion can also result in interfraction motions. In the pelvic region this is often caused by the filling of organs such as the bladder and intestinals (Langen and Jones, 2001; Jaffray *et al.*, 1999). Intrafraction motion is caused by periodic motions, such as breathing and cardiac motion, or due to instant motions, such as gas motion, clenching of muscles and swallowing (Langen and Jones, 2001; Jaffray *et al.*, 1999).

All geometric uncertainties contribute to an error in the alignment between the target and the treatment fields. This error can be separated in systematic and random errors (Van Herk *et al.*, 2000). Systematic errors are deviations between the

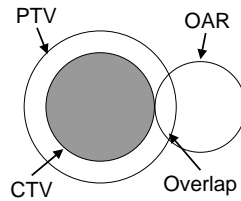


Figure 1.2: Schematic view of a clinical target volume (CTV), planning target volume (PTV) and an organ at risk (OAR). The margin taken for geometrical uncertainties causes an overlapping area, which results a high dose area in the OAR.

average target positioning during the treatment and the planned target position. Since the total dose of a radiotherapy treatment is the sum over all fractions, the systematic error causes a shift in the total dose distribution. Random errors are deviations between each fraction and occur day to day. These result in a blurring of the total dose distribution.

1.4 Management of geometric uncertainties

1.4.1 Position verification using and EPID

In order to minimize geometric uncertainties, position verification is needed. After verification of the position of the target, the position can be corrected using a correction protocol (Bel *et al.*, 1993; De Boer *et al.*, 2001). Most correction protocols aim at minimizing the systematic errors and are off-line. Using an off-line correction protocol, the position of the target is verified after a single treatment session. The next session the position can be corrected. The ultimate goal of position verification is, to ensure, that the target is located at the same position relative to the treatment fields during all radiotherapy fractions. To achieve that goal online position verification and correction should be applied. Both the random and the systematic errors can than be removed.

Many institutes use portal imaging to measure set-up errors by applying a megavoltage film or an electronic portal-imaging device (EPID). Using these portal images, the bony structures can be used as internal markers (Fig. 1.3), of which the location can be verified with respect to their location in the reference position (Hurkmans *et al.*, 2001b). The reference position is thereby the position during the imaging process used for the radiotherapy planning. The use of the bony structures for position verification of the target is indirect, the location of the target should

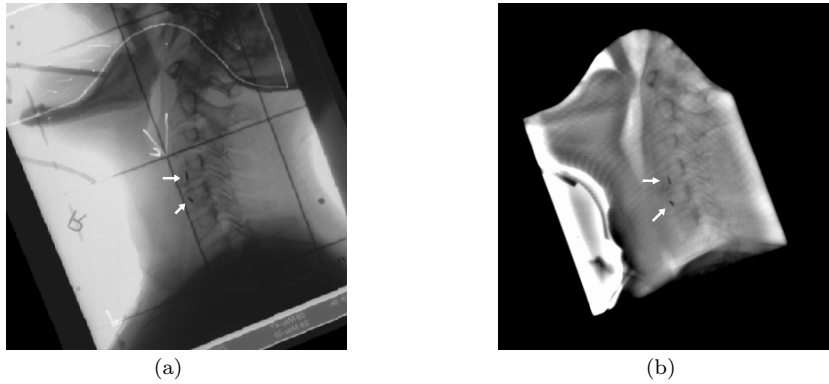


Figure 1.3: An example of a reference image (a) and a portal image (b) taken during the treatment for head-and-neck cancer. Beside the bony structures two markers are visible. The location of markers is indicated by two arrows.

therefore not change relative to the bony structures. For many head-and-neck cancers the targets do not move relative to the bony structure, while for cancers in the pelvic region target volumes may show motions relative to the bony structures. Instead of the use of bony structures, radiopaque markers can be used for position verification (Nederveen *et al.*, 2001a; Shirato *et al.*, 2000; Litzenberg *et al.*, 2002). These markers are usually made of gold. Due to their high electron density, they can be visualized in a portal image (Fig. 1.3). The location of these markers should be fixed relative to the target. The best place to put the markers would be the target itself, since the location of the markers would then be the best representation of the target. This is, however, not possible for each target. Some targets can deform during the radiotherapy course; markers within such targets are not reliable for position verification. Although the use of implanted markers is invasive, it has several advantages. When the target can move relative to the bony structures, the marker, in case its location is fixed to the target, better represents the target location. In that case markers can be used to remove the systematic errors, while using bony structures this is not possible. Another benefit of the use of markers is that the determination is straightforward in images and a small number of monitor units is sufficient to obtain a suitable portal image. This facilitates automatic detection of the markers within the portal images. Marker-based position verification can therefore also be used for measuring intrafraction motions. Furthermore, markers can be detected in small fields as used for IMRT treatments, while the use of bony structures is difficult when only small fields are used.

1.4.2 PTV-CTV margin

The clinical target volume (CTV) should be treated adequately in order to achieve the aim of radical therapy (ICRU Report No. 62, 1999). The CTV is a tissue volume that contains the gross tumor volume (GTV) and/or subclinical malignant disease that must be eliminated (ICRU Report No. 62, 1999). Due to the geometric uncertainties in the location of the CTV relative to the treatment field, a margin should be added to the CTV (Fig. 1.2). If no margins are added to the CTV some tissue may, for part of the treatment move out of the beam. The resulting volume is the planning target volume (PTV). This is a geometrical concept used for treatment planning, and it is defined to select appropriate beam sizes and beam arrangements, to ensure that the prescribed dose is actually delivered to the CTV (ICRU Report No. 62, 1999).

Both the random (σ) and systematic (Σ) positioning errors contribute to the margin between the CTV and the PTV. For a margin that ensures 95 % minimum dose for 90 % of the patients the following recipe was derived by Van Herk *et al.* (2000) when perfect conformation is assumed in 3D and 2D respectively:

$$\text{Margin}(3D) = 2.5\Sigma + 0.7\sigma \quad (1.1)$$

$$\text{Margin}(2D) = 2.15\Sigma + 0.7\sigma \quad (1.2)$$

A similar recipe was derived by Stroom *et al.* (1999) (equation 1.3). The criterion to derive the recipe was that on average more than 99% of the CTV should at least get 95% of the dose.

$$\text{Margin} = 2\Sigma + 0.7\sigma \quad (1.3)$$

The differences between the recipes might be due to the fact that different criterions were used. Both recipes demonstrate the large contribution of the systematic error to the margin. Using position verification to minimize the geometric uncertainties and thus reduce the margin, the main effort should be to reduce the systematic error. This can be achieved using marker-based position verification. The benefit of the use of markers is that it can be used as a direct verification of the target, since these can be placed inside the target (Nederveen *et al.*, 2001a). Systematic errors can therefore be removed for targets loosely attached to the bony anatomy.

1.5 Clinical applications of IMRT

1.5.1 IMRT for breast cancer

Many patients have been successfully treated with breast conserving radiotherapy (Fisher *et al.*, 1989; van Dongen *et al.*, 1992; Morris *et al.*, 1997). The gross tumor

is thereby surgically removed and the entire breast is treated with radiotherapy in order to control the subclinical disease. The aim for breast conserving radiotherapy is to deliver a homogeneous dose of 50 Gy (2Gy/fraction;5 times weekly) to the breast, which can be followed by a small boost dose of 14-20 Gy (2Gy/fraction;5 times weekly) to the tumor bed (Bartelink *et al.*, 2001). The advent of CT made it possible to visualize the anatomy of the breast and to calculate and analyze the three-dimensional dose distribution. The dose homogeneity of the breast has been studied by several groups (Buchholz *et al.*, 1997; Carruthers *et al.*, 1999; Cheng *et al.*, 1994; Neal *et al.*, 1995; Solin *et al.*, 1991). Using conventional techniques, such as wedged fields, it is not always possible to achieve a homogeneous dose distribution due to the complex geometry of the breast. The inhomogeneities typically occur at the entry points, the most caudal en cranial part of the treated volume and the nipple. An inhomogeneous dose is believed to be a contributing factor to the cosmetic result after radiotherapy (Moody *et al.*, 1994), because poor cosmesis occurs more often in patients with large breasts (Gray *et al.*, 1991; Moody *et al.*, 1994; Vrieling *et al.*, 2000) and the dose inhomogeneity of these patients is larger compared to patients with smaller breasts (Buchholz *et al.*, 1997; Cheng *et al.*, 1994; Neal *et al.*, 1995). The dose homogeneity can be improved by beam intensity modulation. Beside the ability to improve the dose homogeneity, IMRT might be used to decrease the dose to the lung and the heart. This is important since side effects due to irradiation of the breast, such as ischemic heart disease (Gyenes *et al.*, 1998) and radiation pneumonitis (Kwa *et al.*, 1998), may occur. Beside setup errors, organ motion due to breathing will contribute to the margin taken for geometrical uncertainties. The intra- and interfraction reproducibility of tangential breast irradiation has been determined using an EPID (Fein *et al.*, 1996; Lirette *et al.*, 1995; van Tienhoven *et al.*, 1991). One of the parameters studied is the central lung distance (CLD), which is the distance from the posterior field margin to the inner chest wall along the horizontal axis of the field. For normal respiratory function, the standard deviation of the intrafraction motion is reported 1-2 mm. The standard deviation of the reported random errors is higher, 2 - 4.4 mm, and the variations in the systematic error are 3-4 mm.

1.5.2 IMRT for Head & Neck cancer

Oropharyngeal cancer

For the treatment of cancers in the head-and-neck region different treatment strategies are used, such as surgery, radiotherapy, chemotherapy or combinations of these modalities. Almost all early oropharyngeal tumors (T1 and T2) are treated with radiation therapy alone. The aim at our department is to deliver a dose of 46-50 Gy (2Gy/fraction;5 times weekly) to the microscopic disease and 70 Gy (2Gy/fraction;5 times weekly) to the macroscopic disease (primary tumor and positive lymph nodes). The dose to the target is often limited by the maximum dose

to critical organs adjacent to the targets, such as the spinal cord and brain (Emami *et al.*, 1991). Another severe complication is xerostomia, caused by irradiation of the salivary glands (Chao *et al.*, 2001; Eisbruch *et al.*, 1999; Roesink *et al.*, 2001). The use of CT made it possible to delineate all target volumes and organs at risk. A simple form of dose painting can be created, when different dose levels are assigned to the individual volumes. The primary tumor and the lymph nodes will thereby receive a different dose, while at the same time the dose to the organs at risk is minimized. In order to develop such a technique, IMRT can be used. With IMRT the different dose levels to the primary tumor and the lymph nodes can be delivered simultaneously. However, other fractionation strategies should than be developed compared to conventionally used (Mohan *et al.*, 2000). Using IMRT it is even possible to deliver a higher dose than conventionally given, in other words to escalate the dose, while sparing surrounding normal tissues. There are several studies indicating that dose escalation might be useful. For oropharyngeal cancer local-regional recurrences after radiotherapy occur most frequently at the site of the original tumor (Pigott *et al.*, 1995). It has also been reported that when using conformal or segmental IMRT most recurrences occurred within the areas judged to be of high risk at the time of the radiotherapy planning (Dawson *et al.*, 2000a). Furthermore it has been shown that a higher total dose and reduction of the treatment time could improve the local control for oropharyngeal tumors (Maciejewski *et al.*, 1989; Withers *et al.*, 1995b).

In order to deliver a high conformal dose distribution and prevent high doses to critical structures, accurate patient positioning is essential. Usually patients treated for head-and-neck cancer are immobilized using a thermoplastic mask. Position verification is performed with a megavoltage film or EPID, where the location of the bony structures within the treatment fields is determined. The random and the systematic error amount to approximately 2 mm (1 standard deviation) (Hurkmans *et al.*, 2001b). Intrafraction displacements have not yet been quantified for patients with head-and-neck cancer.

Preservation of the salivary glands

During radiotherapy of head-and-neck cancers, the parotid gland is often exposed to radiation, which can cause severe reduction of salivary flow and change in salivary composition. This may result in xerostomia, difficulties in mastication and speech, changes of taste, increased risk of carries and oral infections, chronic esophagitis and altered nutrition (Hamlet *et al.*, 1997; Mandel, 1987; Vissink *et al.*, 1988; Wright, 1987). These severe side effects have a negative impact on the quality of life of the patient (De Graeff *et al.*, 1999; Huguenin *et al.*, 1999). Although with IMRT highly conformal plans can be achieved, there is still a significant dose to the parotid gland because the lymph nodes are located adjacent to the parotid glands. The PTV of the lymph nodes will therefore overlap with the parotid glands. When

no reduction of the TCP is allowed, this part of the parotid glands should receive the prescribed dose.

1.6 Outline of this thesis

In chapter 2 the development of a segmental IMRT technique using 3D geometrical information for tangential breast irradiation is presented. The IMRT technique is applied to achieve a homogeneous dose distribution through the entire breast. The shape of the individual segments was obtained from an equivalent path length map of the irradiated volume.

In chapter 3 segmental IMRT is applied for the treatment of oropharyngeal cancer, which is a more complex case than the breast. Different dose levels are delivered to the primary tumor, the CTV of the primary tumor and the CTV of the lymph nodes, while the dose to surrounding organs at risk is minimized. This can be considered a simple form of dose painting. The relation between the quality of the treatment and the number of beams in combination with the number of segments is investigated. This information will be used for developing an efficient and reliable segmental IMRT technique.

Chapter 4 deals with the dose to the parotid gland. Using the segmental IMRT technique presented in the previous chapter, the dose to the parotid gland is reduced without compromising the dose to the targets. Due to the margin taken for geometrical uncertainties, the PTVs will partially overlap with the parotid glands. This causes a high dose area in the parotid glands. The effect of reduction of positioning margins is presented in this chapter.

In chapter 5 the feasibility of the use of implanted gold markers for position verification in the head-and-neck region is investigated using an EPID. Accurate position verification is needed to deliver the dose at the right spot, particularly for highly conformal plans created with IMRT. Markers were implanted in ten patients and the toxicity and the reliability of marker-based position verification was studied.

In chapter 6 intrafraction motions in the larynx are studied. Although most structures in the head-and-neck are relatively immobile, the larynx is a rather mobile organ. Due to the high image quality of the EPID, the displacements of the anatomical structures could be determined for 10 patients during radiotherapy.

A general discussion is presented in chapter 7. Imaging in radiotherapy, IMRT for breast cancer and IMRT for oropharyngeal cancer will be discussed separately.

Chapter 2

An improved breast irradiation technique using three-dimensional geometrical information and intensity modulation

This chapter has been published as

B. van Asselen, C.P.J. Raaijmakers, P. Hofman and J.J.W. Lagendijk 2003 An improved breast irradiation technique using three-dimensional geometrical information and intensity modulation *Radiotherapy and Oncology* **58** 341–347

Abstract

Background and purpose: In spite of the complex geometry of the breast, treatment planning for tangential breast irradiation is conventionally performed using two-dimensional patient anatomy information. The purpose of this work was to develop a new technique which takes the three-dimensional (3D) patient geometry into account.

Materials and methods: An intensity-modulated radiotherapy (IMRT) technique was developed based on the division of the tangential fields in four multi-leaf collimator (MLC) shaped segments. The shape of these segments was obtained from an equivalent path length map of the irradiated volume. Approximately 88 % of the dose was delivered by two open fields covering the whole treated volume. Dose calculations for the IMRT technique and the conventional technique were performed for five patients, using computer tomography (CT) data and a 3D calculation algorithm. A planning target volume (PTV) and ipsilateral lung volume were delineated in these CT data.

Results: All patients showed similar equivalent path length patterns. Analysis of the dose distribution showed an improved dose distribution using the IMRT technique. The dose inhomogeneity in the PTV was 9.0 % (range 6.4–11.4 %) for the conventional and 7.6 % (range 6.5–10.3 %) for the IMRT technique. The mean lung dose was reduced for the IMRT technique by approximately 10 % compared with the conventional technique.

Conclusion: A new breast irradiation technique has been developed which improves the dose homogeneity within the planning target volume and reduces the dose to the lung.

Furthermore, the IMRT technique creates the possibility to improve the field matching in case of multiple field irradiations of the breast and lymph nodes.

2.1 Introduction

Breast conserving radiotherapy is a commonly used treatment for breast cancer. In spite of the complex geometry of the breast, the treatment planning of tangential breast irradiation is conventionally performed using a two dimensional planning system and a two-dimensional (2D) contour of the breast and the lung in the central plane. Optimization of the dose distribution in this plane is performed by manual interactive optimisation of the wedge angle that compensates for the varying contour of the breast. The 3D dose distribution for the tangential breast irradiation has been analyzed using CT data in several studies (Buchholz *et al.*, 1997; Carruthers *et al.*, 1999; Cheng *et al.*, 1994; Hong *et al.*, 1999; Solin *et al.*, 1991; Neal *et al.*, 1995). These studies demonstrated relatively large dose inhomogeneities inside the target volume in some patients. The largest dose inhomogeneities occur particularly in patients with large breast sizes (Buchholz *et al.*, 1997; Moody *et al.*, 1994; Neal *et al.*, 1995).

The dose homogeneity in the breast can be improved by beam intensity modulation (Carruthers *et al.*, 1999; Hong *et al.*, 1999; Evans *et al.*, 1998; Lo *et al.*, 2000). The modulated beams are generally delivered by a physical compensator or by a dynamic multi-leaf collimator (DMLC). The use of physical compensators is, however, time consuming and the use of DMLC requires extensive quality assurance. In our institution therefore a “step and shoot” method is preferred. Since breast irradiation is the most commonly applied technique in our institution the new technique should be straightforward, reliable and efficient. One group reported a method using MLC-shaped wedged fields to improve the dose inhomogeneity (Lo *et al.*, 2000).

In order to obtain complete target coverage with tangential fields, it is unavoidable to irradiate part of the ipsilateral lung. The dose to the lung should be as low as possible, in order to prevent radiation pneumonitis (Kwa *et al.*, 1998) and late fibrosis.

In our institution, a standard technique is used for all tangential breast irradiations (Legendijk and Hofman, 1992). Patients are positioned on a wedged breast-board in order to obtain a vertical match plane between the tangential fields and the supraclavicular and axillary fields in case of multiple field irradiations. Patients lying on a breast-board are difficult to position inside a CT scanner due to the limited size of the bore of the scanner.

If a parasternal field is applied, the match of the tangential fields to the parasternal field is performed in the central plane. Due to the curvature of the thorax, however, the optimal match is not maintained along the whole length of the field

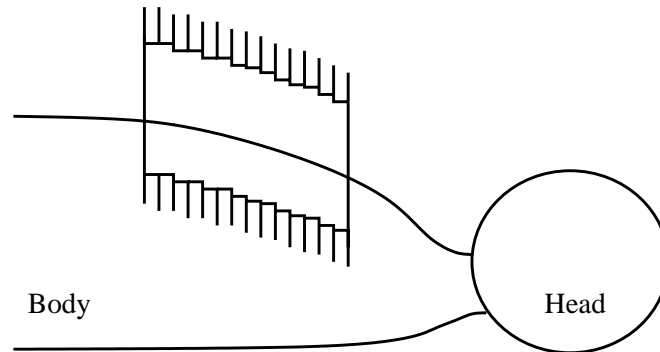


Figure 2.1: The tangential fields are shaped using the multi-leaf collimator, by following the curvature of the thorax. In this way the cranial vertical match plane is maintained without using the breast board.

and using a rectangular field setting, under-dosage or over-dosage in the match region is almost unavoidable.

It was the purpose of our work to develop a new technique for tangential breast irradiation which avoids the above mentioned problems. This technique should fulfil the following criteria: (1) improve the dose homogeneity; (2) maintain a vertical match plane between the tangential fields and the supraclavicular and axillary fields without using a breast-board in order to facilitate the positioning of patients in a CT scanner; (3) have the possibility to match the parasternal field to the tangential fields with the same overlap over the whole length of the field. A new improved breast irradiation technique, developed at our institution, will be described and analyzed in this paper. The parasternal field and supraclavicular and axillary fields are not taken into account in our analysis of the dose distribution.

2.2 Methods and Materials

2.2.1 MLC field shaping

Positioning of the patient without breast board, while avoiding excessive lung irradiation and maintaining a vertical match plane between the tangential fields and the supraclavicular and axillary fields, demands the appliance of complicated shielding techniques (Lebesque, 1986) or the combination of collimator and couch rotations (CaseBow, 1984; Lagendijk and Hofman, 1992). A vertical match plane can, however, also be obtained by applying MLC field shaping (Fig. 2.1). Using the MLC in this way furthermore creates the possibility of shaping the medial

parasternal entrance of the tangential field in order to match it dosimetrically with the parasternal field along the whole length of the field. On the other hand the use of MLC shaping of the tangential fields implies that the wedges cannot be used to optimize the dose distribution since in our linear accelerators (Elekta Oncology Systems, UK) the wedge direction is perpendicular to the leaf direction. Therefore, an intensity-modulated radiotherapy (IMRT) technique had to be developed using MLC field shaping only. The use of MLC field shaping and the 3D optimization of the dose distribution implies further that a 3D CT data set of the patient has to be available.

2.2.2 Volumes of interest

Five patients underwent a planning CT scan. Due to the limited size of the bore of the CT-scanner in combination with the treatment set-up, large patients or large breast board angles could not be included. After positioning, conventional field settings were defined by a radiation oncologist. Although the aim of this work was to abandon the breast board, the patients were scanned in the conventional treatment position using the breast-board in order to compare a new technique with the conventional technique. The patients were positioned according to the local protocol i.e. supine with their hands upon their head (Legendijk and Hofman, 1992). Next, the treatment field was marked by tiny lead wires, in order to visualise the conventionally applied field borders in the CT data. CT scanning was performed with slices spaced at a 5 mm interval, from the cranial side of the acromio-clavicular joint till 2 cm caudal from the submammary fold. In order to analyze the 3D dose distribution, a clinical target volume (CTV, ICRU Report No. 50 (1993)) and lung volume were delineated by the physician. The planning target volume (PTV) was obtained by adding a 1-cm margin to the CTV, except for the skin side of the CTV where the margin was limited to the subcutaneous layer. In order to analyse the dose to the lung the ipsilateral lung volume was drawn. The volumes (Table 2.1) of the organs at risk and the target volumes were determined by a random sampling technique (PLATO EVAL 2.5, Nucletron Ltd). The irradiated lung volume was defined as the lung volume receiving a dose equal or greater than 50% of the prescribed dose for the conventional plan. Besides the above-mentioned volumes, the patient separation in the central plane is shown in Table 2.1. The patient separation is defined as the distance between the lateral and medial entrance point of the posterior border of the treatment field.

2.2.3 Conventional technique

The beam parameters of the tangential beams are conventionally derived from X-ray guided localization. The angle between these beams is chosen in such way that the posterior borders of the lateral and medial fields are coplanar, in order

Table 2.1: The clinical target volume (CTV), planning target volume (PTV), the patient separation in the central plane, the total volume of the ipsilateral lung and irradiated lung volume (ILV)^a.

Patient	CTV [cm ³]	PTV [cm ³]	Patient separation [cm]	Lung volume [cm ³]	ILV [cm ³]
A	257	419	17.2	1556	97
B	71	159	18.2	1974	263
C	233	402	18.0	1159	107
D	140	253	18.0	2008	243
E	943	1283	23.0	1191	405

^a The uncertainty in the calculated volumes is approximately 0.5% (1 SD).

to prevent extra dose to the lung due to the divergence of the beams. In order to apply our standard technique to the CT data set, the posterior borders of the fields were matched with the standard medial and lateral entrance point as displayed by the lead wires. Next, the conventional beam settings were compared with the beam settings derived from the CT data. This comparison resulted in some cases in adjustment of the field settings ($< 5\text{mm}$) to obtain a better coverage of the PTV. For this study it is assumed that the CT data are preferred over the conventional localization data. After adjustment, the 3D dose distribution was calculated using a 3D planning system (PLATO RTS version 2.2, Nucletron Ltd), with a grid space between 3.0 and 3.5 mm. The planning system uses a convolution based pencil-beam model (Bortfeld *et al.*, 1993), with the equivalent tissue-air ratio (ETAR) method (Sontag and Cunningham, 1978) for tissue inhomogeneity corrections. The energy of the beams was chosen to be 6 MV for four patients. For patient E, with the largest breast, 10-MV beams were used. The wedge angles and the weights of the two tangential beams were optimized to obtain a homogeneous dose distribution in the central plane. The dose distribution was normalized at the isocentre in the central plane. The prescribed dose was 50 Gy at the isocentre.

2.2.4 IMRT technique

The dose distribution of a conventional plan usually shows three high dose areas in the central plane, namely at the medial and lateral side of the lung and near the apex of the breast. Conventionally, optimizing of the dose distribution is done by equalizing the dose in these three areas. In this way however, the PTV obtains a relatively high dose at the three high dose areas and a relatively high dose is delivered to the lung itself. The high-dose areas “behind” the lung result from the relatively short equivalent path length through lung tissue compared with sur-

rounding tissue. Although the aim was to improve the 3D dose distribution, the first attempt was to improve the dose distribution in the central plane. The development of the IMRT technique was started by applying an open field to the part of the irradiated volume which contains lung tissue, while the other part of the breast is treated using a wedged field. The dose distribution in the central plane improved using this approach. The wedge, however, had to be abandoned and was therefore mimicked by an intensity-modulated field. The dose distribution in other planes did not improve substantially using the combination of an open part and wedged part of the treatment field. In order to improve the dose distribution in off-axes planes a systematic method had to be developed to deduce the various intensity levels, and thus the shape of the MLC field settings, from the patient geometry. Eventually a method was developed based on the division of the irradiated volume into segments with a similar equivalent path length.

In first approximation, the equivalent path length along a ray line from the focus through the breast is proportional to the dose delivered at a specific depth. In the case of two opposed tangential fields, ray lines with a similar equivalent path length should approximately have the same beam intensity to obtain a homogeneous dose distribution. To test this approach, 2D equivalent path length maps (EPMs) were generated from the CT data set using software developed in our institution. The equivalent path lengths, obtained from ray tracing from the focus of the beam through the CT data set, were projected on a plane perpendicular to the beam axes (Fig. 2.2). The equivalent path length through a voxel was calculated by multiplying the ray length through the voxel by its relative electron density. The total path length was obtained by a summation of the equivalent path lengths of all voxels a ray passes. The relative electron density was determined using a table (Schneider *et al.*, 1996; Knöös *et al.*, 1986) that transfers the Hounsfield units, obtained from the CT data set, to relative electron density. The field size, isocentre and gantry angle used to calculate the EPMs were obtained from the adjusted conventional beam settings.

The translation of such an EPM into optimal MLC field settings and intensity levels is a complex problem. The distance between the minimum and the maximum path length, derived from the EPM, was divided in four discrete, equally spaced intervals. Each interval covers a range of path lengths. The resulting map (Fig. 2.3) is used to obtain the MLC settings. The MLC settings deduced from this map were entered into the 3D planning system by hand enclosing each level with the leaves, except for the largest segment, which was a rectangular open field enclosing the total irradiated volume. In order to simplify the MLC settings, leaf positions where the gap between two opposite leaves was smaller than approximately 10 mm, were not taken into account. In this way a total number of four MLC segments could be obtained for all patients (Fig. 2.4). The 3D dose distribution was calculated using the same adjusted field settings as in the conventional plan. Weighting of the various segments was performed at a point at the centre of the smallest seg-

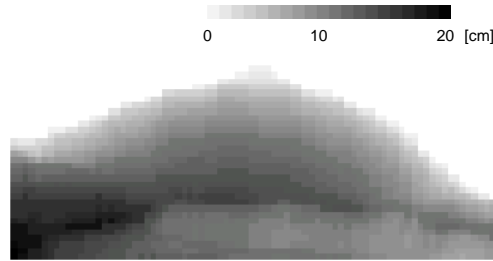


Figure 2.2: An equivalent path length map for tangential breast irradiation (patient A). The left and right side in the figure are cranial and caudal, respectively.



Figure 2.3: The equivalent path length map for the same breast as in Fig. 2.2 divided into four discrete path length intervals.

ment corresponding to the greatest equivalent path length (Fig.2.4). The largest segment delivers most dose to the breast while the other segments are used to obtain a homogeneous dose distribution. Analyses of the dose distribution calculated for two open beams, in off-axes planes showed that the variation in dose was approximately 10-15 %. For our IMRT technique we have chosen that approximately 88 % of the dose to the weighting point was delivered by the largest segments. In order to standardize the weighting procedure, the remaining 12 % were equally divided over the other segments. Finally the weights of the largest segments, the rectangular open fields, were used to improve the homogeneity in the lateral medial and medial lateral direction. The ratio between the dose delivered by these two rectangular segments and the remaining segments was thereby maintained. Normalization and prescription (100 % = 50 Gy) of the plans was performed at the isocentre in the central plane.

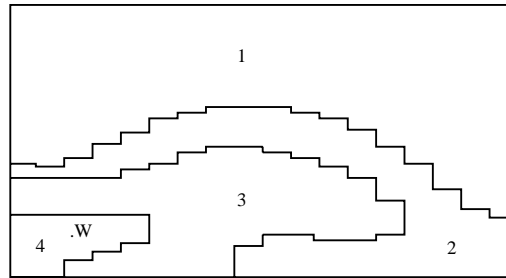


Figure 2.4: The four multi-leaf collimator settings for each intensity level as deduced for the equivalent path length map in Fig. 2.3. The first segment includes the areas 1-4, the second segment the areas 2-4, the third segment the areas 3-4 and the fourth segment area 4. W is the weighting point.

2.2.5 Analysis

After the calculation of the 3D dose distribution, isodose contours were displayed in several planes. Furthermore dose-volume histograms (DVHs) of the conventional and IMRT plan were calculated.

Quantification of the dose distribution was done by calculating $D_{95-5\%}$. Using the DVH two dose values ($D_{95\%}$ and $D_{5\%}$) were extracted; 95% of the PTV receives a dose equal or more than $D_{95\%}$ and 5% of the PTV receives a dose equal or more than $D_{5\%}$. $D_{95-5\%}$ is defined as the difference between $D_{95\%}$ and $D_{5\%}$. These doses are indicators of the low- and high-dose regions in the PTV, respectively. Consequently, $D_{95-5\%}$ indicates the dose range for 90 % of the volume. An advantage of this quantification method is its independence of a normalisation procedure and its potentiality for easy comparison of the dose distributions between patients from different institutes.

In order to analyze the dose to the lung, the average dose to the ipsilateral lung was calculated using a random sampling technique (PLATO EVAL 2.5, Nucletron Ltd).

2.3 Results

2.3.1 Equivalent path length maps

EPMs calculated for the five patients all showed patterns similar to Fig. 2.2. The maximum path length was 19.3, 18.7, 24.6, 18.5 and 24.1 cm for patient A to E, respectively. The equivalent path length changes gradually over the treated volume. Starting from the skin side, the path length increases until the region is

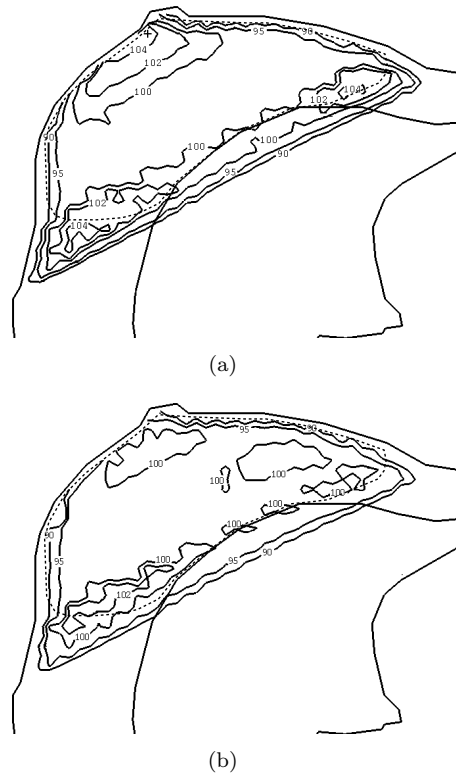


Figure 2.5: The dose distribution in the central plane for the conventional (a) and the intensity modulated radiotherapy treatment (b) technique (patient A). The PTV is delineated by the dashed line.

reached were lung tissue is involved. Due to the low relative electron density of the lung tissue compared with the breast tissue, the equivalent path length through the lung is smaller than that of the adjacent breast tissue. For all patients the path length increased towards the cranial part of the treated volume. Only the patient with the largest breast also showed an area with a large path length in the caudal region.

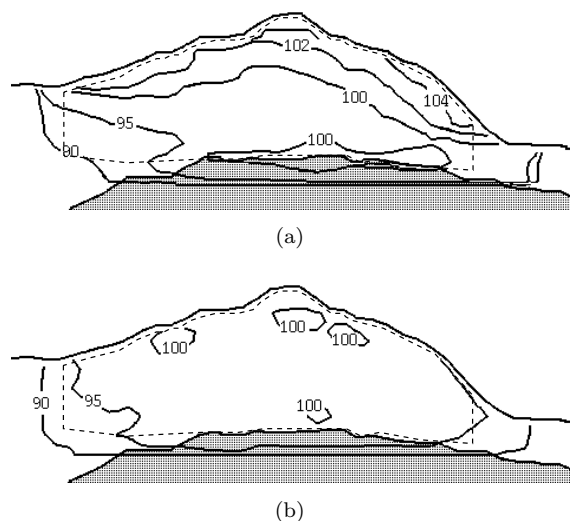


Figure 2.6: The isodose contours displayed in an oblique sagittal plane, calculated for the conventional (a) and the intensity modulated radiotherapy treatment (b) technique (patient A). The plane is perpendicular to the posterior field border of the treatment fields and through the isocenter. The lung tissue is indicated by the gray region. The left and right side in the figure are cranial and caudal, respectively. The PTV is delineated by the dashed line.

Table 2.2: $D_{95-5\%}$ of 5 patients calculated for the conventional (Conv) and the intensity modulated radiotherapy (IMRT) technique (100 % = 50 Gy).

Patient	Conv [%]	IMRT [%]	Ratio $\frac{IMRT}{Conv}$
A	10.5	7.0	0.70
B	8.1	6.6	0.81
C	8.8	7.8	0.87
D	6.4	6.5	1.02
E	11.4	10.3	0.90

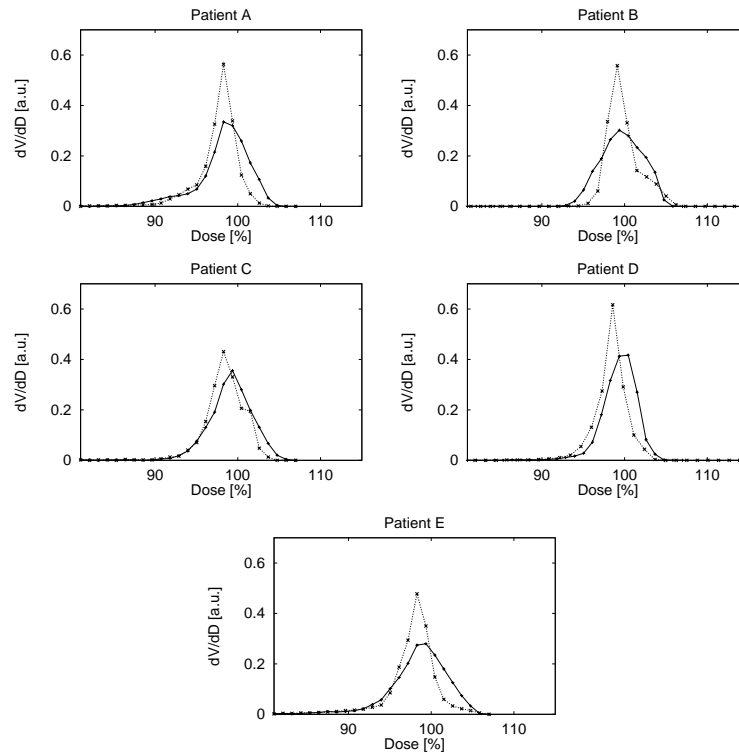


Figure 2.7: Dose-volume histograms calculated for five patients for the conventional (solid line) and intensity modulated radiotherapy (dashed line) treatment technique.

2.3.2 Dose analysis

The dose distributions displayed by isodose contours in the central plane, show an improved dose distribution for the IMRT technique compared with the conventional technique (Fig. 2.5). For the same patient the isodose contours are displayed in an oblique sagittal plane (Fig. 2.6).

The differential DVHs showed improved dose homogeneity for the IMRT technique compared with the conventional technique (Fig. 2.7).

Compared to the conventional technique the $D_{95-5\%}$ decreased in four cases for the IMRT technique with a maximum of 29 % (Table 2.2). However, in one case, the $D_{95-5\%}$ increased by 2 %. The $D_{95-5\%}$ of this patient for the conventional plan is, however, already small compared with that of the other patients and could not be improved. In general, the results show that the dose homogeneity of the IMRT

Table 2.3: Average lung dose of the ipsilateral lung calculated for the conventional (Conv) and the intensity modulated radiotherapy (IMRT) technique.

Patient	Conv [Gy]	IMRT [Gy]	Ratio $\frac{IMRT}{Conv}$
A	4.9	4.1	0.84
B	8.3	7.4	0.89
C	6.1	5.3	0.87
D	7.4	6.6	0.89
E	18.5	17	0.92

plans is the same or better than that of the conventional plan.

Using the IMRT technique, the average dose to the ipsilateral lung decreased with a mean value of 11.8 % (range 8 - 16%) compared with the conventional technique (Table 2.3).

2.4 Discussion

In this work an IMRT technique is presented based on the division of the treatment field in segments with a similar equivalent path length through the breast. Comparison of the DVHs and isodose contours of the IMRT technique with those of our conventional treatment technique showed that the homogeneity of the dose was improved using the IMRT technique.

Part of the low dose region seen in the DVHs is unavoidable, since this is caused by the build-up of the dose in the PTV near the skin. This build-up ensures an acceptable cosmetic outcome of the breast and should therefore be maintained. Only when a tumor is located near the skin (< 1.5 cm) bolus material is placed to increase the dose in that region of the PTV. There was no bolus material used for the patients analyzed in this work.

In order to quantify the dose distribution, the dose difference between 95 and 5 % ($D_{95-5\%}$) of the volume was measured. An advantage of this method is that it is independent of normalization procedures used in different institutions and facilitates comparison with different institutions. The average value of $D_{95-5\%}$ for the conventional plan was 9.2 % (range 6.4 – 11.4 %) and for the IMRT technique 7.6 % (range 6.5 – 10.3 %). The dose distribution for the conventional plan of patient D was the most homogeneous one and could probably not be improved. The most inhomogeneous dose distribution was obtained in the patient with the largest breast. For such patients the use of more intensity levels or optimized weighting of the segments, might result in a further increase of the dose homogeneity.

The inhomogeneity of the dose distribution for tangential breast cancer has been studied by several groups (Buchholz *et al.*, 1997; Carruthers *et al.*, 1999; Cheng *et al.*, 1994; Hong *et al.*, 1999; Solin *et al.*, 1991; Neal *et al.*, 1995) using CT data. It is, however, rather difficult to compare our results with those of other studies because different methods are used to analyze the dose distribution. The methods used by Solin *et al.* (1991) are the closest to our study. They determined the isodose which covers 5 % and 95 % of the volume for a standard wedge plan using CT information and inhomogeneity corrections. On the analogy of this study this would mean a $D_{95-5\%}$ of approximately 15 %. Analyzing 17 patients Carruthers *et al.* (1999) showed a heterogeneity of 12 % (range 8 - 17 %) for a wedged plan and 5 % (range 4 - 7 %) for a IMRT technique using compensators. Their heterogeneity is defined by the difference between the maximum dose and the isodose that just covers the target volume. Evans *et al.* (1998) calculated the volume percentage which received a dose outside the range of 95-105 % of the prescribed dose. They determined an average of 13.2 % for a technique using wedged tangential fields and 3 % for their IMRT technique using physical compensators. Pseudo-CT scans (Evans *et al.*, 1995) were used for their analysis. Using inverse planning to generate intensity-modulated plans, Hong *et al.* (1999) showed an improved dose homogeneity in the PTV, especially in the superior and inferior regions. Lo *et al.* (2000) developed a technique using MLC shaped wedged tangential fields to improve the dose distribution in the breast. A systematic procedure to derive the MLC shaped segments is, however, not presented.

The inhomogeneity of the dose distribution determined for the conventional technique in this work is relatively small. Nevertheless, we showed that we could reproduce or improve the dose homogeneity using our IMRT technique. Furthermore, when a larger inhomogeneity is observed in a patient, tools are now available to improve this. The range of the PTV of the patients we analyzed is large (159 – 1283 cm³). More patients should, however, be analyzed to study our IMRT technique. It should also be noted that, although the target volume was drawn by an experienced physician, there are no standard procedures for delineating a target volume. This could cause inter-physician variability in delineating the target volume. Dose analysis of the conventional target volume, the tissue within 1 cm of the field borders and with exclusion of the lung volume, showed similar dose distributions as that of the PTV.

Dose analysis of the ipsilateral lung showed that the average dose decreased for all patients (range 8 - 16 %). Consequently, the probability for inducing radiation pneumonitis was decreased for the IMRT technique (Kwa *et al.*, 1998). Reducing the myocardial dose was not the aim of this work. However, we used the conventional field set-up and reduced the dose to the lung. Therefore, the myocardial dose for the IMRT technique will probably be less or equal compared to the conventional technique. The dose to the contra-lateral breast will probably be smaller for the IMRT technique since no wedge is used, resulting in a fewer number of

monitor units then conventionally given.

In this work the patients were positioned supine on a breast board following our conventional treatment technique (Lagendijk and Hofman, 1992). The breast board, however, is used to obtain a flat sternum, which is not necessarily needed using MLC field shaping, since the MLC can be used to follow the curvature of the thorax. An advantage of leaving the breast board concept, would be that CT scanning of patients becomes easier. The IMRT technique we described will be tested using CT scans of patients treated without a breast board. The irradiated volume of the lung should thereby be compared between these different treatment positions. Using our IMRT technique it is possible to maintain the axillary and supraclavicular field match, with and without the breast board. The conventional field set-up (Lagendijk and Hofman, 1992) can therefore be used when these fields are necessary. The match between the tangential fields and the parasternal field can be improved using the new technique, because the leaves are positioned in the anterior-posterior direction. The shape of the posterior field border can be adjusted to obtain a uniform dose distribution along the match line of the parasternal and the medial tangential field. This aspect will be analyzed in the near future.

Several other aspects of the IMRT technique need to be further investigated. The deduction of the MLC settings from the EPM was done in this study by eye, ignoring the relatively small areas with slightly different path lengths. Currently software is being developed to generate MLC settings automatically from the EPM. The number of intensity levels was chosen to be four for all patients, which is similar to others groups (Donovan *et al.*, 2000; Tyburski *et al.*, 1999). This approach worked well for the patients we studied. We made the choice for a minimum number of intensity levels to assure a clinically practical technique. Four levels is probably close to the minimum when the dose distribution in off-axis planes is taken into account. The number of intensity levels could, however, be optimised, since the number of intensity levels will influence the homogeneity of the dose distribution. Especially for patients with large breasts the use of more intensity levels will probably result in an increased dose homogeneity. The relation between the optimum number of intensity levels and the geometry of the breast will be further analyzed, since the largest inhomogeneities are usually observed in patients with large breasts. The proportion of the various segments (approximately 88 % for the largest segment and 12 % for the remaining three smaller segments) was based on a first approximation and not on geometrical patient information alone. Although the proportions of the various segments used in this work gave good results, our choice of segment weighting could influence the dose homogeneity and will be further analyzed.

The presented technique currently consumes more time than conventional treatment planning. However, most steps can be easily automated. The time needed for treatment planning will therefore eventually be equal or less than needed for the conventional technique. CT scanning of the patient will then be the only extra

workload. Other practical aspects of the IMRT technique, such as the matching of the tangential field with the parasternal field, are subjects of further research. Film dosimetry using an anthropomorphic breast phantom will be used to verify the dose distribution obtained using the described IMRT technique. When various problems are solved a true inverse planning method will be developed for tangential breast irradiation, i.e. a treatment planning based solely on geometrical information.

2.4.1 Conclusion

An IMRT technique has been developed based on the division of the treatment field in four segments with similar equivalent path lengths through the breast. Analysis of the dose distribution obtained with this technique showed a better, more homogeneous dose distribution compared with that obtained with conventional tangential breast irradiation. The average dose to the ipsilateral lung is reduced using the IMRT technique by approximately 10 % compared with the conventional technique. Furthermore this new technique has the possibility to improve the field match between the tangential fields and the parasternal field, while maintaining the field match between the tangential fields and the axillary and supraclavicular fields.

Chapter 3

Segmental IMRT for oropharyngeal cancer in a clinical setting

This chapter is based on

Bram van Asselen, Homan Dehnad, Chris H.J. Terhaard, Jan J.W. Lagendijk, and Cornelis P.J. Raaijmakers 2003 Segmental IMRT for oropharyngeal cancer in a clinical setting *Radiotherapy and Oncology* (Accepted)

Abstract

Purpose: To develop a segmental intensity-modulated radiotherapy (IMRT) technique for the treatment of oropharyngeal cancer.

Methods and Materials: Eight patients previously treated for oropharyngeal cancer were replanned with segmental IMRT. The dose distribution was optimized using beam geometries consisting of 3, 5, 7 and 9 equiangular beams. The optimization procedure resulted in a theoretical fluence for each beam. In order to vary the number of segments, the optimized fluence was divided in four different equidistant levels. The final dose distribution was calculated using clinically deliverable segments obtained from optimized fluence.

Results: For our segmental IMRT technique the dose homogeneity within the target volumes improved when the total number of segments increased and reached a saturation level at approximately 150 segments. Seven beams were sufficient to achieve the saturation level for dose homogeneity. The mean dose to the parotid glands depended on the beam geometry and tumor location and did not depend on the number of segments. On average the mean dose to the contralateral parotid gland was 35.7 Gy (27.1 - 39.9 Gy) for all seven beam plans.

Conclusion: Seven beams are sufficient to achieve an acceptable dose homogeneity within the target volumes and significant parotid sparing. These results will be used to introduce IMRT in routine clinical practice.

3.1 Introduction

Due to the complex geometry of the various target volumes and organs at risk, it is useful to apply intensity-modulated radiotherapy (IMRT) for the treatment of oropharyngeal cancers. Most studies concerning the IMRT treatment of oropharyngeal cancers (Vineberg *et al.*, 2002; Chao *et al.*, 2000; Wu *et al.*, 2000; van Asselen *et al.*, 2002), focus on the sparing of the parotid glands, since xerostomia is a severe complication of irradiation of the head-and-neck region (Roesink *et al.*, 2001; Eisbruch *et al.*, 1999). Besides the ability to deliver highly conformal dose distributions, IMRT can be used to deliver different dose levels to different target volumes at the same time, such as the tumor and the electively treated lymph nodes. This ability can also be used to improve the tumor control probability (TCP) by increasing the dose to the target volume, without increasing the dose to the surrounding tissues (Nederveen *et al.*, 2001b; Wu *et al.*, 2000; Mohan *et al.*, 2000).

The number of beams, the beam orientations and the number of segments, when using a segmental MLC delivery technique, are important parameters for the optimization process of an IMRT plan and result in a vast amount of degrees of freedom for the optimization process.

Optimization of beam orientation for IMRT has been studied by several groups (Pugachev *et al.*, 2001; Rowbottom *et al.*, 2001; Söderström and Brahme, 1995; Stein *et al.*, 1997). In most of these studies, beam orientation optimization resulted in improved dose distributions, when a small number of beams (<5) was applied (Rowbottom *et al.*, 2001; Söderström and Brahme, 1995; Stein *et al.*, 1997). The clinical introduction of beam orientation optimization is, however, hampered by the long computation times (Pugachev *et al.*, 2001; Rowbottom *et al.*, 2001). Consequently, IMRT is often clinically introduced using a fixed beam geometry (Nederveen *et al.*, 2001b; Vineberg *et al.*, 2002; Zelefsky *et al.*, 2000; Wu *et al.*, 2000). Generally nine beams are considered to be sufficient (Bortfeld *et al.*, 1990; Mohan *et al.*, 1995). In most recent planning studies concerning IMRT for the treatment of oropharyngeal cancers, nine equiangular coplanar beams were used (Manning *et al.*, 2001; Vineberg *et al.*, 2002; Wu *et al.*, 2000). Wu *et al.* (2000) reported that the quality of IMRT plans improved with increasing number of beams, up to 9 beams. The differences between various beam geometries were, however, not fully quantified. Both Vineberg *et al.* (2002) and Manning *et al.* (2001) did not show data that supported their choice of nine beams.

In our institute segmental IMRT, also known as step-and-shoot IMRT, is used (Nederveen *et al.*, 2001b), in contrast with the use of dynamic MLC in the above mentioned planning studies. For segmental IMRT, the optimal fluence maps obtained by an inverse planning process, are divided in a discrete number of intensity levels. By increasing the number of intensity levels, a better approximation of the optimal fluence map is obtained. The use of segmental IMRT has the advantage

of less complicated quality assurance procedures compared to dynamic MLC. For practical implementation, the total number of MLC segments is an important parameter, since the treatment time is closely related to the number of segments. The use of many segments will not only result in long treatment times but will also result in many small segments with few monitor units. This might lead to unacceptable uncertainties in the treatment delivery (Que, 1999). Potter *et al.* (2002) reported that the treatment efficiency, represented by the total number of MLC segments, firstly depended on the number of intensity levels used and secondly on the segmentation technique used. The number of intensity levels used to obtain results close to the optimal intensity maps was 5 to 10 (Chui *et al.*, 2001; Keller-Reichenbecher *et al.*, 1999; Potter *et al.*, 2002).

The relation between the quality of a treatment plan and the number of beams in combination with the number of segments is important for the clinical introduction of segmental IMRT. This relation has only been studied for two individual head-and-neck cases (Keller-Reichenbecher *et al.*, 1999). It was the purpose of this work to investigate this relation in detail for the IMRT treatment of oropharyngeal cancers and lymph nodes level II-IV in a clinical setting. Few beams with many segments, i.e. a better approximation of the optimized fluence, might give similar results than many beams with few segments. For this purpose, the planning software (PLATO) and linear accelerator (Elekta) available at our department will be used. The results will be used for developing an efficient and reliable segmental IMRT technique.

Table 3.1: The original tumor site and TNM classification.

Patient	Tumor site	TNM		
1	ant.* faucial pillar	T ₁	N ₀	M ₀
2	tonsil	T ₁	N ₀	M ₀
3	tonsil	T ₂	N ₀	M ₀
4	tonsil	T ₂	N ₀	M ₀
5	tonsil	T ₂	N ₀	M ₀
6	base of tongue	T ₂	N ₀	M ₀
7	vallecula	T ₃	N ₀	M ₀
8	tonsil	T ₃	N ₀	M ₀

* anterior

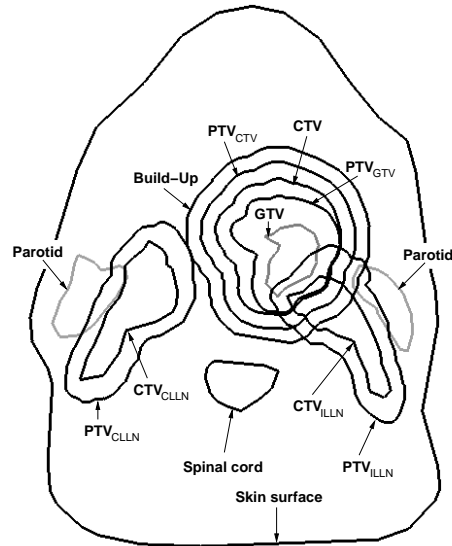


Figure 3.1: The contours of various volumes of interest delineated in a transversal plane. For the primary tumor the gross tumor volume (GTV) and the clinical target volume (CTV) are delineated as well as the planning target volume (PTV) of the GTV (PTV_{GTV}) and the CTV (PTV_{CTV}). Furthermore the CTV and the PTV of ipsilateral and the contralateral lymph node containing regions (ILLN and CLLN) are delineated. Finally the build-up region around the primary target is shown.

3.2 Method

3.2.1 Patients

Eight patients previously treated with conventional radiotherapy for oropharyngeal carcinoma at our institute (Table 3.1), were replanned for this study. All patients underwent a planning computer tomography (CT) scan with 3-5 mm slice intervals, which was transferred to our treatment planning system (PLATO RTS 2.4, Nucletron Ltd., Veenendaal, NL). The clinical target volume (CTV) of the lymph node containing regions, the CTV of the primary target and the organs at risk (OAR; the parotid glands, the brain and the spinal cord) were delineated by a physician (Fig. 3.1). According to the protocol used in our department, the margins necessary to account for microscopic invasion, applied to the GTV to obtain the CTV of the primary tumor differ for each direction: 2 cm cranial; 1 cm caudal,

ventral and medial; 0.5 cm lateral and dorsal. For the delineation of the CTV of the lymph node containing regions the guidelines of Wijers *et al.* (1999) and Nowak *et al.* (1999) were used. The cranial border of the lymph node containing region is at the base of skull for both sides. A margin of 5 mm was applied to each CTV to take into account the set-up uncertainties and organ motion, resulting in the planning target volume (PTV) of the CTV of the primary tumor (PTV_{CTV}), the PTV of the ipsilateral lymph nodes (PTV_{ILLN}) and the PTV of the contralateral lymph nodes (PTV_{CLLN}). No margins were applied to the organs at risk. The intention was to deliver an extra dose to the primary tumor, therefore an extra volume was delineated (PTV_{GTV}), which is the GTV with an extension of 5 mm. Furthermore an extra volume was delineated around the PTV_{CTV} with a margin of 5 mm in order to guide the optimization process. The optimization program can be forced to deliver the build-up of the dose to the prescribed dose to the primary PTV inside this volume (Fig. 3.1). Thus when the primary PTV overlaps with the PTV of the lymph node containing region, the dose gradient from the dose prescribed to the lymph nodes to the dose prescribed to the primary target should be within this volume. All the extensions were limited in the region containing the skin, where the PTV was adjusted by hand when necessary to assure a minimal distance of 5 mm between the PTV and the skin. The minimal margin between the PTVs and the spinal cord and the brain was approximately 10 mm.

3.2.2 Dose prescription

Conventionally, the prescribed dose to the lymph nodes is 50 Gy (2 Gy/fraction; 5 times weekly) and the prescribed dose to the primary tumor 70 Gy (2 Gy/fraction; 5 times weekly) in our institute. In the presented study, the primary disease and the electively treated regions are treated simultaneously with the same number of fractions. Therefore a different fractionation is needed. The data of Mohan *et al.* (2000) were used to determine the fractionation schedule, using a α/β ratio of 20 Gy and an accelerated tumor clonogen doubling time of 4 days. This resulted in a prescribed dose of 54 Gy (1.8 Gy/fraction; 5 times weekly) for the elective irradiation of the lymph nodes and a prescribed dose of 66 Gy (2.2 Gy/fraction; 5 times weekly) for the CTV of the primary tumor. An extra dose of 3 Gy was planned for the GTV in order to increase the TCP, resulting in a total prescribed dose to the GTV of 69 Gy (2.3 Gy/fraction; 5 times weekly). The dose to all target volumes was delivered in 30 fractions, resulting in a simultaneous integrated boost IMRT strategy (Mohan *et al.*, 2000). The maximum dose allowed to the CNS and the spinal cord was 45 Gy. Since the parotid glands are located adjacent to the lymph node containing regions, part of the volume is overlapping with the PTV of the lymph node containing regions, which should receive the prescribed dose. The homogeneous irradiation of the target volumes was the most important aim. Sparing of the parotid gland will be obtained by reducing the dose to the none

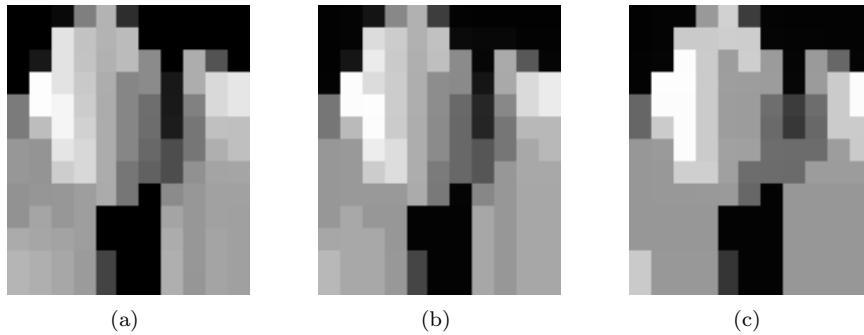


Figure 3.2: The optimized fluence map for an IMRT beam (a) and the fluence after sequencing for segmental IMRT, dividing the intensity values in 15 (b) and 5 (c) equidistant levels.

overlapping parts without affecting the dose to the target volumes (van Asselen *et al.*, 2002).

3.2.3 Inverse planning

IMRT plans were generated using the inverse treatment-planning module ITP of PLATO (version 1.0). This is a commercially available version of the KonRad program, developed by the Bortfeld group (Bortfeld *et al.*, 1993). The ITP module optimizes the fluence for a fixed beam geometry to obtain a dose distribution that best fits a series of dose constraints. For the target volumes a maximum and minimum dose is specified. For organs at risk only a maximum dose is specified. The relative weight of these constraints is tuned with so called 'penalties'. All dose constraints are related to a given contour. Therefore the judicious choice of contours is important for dose painting. When the contours are overlapping, the overlapping volume is assigned to one of the volumes during the optimization process. The parotid glands for example overlap with the PTV of the lymph nodes. During the optimization the overlapping volume is considered to be PTV, since the main goal is to deliver the prescribed dose to the lymph nodes and not reducing the dose to the parotid gland.

A standard set of dose constraints (van Asselen *et al.*, 2002) was determined by systematically varying the penalties, minimum en maximum dose values. For this purpose we used a generic patient including all PTVs and OARs. The starting point was to irradiate only the PTVs without considering the organs at risk. When acceptable dose homogeneity was achieved within the PTVs, organs at risk were added to the optimization process. Since the dose constraints are relative to each

other, the settings of the target volumes did not need to be adjusted and the constraints of the organs at risk could slowly be increased in relative importance. Increasing the penalty was stopped when the volume of the PTVs receiving 95% of the prescribed dose reduced significantly. After obtaining the standard set, it was tested on 3 other patients using three different beam geometries. In each case, clinically acceptable results were obtained and further individual adjustments of the constraints only resulted in mild changes in the dose parameters. In this way a set of dose constraints was obtained which ensures dose homogeneity to the PTVs. This standard set, using moderate sparing for the parotid glands (van Asselen *et al.*, 2002), was then used for all IMRT plans presented in this paper.

During the optimization, a fluence matrix for each beam angle is generated and iteratively adjusted resulting in a dose distribution matching the prescription as closely as possible. For the delivery of the optimized fluence we use step-and-shoot IMRT applying the Elekta MLC (Elekta Oncology Systems, Crawley, UK). The standard ITP sequencer for the Elekta MLC was used for the sequencing procedure. The optimized intensity values of each fluence map were therefore subdivided into a number of equidistant levels. This sequencer is based on the algorithm of Convery and Webb (Convery and Webb, 1998) and tends to minimize the effect of the transmission of the collimators, the leafs and the tongue-and-groove region. In order to minimize the number of segments, a 1-D median filter is applied to the theoretical fluence with a width of 3 bixels. An example of an optimized fluence map and the resulting sequenced fluence map is shown in figure 3.2.

The fluence matrix had a resolution of $1 \times 1 \text{ cm}^2$ in the isocenter. The resolution of the dose calculation matrix, for the iterative dose optimization, is 2.9 mm. After sequencing, the dose distribution as actually delivered, is recalculated using a 3D planning system (PLATO RTS version 2.5) using a resolution of 3–4 mm for the dose calculation matrix.

For each patient, the dose distribution was optimized using a different number of equiangular beams (3, 5, 7 and 9), with the gantry angle of the first beam at 0 degrees. The number of segments cannot be varied in a direct way.

Theoretical fluence with a continuous intensity distribution was converted into a deliverable fluence with distinct intensity levels using 5, 7, 10 or 15 equidistant intensity levels. It should be noted that the number of resulting segments in a beam could be much larger than the number of intensity levels. The variations in number of beams and intensity levels resulted in 16 dose distributions for a single patient.

3.2.4 Analysis of the dose distribution

The dose received by 95 % of the PTV (D_{95}) and the dose received by 5 % of the PTV (D_5) were calculated. The difference between the D_{95} and D_5 , D_{95-5} , was used as a parameter indicating the homogeneity of the dose distribution. The

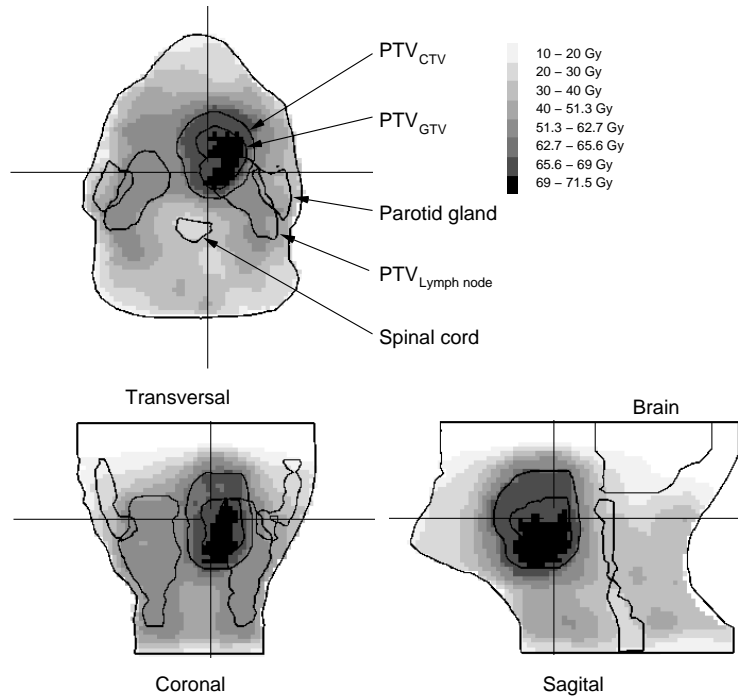


Figure 3.3: An example of the dose distribution in a transversal, coronal and sagittal plane. The cross wire in each plane indicates the intersection of the other two planes. The volumes of interest are delineated. The doses values 51.3, 62.7 and 65.6 Gy are the 95 % doses of the lymph nodes, PTV_{CTV} and PTV_{GTV} respectively.

volume receiving less than 95 % of the prescribed dose ($V_{<95\%}$) and more than 105 % of the prescribed dose ($V_{>105\%}$) were used as parameters indicating underdosages and overdosages respectively. For the PTV of the lymph nodes the volume receiving less than 90 % of the prescribed dose was also calculated. Furthermore, the mean dose to the target volumes was calculated. For the PTV_{CTV} the dose distribution for the part which was not overlapping with the PTV_{GTV} was used in the analysis, since the overlapping part should receive the dose to the PTV_{GTV}. Consequently the PTV_{CTV} is a shell around the PTV_{GTV}. The PTVs of the lymph nodes are overlapping with the PTV_{CTV}. In the analysis of the dose distribution only the part which is not overlapping is taken into account because the overlapping part should receive the dose prescribed to the PTV_{CTV}.

The mean dose to the parotid glands was calculated, including the overlapping

volume, since the mean dose is the best known predictor for the salivary function of the parotid glands after radiotherapy and can be used to calculate the NTCP for xerostomia (Roesink *et al.*, 2001; Eisbruch *et al.*, 1999). The data of Roesink *et al.* (2001) were used to calculate the NTCP for the parotid glands using the model of Lyman (1985) with a TD_{50} of 39 Gy, a slope parameter m of 0.45 and a volume parameter n of 1 (one year after radiotherapy). For statistical analysis of the mean dose to the parotid glands a One-Way ANOVA procedure was used. Differences were considered to be statistically significant when $p < 0.05$.

In order to evaluate the dose to the spinal cord and the CNS the maximum dose was calculated (D_{max}). The maximum dose was defined as the highest dose delivered to a total volume of at least 1 cm³.

The dose to the body, i.e. the volume not containing the target volumes or organs at risk, was studied by determining the volume of the body receiving more than 60 Gy and 70 Gy ($V_{>60Gy}$ and $V_{>70Gy}$).

3.3 Results

3.3.1 Primary tumor

Highly conformal dose distributions were obtained using IMRT for the treatment of oropharyngeal cancers (Fig. 3.3). The mean dose to the PTV_{GTV} was on average 69.4 ± 0.8 Gy (1 standard deviation, SD), which was close to the prescribed dose for this volume. The mean dose to the PTV_{CTV} was on average 66.7 ± 0.7 Gy (1 SD). The dose homogeneity, indicated by D_{95-5} , of the dose distribution within the PTV_{GTV} and the PTV_{CTV} varied for the different combinations of numbers of beams and intensity levels (Fig. 3.4). In general, the dose homogeneity increased when the total number of segments increased. The dose homogeneity was independent of the beam geometry. In other words, the dose homogeneity was similar when the IMRT plans for various beam geometries had a similar total number of segments. Only for the PTV_{CTV} irradiated with the 3 beams this was not the case, similar number of segments resulted in worse dose homogeneity compared to irradiation with 5 beams. When more than approximately 100 segments are used, however, only limited further improvement in dose homogeneity was observed (Fig. 3.4).

The part of the PTV_{GTV} which received a dose less than 95 % of the prescribed dose was small (< 1 % of the volume) when more than approximately 100 segments were used (Table 3.2). The underdosed part of the PTV_{CTV} was larger and increased when fewer beams were used (Table 3.2). The overdosed area of the PTV_{GTV} was relatively small for most cases. On average $V_{>105\%}$ was 7.2 ± 13.6 (1 SD) %, 3.3 ± 4.1 (1 SD) %, 0.9 ± 1.7 (1 SD) % and 1.8 ± 5.0 (1 SD) % for 3,

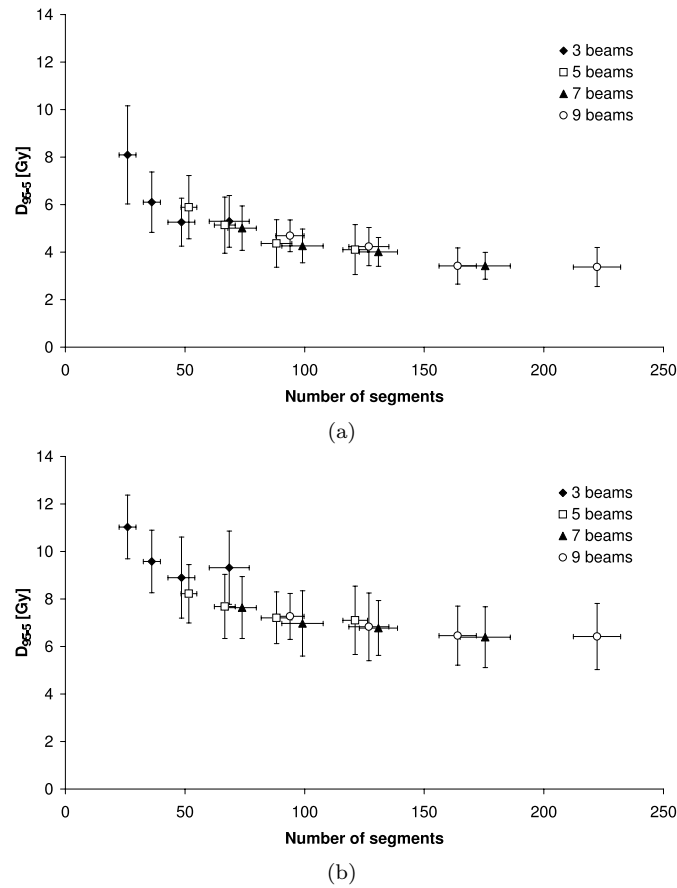


Figure 3.4: The dose homogeneity of the PTV_{GTV} (a) and PTV_{CTV} (b) as a function of the total number of segments for 3, 5, 7 and 9 beams. Each data point is the mean value of 8 patients. The error bar indicates 1 standard deviation.

5, 7 and 9 beams respectively. The overdosed volume of the PTV_{CTV} was larger than that of the PTV_{GTV} due to the dose gradient, from 66 to 69 Gy, which is located in this shell around the PTV_{GTV} . On average the $V_{>105\%}$ of the PTV_{CTV} was 14.4 ± 9.6 (1 SD) %, 13.1 ± 7.1 (1 SD) %, 10.4 ± 4.3 (1 SD) % and 12.9 ± 5.0 (1 SD) % for 3, 5, 7 and 9 beams respectively. The $V_{>105\%}$ increased when fewer segments were used.

Table 3.2: The volume (%) receiving a dose lower than 95 % of the prescribed dose of the planning target volume of the gross tumor (PTV_{GTV}), clinical target volume (PTV_{CTV}), the contra- and ipsilateral lymph node containing region (PTV_{CLLN} and PTV_{ILLN}) for different combinations of number of beams and intensity levels used for sequencing. Beside the mean (m) $V_{<95\%}$ over 8 patients, the standard deviation (SD) is shown.

beams	levels	segm.	PTV_{GTV} m (SD)	PTV_{CTV} m (SD)	PTV_{CLLN} m (SD)	PTV_{ILLN} m (SD)
3	5	26	11.4 (16.6)	15.3 (6.6)	14.2 (5.3)	6.0 (4.7)
3	7	36	4.1 (3.6)	12.5 (5.6)	11.8 (5.0)	6.2 (4.2)
3	10	49	2.4 (2.1)	11.6 (5.7)	11.0 (4.7)	5.4 (4.4)
3	15	69	2.8 (2.1)	12.1 (5.3)	11.3 (4.7)	4.8 (3.8)
5	5	52	2.1 (2.2)	6.3 (3.4)	7.6 (4.6)	9.3 (6.3)
5	7	67	2.1 (1.7)	6.5 (3.0)	6.9 (3.6)	6.1 (3.5)
5	10	88	0.4 (0.3)	5.2 (2.4)	6.0 (3.0)	3.9 (1.8)
5	15	121	0.2 (0.2)	4.6 (2.2)	7.1 (5.7)	4.3 (2.2)
7	5	74	1.8 (2.5)	5.3 (3.8)	6.2 (2.9)	4.3 (2.5)
7	7	99	0.6 (1.2)	4.8 (3.1)	4.9 (2.6)	3.6 (2.1)
7	10	131	0.3 (0.5)	4.2 (2.2)	4.3 (2.6)	3.4 (2.0)
7	15	176	0.1 (0.1)	4.0 (2.3)	4.4 (2.7)	3.3 (2.3)
9	5	94	0.7 (1.2)	4.4 (2.5)	4.2 (2.6)	3.9 (2.0)
9	7	127	0.1 (0.2)	3.4 (1.8)	3.7 (2.6)	3.4 (2.5)
9	10	164	0.1 (0.2)	3.6 (1.8)	3.2 (2.4)	3.0 (2.2)
9	15	222	0.1 (0.1)	3.4 (1.8)	2.9 (2.1)	2.9 (1.7)

3.3.2 Lymph nodes

The mean dose to the PTV of the ipsilateral lymph nodes (PTV_{ILLN}) and the PTV of the contralateral lymph nodes (PTV_{CLLN}) was on average 55.5 ± 0.7 Gy and 55.0 ± 0.5 Gy (1 SD) respectively. The dose homogeneity of the PTV_{ILLN} (Fig. 3.5) improved, as was observed for the primary targets, when the total number of segments increased and did not depend on the number of beams. This was not the case for the dose homogeneity of the PTV_{ILLN} for the 3-beam plans. The dose homogeneity of the PTV_{CLLN} however, showed a different trend. For each beam geometry the saturation level was reached at a different value of dose homogeneity. In other words, the dose homogeneity increased with increasing number of beams

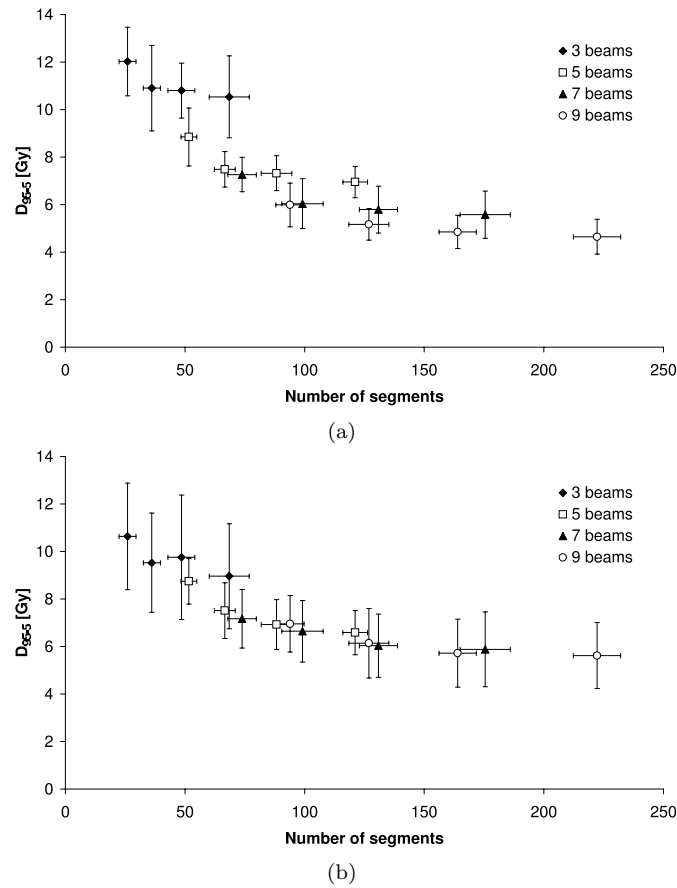
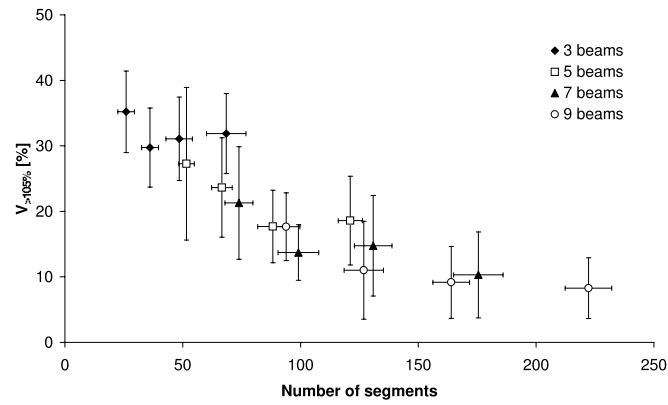


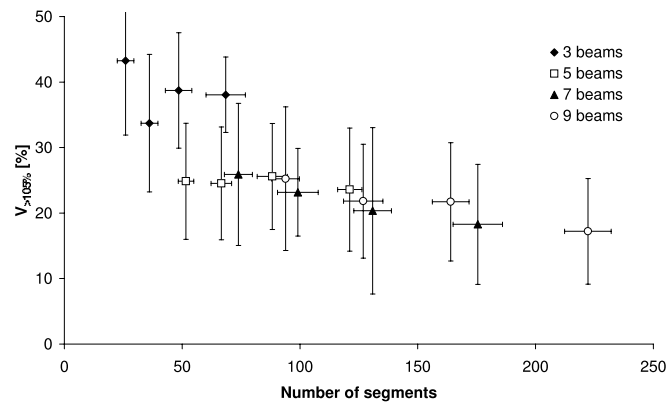
Figure 3.5: The dose homogeneity of the PTV_{CLLN} (a) and PTV_{ILLN} (b) as a function of the total number of segments for 3, 5, 7 and 9 beams. Each data point is the mean value of 8 patients. The error bar indicates 1 standard deviation.

for a similar total number of segments.

The $V_{<95\%}$ increases when a smaller number of intensity levels was chosen and for a smaller number of beams (Table 3.2), especially for the contralateral part of the lymph nodes. The volume receiving less dose than 90 % of the prescribed dose ($V_{<90\%}$) for the PTV_{ILLN} was smaller than 1 % for the plans with more than approximately 90 segments. For a smaller number of segments $V_{<90\%}$ amounted to 1-2 %. For the PTV_{CLLN} , $V_{<90\%}$ was on average 4.2, 1.6, 1.3 and 0.8 % for 3, 5, 7 and 9 beams respectively. The overdosage of the lymph nodes was relatively



(a)



(b)

Figure 3.6: The volume receiving more than 105 % of the prescribed dose ($V_{>105\%}$) to the contralateral (a) and ipsilateral (b) lymph node containing region. Each data point is the mean value of 8 patients. The error bar indicates 1 standard deviation.

large (Fig. 3.6), especially for the ipsilateral part which was close to the high dose areas. It was also observed that the overdosed volume depended on the number of beams and number of segments, especially for the contralateral side.

3.3.3 Spinal cord and brain

On average D_{max} of the brain was 33.6 Gy (range 11.4 – 46.8 Gy). For one case, with 3 beams and 7 intensity levels, the maximum dose did exceed 45 Gy. The average of the maximum dose to the spinal cord was 32.6 Gy and did not vary much from patient to patient (range 30.2 – 37.5 Gy).

3.3.4 Body

No large difference was observed between the high dose volumes for 5, 7 and 9 beams. On average $V_{>60Gy}$ and $V_{>70Gy}$ were 34.2 cm³ (range 13.1 – 59.0 cm³) and 0.4 cm³ (range 0.0 – 2.3 cm³) respectively. These volumes decreased when more segments were used. The high dose volume of the body for 3 beams was larger than for the other beam geometries. On average $V_{>60Gy}$ and $V_{>70Gy}$ were 45.2 cm³ (range 11.6 – 81.8 cm³) and 3.0 cm³ (range 0.0 – 9.7 cm³) respectively. High dose volumes in the body appeared not only near the target volume but also in the posterior part of the neck for the 3-beam geometry.

3.3.5 Parotid glands

The mean dose to the parotid glands did not depend on the number of intensity levels. The variation in mean doses for a varying number of intensity levels using the same beam geometry was smaller than 0.5 Gy. The mean dose was, however, influenced by the beam geometry, especially for the contralateral parotid gland (Fig. 3.7). On average the mean dose to the contralateral parotid gland was 32.6 Gy for the 5 beam plans. This was lower than the average mean dose for the 3, 7 and 9 beam plans, which amounted to 38.0, 35.7 and 34.4 Gy, respectively. Although small, the difference in the mean doses for the different beam geometries were statistically significant ($p < 0.001$). There was no statistically significant difference between the mean doses of the ipsilateral parotid gland (on average 42.6 Gy) calculated for the 5, 7 and 9 beam plans. The mean dose for the 3 beam geometry was on average 45.3 Gy, and was significantly higher ($p < 0.001$) than the mean doses of the other beam geometries.

NTCP values were calculated using the mean doses to the parotid glands. This resulted in mean NTCP values for the contralateral parotid gland of 0.48, 0.36, 0.43 and 0.40 for the 3, 5, 7 and 9 beam plans, respectively. For the ipsilateral parotid gland the NTCP values were higher, 0.64 for the 3 beam plan and approximately 0.58 for the other beam geometries.

3.3.6 Segments

The total number of segments after sequencing ranged from 22 to 234 depending on the number of beams and intensity levels. The differences between the seg-

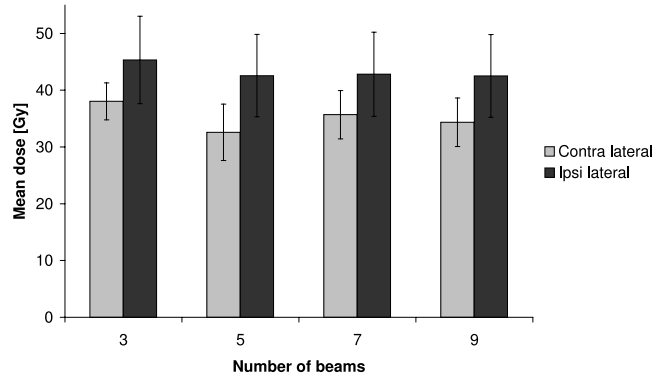


Figure 3.7: The mean dose for the contralateral and ipsilateral parotid gland for 3, 5, 7 and 9 beams. The mean dose is averaged over 8 patients and 4 numbers of intensity levels. The error bar indicates 1 standard deviation.

mented fluence map and the optimized fluence map were small when 15 intensity levels were used, while for 5 intensity levels distinct differences were observed (Fig. 3.2). There was a linear relation between the number of intensity levels and the resulting number of segments after the sequencing process (Fig. 3.8). The number of segments for a single beam was approximately 1.4 times the number of intensity levels. The delivery time of an IMRT plan with 7 beams and approximately 80 segments was 13-14 minutes. For approximately 150 segments the IMRT plans were executed in 24-26 minutes. The delivery times were reduced by approximately 2 minutes when 5 beams were used with a similar number of segments.

3.4 Discussion

In this planning study on the segmental IMRT treatment of oropharyngeal tumors and lymph nodes level II-IV, various combinations of beam geometries and intensity levels were investigated. The dose homogeneity within the target volumes mainly depended on the total number of segments and was only slightly influenced by the number of beams. For the PTV_{GTV} , PTV_{CTV} and PTV_{ILLN} the dose homogeneity, using 5, 7 and 9 beams, was similar when the total number of segments was similar. For the contralateral lymph nodes, however, the dose homogeneity improved for plans with a constant number of segments when more beams were used. The difference in dose homogeneity between the plans with 7 or 9 beams with many segments was small for all target volumes, indicating that more than 7

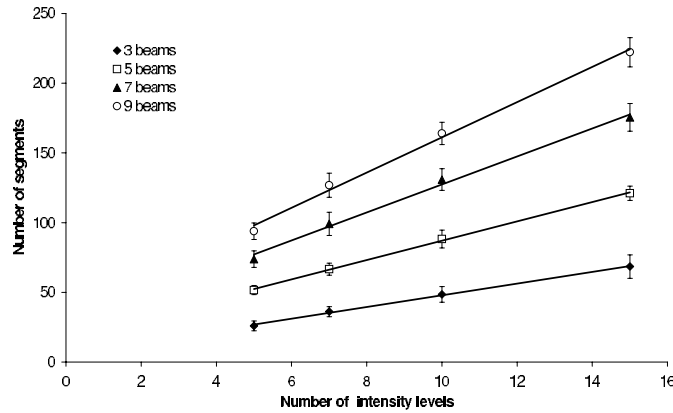


Figure 3.8: The total number of intensity levels in which the theoretical fluence is divided and the resulting total number of segments after sequencing.

beams are not needed. In a study of Wu *et al.* (2000), IMRT using various beam geometries was analyzed. Although not quantified in detail, they reported that the quality of the IMRT plan improved when the number of beams increased, up to 9 beams. Vineberg *et al.* (2002) used 9 beams for the IMRT treatment of oropharyngeal cancer, in order to have sufficient degrees of freedom to achieve high-quality dose distributions. Although beam optimization becomes less important when 7 or more beams are used (Stein *et al.*, 1997; Söderström and Brahme, 1995; Rowbottom *et al.*, 2001), Pugachev *et al.* (2001) showed improvements in the dose distribution for a nasopharyngeal case using 9 noncoplanar beams when beam angle optimization was applied.

The underdosage of the PTV_{GTV} was small (Table 3.2). $V_{<95\%}$ amounted to 0.1 – 0.3 %, for the 7- and 9-beam plans with many segments. For the PTV_{CTV} the $V_{<95\%}$ was larger and amounted to 3 – 4 % for the IMRT plans with the best dose homogeneity. The volumes within the target volume receiving a dose lower than 95 % of the prescribed dose were always located near the border of the volume. In most cases they were observed at the posterior side of the PTV, relatively close to the spinal cord and the brain. The $V_{<95\%}$ of the PTV of the lymph nodes were comparable with the $V_{<95\%}$ of the PTV_{CTV} . Since most of the PTV of the lymph nodes received a dose larger than 90 % of the prescribed dose (on average 99 % of the PTV) this will still result in low risk of metastasis (Withers *et al.*, 1995a).

Although the dose homogeneity to the target volumes was considered the most important, it was possible to achieve mean doses to the contralateral parotid gland of approximately 35 Gy, the dose to the ipsilateral gland was approximately 10 Gy higher. Using conventional conformal techniques mean doses of approximately

50 – 70 Gy are obtained. For the IMRT plans this results in a NTCP value of approximately 0.40 for the contralateral parotid gland. Several groups studied the IMRT treatment of oropharyngeal cancers and elective irradiation of the lymph nodes. Vineberg *et al.* (2002) reported mean doses ranges of approximately 17 – 34 Gy and 28 – 53 Gy for the contralateral and ipsilateral parotid glands respectively, using a contralateral parotid-sparing protocol (Eisbruch *et al.*, 1998). The homogeneity of the dose in the target volumes was within 5 % of the prescribed dose. Using a simple three-dimensional conformal radiotherapy technique with beam intensity modulation van Dieren *et al.* (2000) reported a mean dose to the parotid glands of 41.5 Gy, while the PTV was fully covered by the 95 % isodose surface for most plans. Chao *et al.* (2000) reported a mean dose of 22.4 ± 5.22 Gy (1 SD) for irradiations involving the primary tumor and neck nodes. The mean volume of the targets receiving less than 95 % of the prescribed dose was 3 ± 1.4 % (1 SD). A tomotherapy-based IMRT system was used. Using a planning organ-at-risk volume and a dynamic multileaf collimation technique, Manning *et al.* (2001) reported that 0.1 ± 0.0 % (1 SD) of the contralateral parotid received a dose more than 30 Gy for three cases. The coverage of the elective treated volume (ETV) was however, diminished, i.e. 92.5 ± 4.4 % (1 SD) of the ETV received a dose higher than or equal to the prescribed dose (54 Gy). Variation in the mean dose to the parotid gland and target dose homogeneity reported by the various groups may be the result of different treatment planning strategies and different IMRT delivery techniques. Also the volumes will not always be delineated in the same way. For example, the cranial border of the lymph node containing region is at the base of skull for both sides in our study, while others might lower the cranial border in order to spare the contralateral parotid gland. The influence of lowering this cranial border and the associated risks are currently investigated.

The mean dose to the parotid glands did not decrease using additional beams. In this paper, the mean dose to the contralateral parotid gland was statistical significantly lower for 5 beams than for the other beam geometries. This might be due to the fact that in the five-beam geometry, a favorable beam angle is present. Another reason might be the use of a fixed set of dose constraints and penalties independent of the beam geometry. The reason for this effect will be further investigated. There was also no effect of the number of intensity levels on the mean dose to the parotid gland. Using more intensity levels might result in a sharper dose gradient between the parotid glands and the lymph nodes. The mean dose, which is the best known prognostic factor for xerostomia (Roesink *et al.*, 2001; Eisbruch *et al.*, 1999), is, however, not very sensitive to a sharper dose gradient and is dominated by the overlapping volume receiving the prescribed dose (54 Gy). Keller-Reichenbecher *et al.* (1999) reported for two head-and-neck cases that using additional beams and intensity levels, it was possible to improve the dose homogeneity in the target volume. This, however, did not automatically result in a better sparing of OARs. For a nasopharyngeal case, Chui *et al.* (2001), reported

that increasing the number of levels resulted in improved target coverage, but the critical organ protection was little affected.

The total number of segments after sequencing ranged from 22 to 234 depending on the number of beams and intensity levels. The absolute number of resulting segments depends on the sequencing technique (Chui *et al.*, 2001; Potter *et al.*, 2002; Que, 1999). The number of segments needed per field per intensity level was 1.4, which is similar to the value of 1.3 (± 0.2) determined by Potter *et al.* (2002) for three head and neck cases. The number of segments is also influenced by the resolution of the fluence matrix. Although a finer resolution might result in an improved dose distribution, it could also result in more segments and thus in longer treatment times. We therefore choose for a resolution of $1\text{ cm} \times 1\text{ cm}$ in this work and will further investigate the influence of a higher resolution.

When the total number of segments increased from approximately 100 to approximately 150, relatively little improvement in dose homogeneity was observed. When many segments are used, the individual segments will become smaller. The use of many small segments has dosimetric disadvantages such as a larger contribution from leaf transmission and uncertainties caused by small field dosimetry. Furthermore, many segments result in longer treatment times and consequently an increased risk for intrafraction motion of the patient (van Asselen *et al.*, 2003). The optimization in radiotherapy is a multi-parameter problem. Parameters such as treatment modality, beam energy, number and orientation of beams and the fluence profiles all require optimization to obtain the best possible treatment plan for an individual patient (Rowbottom *et al.*, 1999). The optimization of all parameters requires too much time even on a research basis. We therefore choose a reasonable sub-set of these parameters and investigated for this sub-set the best clinically achievable treatment plan. The patients were all planned using the same parameters, what makes the introduction of IMRT more easy since this would be less time consuming than individually optimize the parameters for each patient. Individual optimization might, however, result in a slightly better treatment plan. Although the optimal plan for each individual patient might not be achieved using the class solution, the presented IMRT plans resulted, however, in highly conformal and clinically acceptable plans. The findings of this paper are now used for the clinical introduction of IMRT for the treatment of oropharyngeal tumors at our department and can be used as a starting point for further improvements.

3.5 Conclusion

A subset of treatment parameters has been investigated for the segmental IMRT treatment of oropharyngeal cancers and the elective treatment of the lymph nodes level II-IV. Significant parotid sparing was obtained for 5, 7 and 9 beams, with acceptable dose homogeneity within the target volumes and dose escalation in the

GTV. The dose homogeneity in the PTVs depended mainly on the total number of segments and was only slightly influenced by the number of beams. The number of segments did not influence the mean dose to the parotid glands. When only the dose distribution to the target volumes is considered, 7 beams and a total of approximately 100 segments were sufficient to achieve a highly conformal and homogeneous dose distribution. Between 100 and 150 segments little improvement in the dose distribution was observed.

Chapter 4

The dose to the parotid glands with IMRT for oropharyngeal tumors: the effect of reduction of positioning margins

This chapter has been published as

B. van Asselen, Homan Dehnad, C.P.J. Raaijmakers, J.J.W. Lagendijk and Chris H.J. Terhaard 2001 The dose to the parotid glands with IMRT for oropharyngeal tumors: the effect of reduction of positioning margins *Radiotherapy and Oncology* **64** 197–203

Abstract

Purpose: The aim of this paper is to quantify the importance of the reduction of positioning margins applied to the clinical target volume (CTV) on the dose distribution of the parotid gland for different intensity modulated radiotherapy (IMRT) strategies for the treatment of oropharyngeal cancer.

Methods and Materials: CTVs and organs at risk were delineated in the planning computed tomographic (CT) scans of three patients. Margins of 0, 3, 6 and 9 mm were applied to the CTVs in order to obtain the planning target volumes (PTVs). Three IMRT strategies were used to optimize the dose distribution.

Results: The analysis of the three IMRT strategies resulted in: (1) an optimal dose distribution in the PTV, (2) optimal dose distribution in the PTV while sparing the parotid gland and (3) more parotid gland sparing but at expense of the dose homogeneity in the PTV. The mean parotid dose increased linearly with increasing margin by approximately 1.3 Gy per mm. As a result the normal complication probability (NTCP) for xerostomia decreased when smaller margins were applied. Reducing the margin from 6 to 3 mm resulted in an NTCP reduction of approximately 20 %.

Conclusion: Reducing the CTV-PTV margin by improving the patient position accuracy may lead to a significant reduction of NTCP for the IMRT treatment of the oropharyngeal tumors and lymph nodes level II.

4.1 Introduction

A common and severe complication of the irradiation of cancers in the head and neck region is xerostomia. The level of xerostomia for an individual case depends on the location of the main salivary glands relative to the target volumes. In case of oropharyngeal tumors, at least one parotid gland is located near the primary tumor and both are located adjacent to the lymph node containing region level II, which are treated electively. Irradiation of the main salivary glands is therefore inevitable, which can cause reduction of the salivary flow and change in salivary composition leading to a number of clinical sequela including xerostomia, difficulties in mastication and speech, changes of taste, increased risk of caries and oral infections, chronic esophagitis and altered nutrition (Hamlet *et al.*, 1997; Mandel, 1987; Vissink *et al.*, 1988; Wright, 1987). These severe side effects have a negative impact on the quality of life of the patient (De Graeff *et al.*, 1999; Huguenin *et al.*, 1999).

Conventionally two opposed lateral fields are used for the irradiation of the oropharynx. Therefore dose values up to the prescribed dose (50-70 Gy) cannot be avoided to the parotid glands. In a prospective study Roesink *et al.* (2001) showed that a normal tissue complication probability (NTCP) of 50 % for xerostomia is obtained when the mean dose to the parotid glands is 39 Gy. Eisbruch *et al.* (1999) reported a mean dose of 28.4 Gy for a NTCP of 50 % . Lower NTCP values (< 50 %) and thus lower mean doses are, however, desirable.

Various studies showed reduction of the dose to the parotid glands using intensity modulated radiotherapy (IMRT) (De Neve *et al.*, 1999; Butler *et al.*, 1999; Wu *et al.*, 2000; Manning *et al.*, 2001; Eisbruch *et al.*, 1998). With IMRT it might therefore be possible to preserve the function of the parotid glands, while the target volumes still receive an acceptable dose. The reduction of the dose is depends on the exact implementation of the IMRT technique, which determines the steepness of the dose gradient between the parotid glands and the PTVs. Secondly, the margins applied to the clinical target volume (CTV) in order to obtain the planning target volume (PTV) are important. These margins can cause overlapping areas between the PTVs and the parotid glands, unavoidably leading to high dose regions in these glands. The size of these margins depends on set-up uncertainties (Hurkmans *et al.*, 2001b; De Boer *et al.*, 2001) and organ motion. Improving the positioning of patients and position verification results in smaller margins, and might consequently result in a lower NTCP for xerostomia.

It is the purpose of this work to quantify the influence of the CTV-PTV margin, i.e. the importance of more accurate position verification, on the dose distribution of the parotid glands and secondly to investigate the influence of different IMRT strategies to the dose to the parotid glands and the PTVs for the irradiation of oropharyngeal tumors and lymph nodes level II.

4.2 Materials and method

4.2.1 Patients

The data of three patients with oropharyngeal tumors were used. Patient A had a tumor localized in the anterior faucial pillar (T1N0M0), patient B had a tumor localized in the tonsil (T2N0M0) and the tumor of patient C was localized in the vallecula (T3N0M0). A planning computer tomography (CT) with 3 mm slice intervals was available for these patients. The CT-images were transferred to our treatment planning system (PLATO RTS 2.4, Nucletron Ltd., Veenendaal, NL), where the CTV of the lymph node containing regions, the CTV of the primary target and the organs at risk (OAR; the parotid glands, the brain and the spinal cord) were delineated by a physician. According to the protocol used in our department, the margins applied to the GTV to obtain the CTV of the primary tumor differ for each direction: 2 cm cranial; 1 cm caudal, ventral and medial; 0.5 cm lateral and dorsal. For the delineation of the CTV of the lymph node containing regions the guidelines of Wijers *et al.* (1999) and Nowak *et al.* (1999) were used. The volumes of the CTVs of the primary tumor were 97.2, 70.2 and 68.6 cm³ for patient A, B and C, respectively. The mean volume of the parotid glands was 26.3 cm³ (range 22.4–31 cm³).

Margin of 0, 3, 6 and 9 mm were applied to the CTV in three dimensions using an automatic volume extension (PLATO VSS). This resulted in four different PTVs for each of the three CTVs of an individual patient (Fig. 4.1). The margin was a multiple of 3 mm since the CT was taken with 3 mm intervals. The extension of the CTV was limited in the region containing the skin, where the PTV was adjusted by hand when necessary to assure a minimal distance of 5 mm between the PTV and then skin. The minimal margin between a PTV and the spinal cord was approximately 10 mm. An extra volume was delineated around the PTV of the primary target with a margin of 5 mm to the PTV in order to steer the dose distribution. The optimization program can be forced to deliver the build-up of the dose to the prescribed dose to the primary PTV inside this extra volume. Thus when the primary PTV overlaps with the PTV of the lymph node containing region, the dose gradient from the dose prescribed to the lymph node containing region (54 Gy) to the dose prescribed to the primary target (66 Gy) will be located in this volume.

4.2.2 Intensity modulated radiotherapy planning

IMRT plans are generated using the inverse treatment planning module ITP of PLATO. This module is a commercially available version of the KonRad program, developed by the Bortfeld group (Bortfeld and Schlegel, 1993). The ITP module optimizes the fluence for a fixed beam geometry to obtain a dose distribution that best fits a series of dose constraints. For the target volumes a maximum and

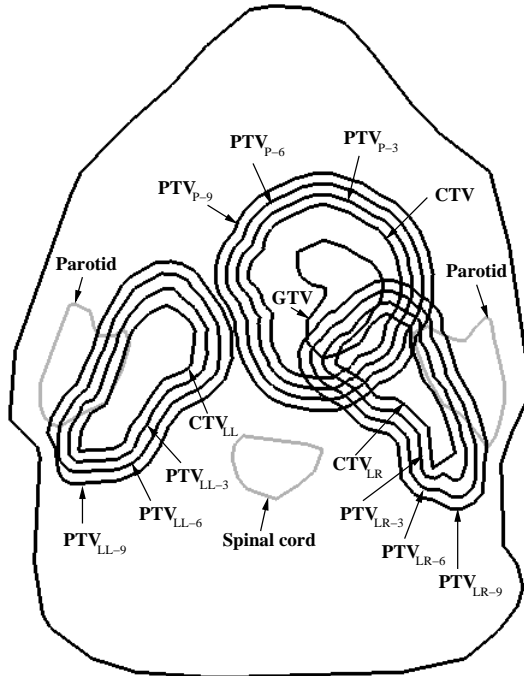


Figure 4.1: The contours of patient B delineated in a transversal plane. The PTVs of the primary tumor (PTV_{P-x}) and the right and left lymph node containing region (PTV_{LL-x} and PTV_{LR-x} respectively) are shown for different margins applied to the CTVs. The number in the subscript indicates the applied margin in millimeters.

minimum dose is specified, for OARs only a maximum dose. The relative weight of these constraints is tuned with so-called 'penalties'. All dose constraints are related to a given contour. Therefore the judicious choice of contours is important for dose painting.

During the optimization, a fluence matrix for each beam angle is generated and iteratively adjusted resulting in a dose distribution matching the prescription as closely as possible. For delivering such a fluence in practice, we plan to use step-and-shoot IMRT, i.e. the modulated fluence is realized by delivering a discrete number of irregularly shaped fields. The theoretical fluence with a continuous intensity distribution is converted into a deliverable fluence with distinct intensity

levels using sequencer software developed at our institute and incorporated into the ITP software. The fluence matrix had a resolution of $1 \times 1 \text{ cm}^2$ in the isocenter. The resolution of the dose calculation matrix, for the iterative dose optimization, is 2.9 mm. After optimization, the dose distribution is recalculated with a three-dimensional (3D) planning system (PLATO RTS version 2.4) using a resolution of 1.6 mm for the dose calculation matrix.

The prescribed dose to the PTV of the primary tumor was 66 Gy (2.2 Gy/fraction; five times weekly), which is radiobiologically similar to 70 Gy (2 Gy/fraction; five times weekly). For the elective irradiation of the lymph node containing regions 54 Gy (1.8 Gy/fraction; five times weekly) was prescribed, equivalent to 50 Gy in 25 fractions. The dose to the target volumes was delivered in a total of 30 fractions, resulting in a simultaneous integrated boost strategy, i.e. different dose levels are simultaneously delivered to different tissues in a single treatment session (Mohan *et al.*, 2000). The maximum dose to the brain and the spinal cord was 45 Gy.

In order to achieve a standard set of beam parameters and dose constraints which can be used for the IMRT calculations, the number of beams and the value of the penalties were systematically varied. This resulted in a beam geometry consisting of seven coplanar beams equidistant, with the gantry angle of the first beam at 0° . Beside the beam geometry, a standard set of dose constraints (Table 4.1) was determined, which resulted in homogeneous dose distributions within the target volumes and acceptable doses to the organs at risk. Fifteen intensity levels were chosen for each beam. This is the maximum which can be chosen for step-and-shoot IMRT.

For each margin, three different optimization strategies concerning the sparing of the parotid glands were analyzed. In other words, three different sets of dose constraints for the parotid glands are used in this paper:

- set 1 The dose to the parotid gland is not taken into account during the optimization process of the target volumes.
- set 2 A penalty is assigned to the parotid gland which limits the dose during the optimization process. The parotid is thus actively spared.
- set 3 A more extreme version of the second set (a higher penalty), where the optimization process is forced to reduce the dose to the parotid glands further.

The penalty settings for the parotid glands were 0, 1 and 10 for dose constraint set 1, 2 and 3 respectively. The three different sets were used to determine the amount of parotid sparing that can be achieved and to investigate the relation between the sparing of the glands and the dose distributions in the PTVs.

It should be realized that the beam geometry and the set of dose constraints for the volumes involved were the same for all 36 (3 patients \times 4 margins \times 3 dose constraint sets for the parotid glands) IMRT plans, the constraints of the parotid glands excluded.

Table 4.1: The settings used for the optimization in PLATO ITP. The penalty setting for the parotid glands (x) is varied.

VOI	max dose	penalty	min dose	penalty
PTV _{primary tumor}	66	100	66	100
PTV _{build-up}	66	100	66	1
PTV _{lymph node}	54	100	54	100
Body	40	10	-	-
Spinal cord	30	100	-	-
Brain	30	100	-	-
Parotid gland	20	x	-	-

4.2.3 Analysis

In our institute the salivary function of 108 patients treated with radiotherapy for various malignancies in the head and neck region was studied in detail (Roesink *et al.*, 2001). The data were fitted using the NTCP model proposed by Lyman (1985). The data analysis showed that the mean dose to the parotid glands is a predictor for the salivary function of the glands after radiotherapy and can be used to calculate the NTCP. Therefore we calculated the mean dose to the parotid glands in order to predict the NTCP value for the IMRT plans. Beside the data of Roesink *et al.* (2001), the data of Eisbruch *et al.* (1999) were used to compare the results for two different clinically obtained NTCP curves. Both used a maximum likelihood estimation of the NTCP model but found different parameter values. For the same endpoint, i.e. less than 25 % of the baseline flow value at 1 year post-radiotherapy, Roesink *et al.* (2001) found $TD_{50} = 39$ Gy and a slope $m = 0.45$ versus a $TD_{50} = 28.4$ Gy and slope $m = 0.18$ reported by Eisbruch *et al.* (1999). A smaller value for m results in a steeper NTCP curve.

A two-tailed paired *t*-test, using the Bonferroni correction for multiple testing, was used for statistical analysis of the mean dose. In the remainder of this paper, differences were considered to be statistically significant when $P < 0.05$.

Beside the analysis of the dose volume histograms (DVHs), the dose to the PTVs was evaluated by calculating the dose received by 95 % of the PTV (D_{95}), the dose received by 5 % of the PTV (D_5) and the mean dose. For the spinal cord and the brain, the dose received by 1 cm³ (D_{max}) was evaluated, which is used as an indicator of the maximum dose. The PTV of the primary target partially overlaps the lymph node containing region (Fig 4.1). In the analysis of dose distribution of the lymph node containing region, only the part of the lymph nodes which is not overlapping the PTV of the primary tumor is taken into account.

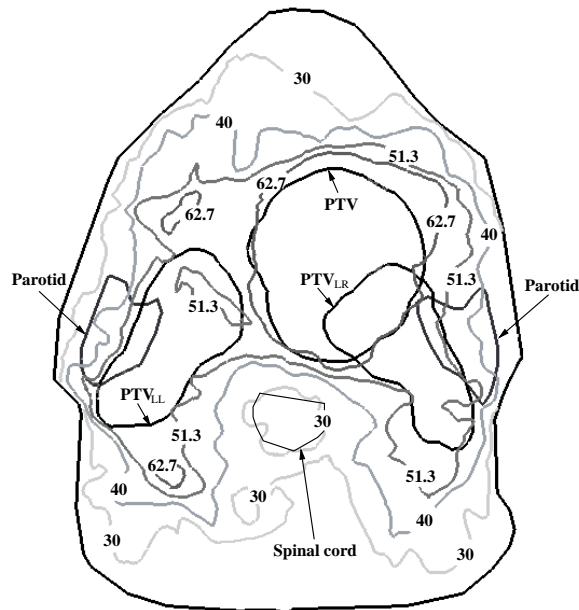


Figure 4.2: Dose distribution in a transversal plane obtained using 7 equidistant beams. A margin of 6 mm and dose constrain set 2 were used. The isodose of 30, 40, 51.3 (= 95 % of 54 Gy) and 62.7 (= 95 % of 66 Gy) Gy are shown. Furthermore the contours of the volumes of interest are shown.

4.3 Results

4.3.1 Target volumes

In general, highly conformal dose distributions were obtained using seven beams and 15 intensity levels (Fig. 4.2). The mean dose to the various PTVs was close to the prescribed dose. The average mean dose (averaged over all 36 plans) to the PTV of the primary tumor was 66.2 Gy (range 65.4–67 Gy). For the PTV of ipsilateral and contralateral lymph node containing region this the average mean dose was 54.8 Gy (range 54.4–55.3 Gy) and 54.5 Gy (range 53.7–55.2 Gy) respectively. The homogeneity of the dose distribution was different for the three sets of dose constraints. The dose distribution calculated using set 1 or 2 were comparable when the same margin was applied (Fig. 4.3), indicating that parotid sparing was obtained without compromising the dose homogeneity in the PTVs. However, using the dose constrain set 3, part of the lymph node containing regions did receive a lower dose compared to the calculations for set 1 and 2 (Fig. 4.3). This was the case

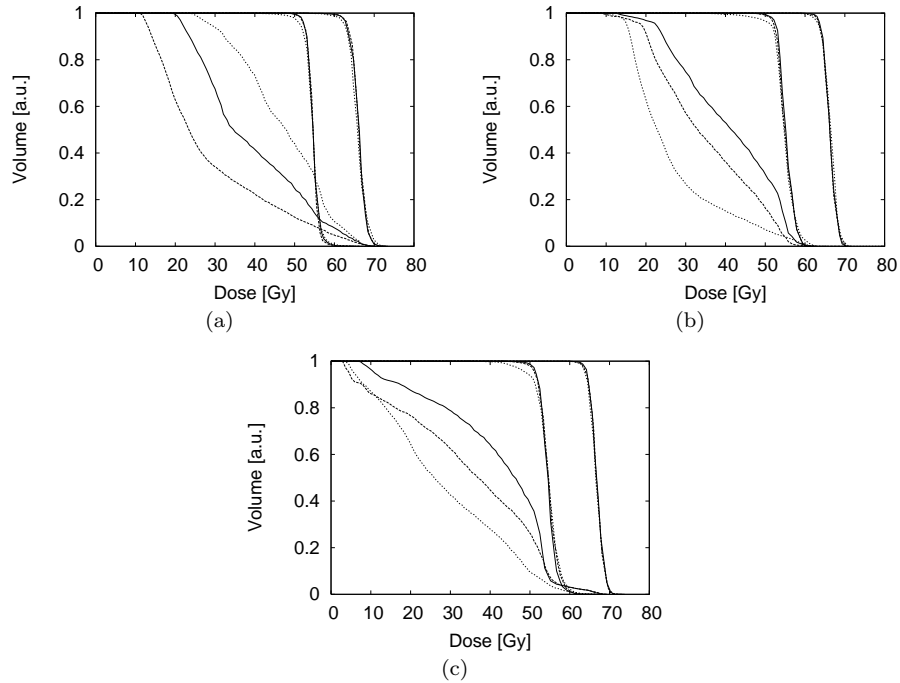


Figure 4.3: The DVHs of the PTV of the primary tumor (3 right curves), the ipsilateral lymph node containing region (3 curves in the middle) and the ipsilateral parotid gland (3 left curves) for the 3 patients (a, b and c) calculated for 3 sets of dose constraints: no active sparing (solid line), moderate sparing (dashed line) and heavy sparing (dotted line). A margin of 6 mm was applied to the CTV.

for all patients and all margins used. The dose distributions of the PTVs calculated for larger margins were slightly more inhomogeneous. The difference between D_{95} and D_5 , which characterizes the slope of the DVH, did not exceed 1 Gy for the PTV of the primary tumor and the contralateral lymph containing region when enlarging the margin for the same dose constrain set. In other words, 90 % of the volume received a dose within a dose interval of 1 Gy. For the ipsilateral lymph node containing region, values up to 2 Gy were calculated for a margin of 9 mm.

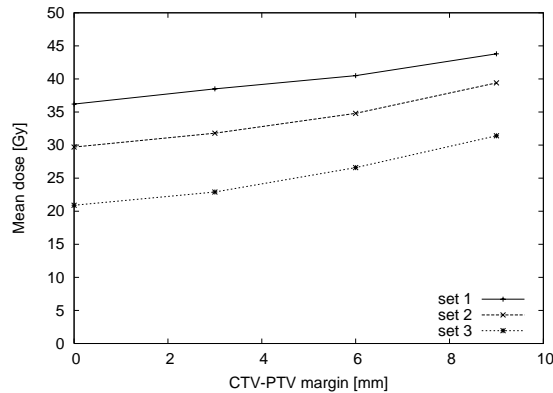


Figure 4.4: The mean dose to the ipsilateral parotid gland of patient B as a function of the margin applied to the CTV for 3 dose constrain sets.

4.3.2 Spinal cord and brain

The maximum dose to the spinal cord and the brain were well below 45 Gy (table 4.2). The dose to the brain was not exceeding 42.9 Gy and the dose to the spinal cord was not exceeding 32.5 Gy for all plans. The average D_{max} of the spinal cord was similar for the three patients with relatively small ranges. The variation in the D_{max} of the brain was however larger and differed from patient to patient. In contrast with the D_{max} of the spinal cord, the D_{max} of the brain increased slightly when the margin was enlarged.

4.3.3 Parotid gland

The mean dose to the parotid gland was largely influenced by the IMRT strategy (Table 4.3). Using set 2, the mean parotid dose was reduced compared to the calculation using set 1 by approximately 6 Gy. For dose constrain set 3 the mean

Table 4.2: The average D_{max} and its range of all IMRT plans for the spinal cord and the brain.

	Brain	Spinal cord
	average D_{max} (range) [Gy]	average D_{max} (range) [Gy]
patient A	30.5 (25.6–34.7)	31.5 (30.4–32.3)
patient B	37.5 (32.6–42.9)	29.9 (28.9–30.7)
patient C	23.8 (18.6–29.6)	30.1 (29.1–31.5)

Table 4.3: The average mean dose ($SD \leq 8\%$) to the parotid glands (\bar{D}) and the NTCP (using the data of Roesink *et al.* (2001)) of the parotid glands for three sets of dose constraints and four different margins between the CTV and PTV.

	margin [mm]							
	0		3		6		9	
	D [Gy]	NTCP	D [Gy]	NTCP	D [Gy]	NTCP	D [Gy]	NTCP
set 1	34.9	0.41	38.4	0.49	42.1	0.57	45.1	0.64
set 2	28.6	0.28	32.3	0.35	36.2	0.44	39.4	0.51
set 3	21.5	0.16	24.3	0.20	28.7	0.28	32.7	0.36

dose of the parotid glands could be reduced further by approximately 7 Gy. The mean parotid dose increased approximately linearly with increasing margin, for all parotid glands and the various set of dose constraints used (Fig. 4.4). The relation between the margin and the mean dose was fitted by linear regression, for each gland and for every dose constraint set separately. This resulted in an average slope of 1.3 ± 0.2 (1 SD = standard deviation) $\frac{\text{Gy}}{\text{mm}}$ for 18 fits. Consequently, when the margin is increased by 1 mm, the mean dose to the parotid gland will increase by approximately 1.3 Gy. The differences in mean dose between the IMRT plans calculated using the three different sets and between the four different margins were all statistically significant ($P < 0.001$).

NTCP values (Table 4.3) were calculated using the averaged mean dose of the parotid glands and the NTCP data of Roesink *et al.* (2001). The range of NTCP values was 0.16 – 0.63, depending on the margin and the IMRT strategy. The relation between the margin and the NTCP was also approximately linear (Fig. 4.5 A). When a margin of 6 mm was used together with dose constraint set 2, i.e. sparing of the parotid glands without compromising the dose homogeneity in the PTVs, the average NTCP was 0.44. Using a margin of 3 mm the NTCP reduced by approximately 20 % to a value of 0.35. The NTCP values were also calculated using the data of Eisbruch *et al.* (1999) (Fig. 4.5 B). Only for set 3 (NTCP range 0.09–0.80) and set 2 (NTCP range 0.54–0.98), with small margins, low NTCP values could be achieved using the data of Eisbruch *et al.* (1999). The range calculated for set 1 was 0.90–1.00.

For each margin, the PTVs are overlapping the parotid glands. The result is that a smaller part of the parotid gland (table 4.4) could be spared during the optimization process when the margin was increased. The volume of the parotid gland overlapped by the PTVs, relative to its original volume (relative overlapping volume) correlated linearly with the mean dose (Fig. 4.6). The data were fitted by linear regression. When the relative overlapping volume of the parotid glands in-

Table 4.4: The volume [cm³] of the parotid glands (I = ipsilateral, C = contralateral) that is not overlapping the PTVs for 0, 3, 6, 9 mm margin between the CTV and the PTV.

	patient A		patient B		patient C	
	I	C	I	C	I	C
margin 0	27.4	31	26.1	22.4	25.6	25.4
margin 3	25.5	29.8	24.8	21.1	22.8	22.6
margin 6	23.1	27.5	22.5	18.3	19.4	19.2
margin 9	20.4	24.9	19.9	15.5	16.1	16.0

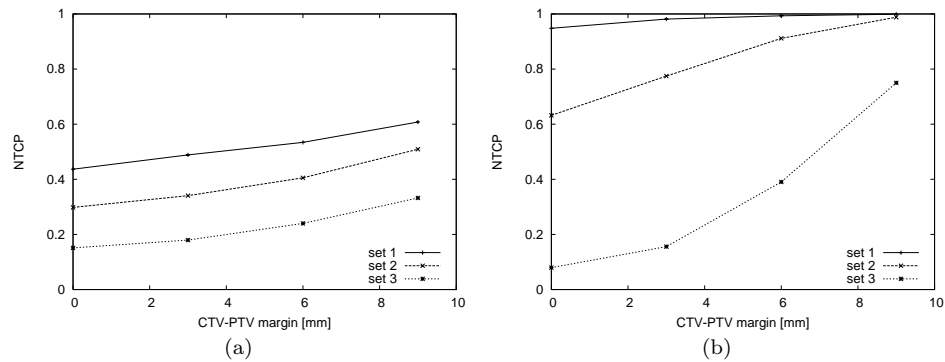


Figure 4.5: The correlation between the NTCP and the margin applied to the CTV calculated for 3 dose constrain sets using the data of Roesink *et al.* (2001) (a) and Eisbruch *et al.* (1999) (b). Data of Fig. 4.4 are used.

creased by 10 %, the mean dose to the parotid glands increased by approximately 3.5 Gy.

4.4 Discussion

In this work, the influence of the margins applied to the CTV on the dose to the parotid gland for the treatment of oropharyngeal cancer was quantified. As expected the mean dose to the parotid glands increased when the margin between the CTV and the PTV was enlarged. The parotid gland will, however, receive a substantial dose even for very small margins, since it is located adjacent to the lymph node containing region level II. The correlation between the mean dose and the margin was approximately linear, with a slope of $1.3 \frac{\text{Gy}}{\text{mm}}$, i.e. enlarging

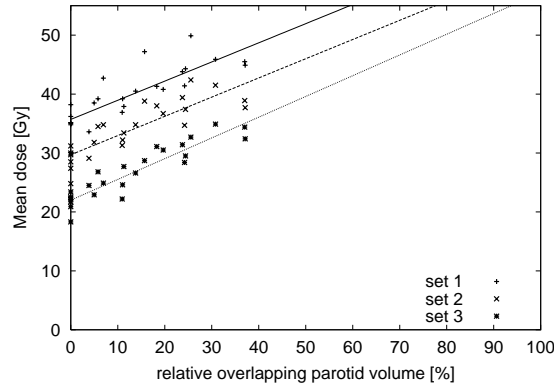


Figure 4.6: The correlation between the mean parotid gland dose and the relative overlapping volume of the parotid gland, i.e. the volume that is overlapping the PTV, for 3 dose constrain sets. The data are fitted by linear regression ($y = ax + b$): $y_{set1} = 0.33x + 35.7$ ($r = 0.66$, dashed line), $y_{set2} = 0.33x + 29.7$ ($r = 0.72$, solid line) and $y_{set3} = 0.35x + 20.0$ ($r = 0.84$, dotted line)

the CTV-PTV margin with 1 mm results in an increment of the mean dose to the parotid gland of approximately 1.3 Gy. Consequently, the NTCP decreased for smaller margins. Decreasing for example the margin from 6 to 3 mm, without compromising the homogeneity of the dose distribution in the lymph nodes, results in a reduction of 20 % in NTCP, showing the benefit of reducing the margins. The dose distribution has been analyzed for three different dose constrain sets, resulting in: an optimal dose distribution in the PTV (set 1), optimal dose distribution in the PTV while sparing the parotid gland (set 2) and more parotid gland sparing but at the expense of the dose homogeneity (set 3). Using set 2 instead of 1, it is possible to reduce the dose to the parotid gland while the dose distribution to the PTVs remains the same. Using set 3 it is possible to reduce the dose to the parotid glands further, but part of the lymph node containing regions received a lower dose compared to the calculations for set 1 and 2 (Fig. 4.3). This was the case for all margins used. Although the NTCP could be decreased substantially, for example for a fixed margin of 6 mm and using set 3 instead of set 2 the NTCP was reduced from 0.44 to 0.28, these low dose regions might cause a lower TCP for the lymph node containing regions. Using set 3 instead of set 2 might thus have clinical consequences, not only for the NTCP but also for the TCP. When reducing the dose to an OAR, the dose distribution within the target volumes should be carefully monitored. It should therefore be investigated whether these

low dose regions in the elective PTV are of high risk regarding local failure, before dose reduction to the parotid glands using set 3 can be applied.

The mean volume of the parotid glands was 26.3 cm³ (range 22.4–31.0 cm³), which is comparable to the mean value of 26.4 cm³ (range 12.9–46.4 cm³) reported in literature (Roesink *et al.*, 2000). Consequently, in this work no extreme volumes of the parotid gland were studied. More extreme volumes of the parotid glands or parotid glands which are located more caudal or cranial, probably show a similar dependency of the mean dose on the margin. Since the mean dose depends on the relative overlapping volume of the parotid gland, it might be different for a specific margin. The mean dose of a more caudal located gland will be larger than a more cranial situated gland.

The relation between the NTCP, calculated using data of Roesink *et al.* (2001), and the margin is approximately linear (Fig. 4.5 a). This can be explained by the fact that the slope of the NTCP curve is relatively smooth. The NTCP curve of Eisbruch *et al.* (1998) is, however, steeper and has a lower TD₅₀ (28.4 Gy) compared to the data of Roesink *et al.* (2001). Therefore, the NTCP will increase faster with increasing dose compared to the NTCP values calculated for the data of Roesink *et al.* (2001).

The choice of a higher resolution of the fluence matrix might improve the steepness of the dose gradient between the parotid glands and the PTVs and therefore reduce the dose to the parotid glands. This will be investigated in the near future. However, since the parotid glands are adjacent to the lymph node containing region, it is anticipated that they will still receive a substantial dose.

The use of less than seven beams for the IMRT treatment might reduce the complexity of the IMRT plans. Less beams might however result, in less homogeneity in the target volumes. Since the number of beams was not a optimization parameter in this paper, a number of beams was chosen with acceptable dose homogeneity in the target volumes. A detailed investigation of the effect of the number of beams on the dose distribution will be reported in the near future.

Accurate delineation of the target volumes is important when using IMRT, since the target volumes and OARs are adjacent to each other and a high dose is delivered to the target volumes. In this study we used CT images for the delineations of the volumes. Other imaging modalities such as Magnetic Resonance Imaging (MRI) might improve the delineation of various structures. MRI has, however, the disadvantage of lack of electron density information, which is important for an accurate treatment planning. In order to improve the delineation process CT-MRI matching (Rasch *et al.*, 1997) might be used, since this allows the simultaneous use of both image modalities.

With the currently available positioning equipment it is possible to achieve a standard deviation of the systematic and the random error of 2 mm or less for head and neck treatment techniques (Hurkmans *et al.*, 2001b; De Boer *et al.*, 2001). With the use of correction protocols, the systematic error can be reduced to 1 mm

(De Boer *et al.*, 2001). Although it is often mentioned that accurate patient positioning during the treatment sessions is of crucial importance, margins which take into account the systematic and random errors, are not always explicitly stated in literature. For head and neck cases van Dieren *et al.* (2000), Eisbruch *et al.* (1998) and Hunt *et al.* (2001) used a margin 5 , 5 and 10 mm respectively. Using our conventional position verification tools, where anatomical structures are matched using portal images, a margin of 6 mm will be used for head and neck patients. In order to reduce the margin, and thus reduce the dose to the parotid glands, the patient position has to be more accurate. Using stereotactic immobilization systems instead of the conventionally used head masks might improve the positioning accuracy during the treatment. Stereotactic immobilization systems are however usually patient unfriendly. Using dental casts the immobilization might also be improved, this type of immobilization can however not be used for all patients. At our department implanted gold markers (Nederveen *et al.*, 2000, 2001a) are used for daily position verification of the prostate and will eventually be used for online position verification. The same approach will be used for the position verification for head and neck cases. The advantage of the use of markers compared to the matching of anatomical structures is that the automatic detection of the gold markers is accurate and fast. Especially for complex IMRT plans with seven different beam angles, matching of anatomical structures will be more difficult compared to the position verification using gold markers. Two orthogonal fields might be added for position verification purposes. The adding of extra fields for position verification is however in contradiction with the use of IMRT. Using the gold markers for position verification it might be possible to reduce the margin to 3 mm. As has been shown in this study this may result in a NTCP reduction of approximately 20 %.

4.5 Conclusion

The mean dose to the parotid gland decreased when smaller margins are applied to the CTV for the IMRT treatment of the oropharynx. Reducing the margin with 1 mm results in an decrease of the mean parotid dose by approximately 1.3 Gy. Therefore, more accurate patient positioning, resulting in smaller margins, results in a lower NTCP for xerostomia.

For a fixed margin the dose to the parotid glands can be reduced, using a more optimal dose constraint set for the parotid glands. The parotid glands, however, will receive a substantial dose and eventually a compromise has to be made between the dose in the lymph node containing region and the dose to the parotid gland.

Chapter 5

Implanted gold markers for position verification during irradiation of head-and-neck cancers: a feasibility study

This chapter has been submitted for publication as
Bram van Asselen, Homan Dehnad, Cornelis P.J. Raaijmakers, Jan J.W. Lagendijk, and Chris H.J. Terhaard 2003 Implanted gold markers for position verification during irradiation of head-and-neck cancers: a feasibility study *International Journal of Radiation Oncology Biology Physics*

Abstract

Purpose: To assess the toxicity and reliability of the use of implanted gold markers for position verification during the irradiation of head-and-neck cancer.

Methods and Materials: Ten patients with localized head-and-neck tumors received two gold markers in the parapharyngeal region. The acute and late radiation related toxicity were scored prospectively, using common toxicity criteria. The patients were immobilized during irradiation using a five-point mask. The marker location was detected in portal images taken with an a-Si flat panel imager. The intermarker distance as well as the interfraction motion of the markers was determined for all patients.

Results: No acute major complications were observed. The acute toxicity grade was not larger than normally detected. The markers were visible in all images. A small time trend was observed in the intermarker distance for three patients. For these patients at least one marker was located in the mucosa or pharyngeal constrictor muscle. Deeper seated gold markers did not show a time trend in intermarker distance. The random positioning uncertainty determined using the markers was on average 1.1 and 1.4 mm (1 standard deviation) in the caudal-cranial and anterior-posterior direction respectively.

Conclusion: The use of implanted gold markers for position verification during radiotherapy of head-and-neck patients seems safe and feasible. To avoid any chance of migration, markers should be placed in deep muscular compartments.

5.1 Introduction

In order to reduce geometric uncertainties during the treatment, patients treated for head-and-neck cancer are usually immobilized using a mask. For position verification purposes, portal images can be taken during the treatment fractions using an electronic portal imaging device (EPID) or mega-voltage films. Usually portal images are taken of lateral and anterior-posterior fields. The internal bony structures visible within the portal image are then aligned with those in the reference image (De Boer *et al.*, 2001; Gilbeau *et al.*, 2001; Hurkmans *et al.*, 2001b). Random and systematic errors of approximately 2 mm (1 standard deviation) have been reported (De Boer *et al.*, 2001; Gilbeau *et al.*, 2001; Hurkmans *et al.*, 2001b). A disadvantage of this procedure is that the delineation and matching of bony structures is relatively time consuming. Furthermore, the projection of bony structures can sometimes be difficult to interpret, especially when these structures are rotated relative to the reference position and/or the field size is relatively small.

Instead of using anatomical landmarks, implanted gold markers can be used for position verification (Crook *et al.*, 1995; Vigneault *et al.*, 1997; Alasti *et al.*, 2001; Shirato *et al.*, 2000; Litzenberg *et al.*, 2002; Dehnad *et al.*, 2003). These markers should not be too large, because large markers can result in more tissue damage. The markers should, however, be large enough to be visible in a portal image taken with an EPID. Using an a-Si flat-panel imager it is possible to visualize markers, which have a size, a diameter of 1.0 mm and length of 5 mm, which is clinically acceptable (Nederveen *et al.*, 2001a). Although this approach is invasive, it has several advantages. The markers can be detected easily within a portal image made with 1-2 monitor units (MU; Nederveen *et al.* (2001a)) and the determination of the three-dimensional coordinates of a marker is straightforward. Furthermore the detection of the markers can be automated more easily. These advantages make it possible to use marker-based position verification for daily on-line position corrections. The use of markers instead of bony structures might also be useful when applying IMRT, using multiple field angles and small segments.

The use of gold markers for positioning verification has been reported mainly for the irradiation of the prostate and organs within the thorax or upper abdomen (Crook *et al.*, 1995; Vigneault *et al.*, 1997; Dawson *et al.*, 2000b; Nederveen *et al.*, 2001a; Alasti *et al.*, 2001; Litzenberg *et al.*, 2002; Shirato *et al.*, 2000). Murphy *et al.* (2000), used implanted markers for radiosurgery for the spine and pancreas. In a study of Gall and Verhey (1993), the use of implanted radiopaque fiducial markers was tested using a skull phantom. Although it was mentioned that the technique was implemented for positioning patients for proton beam therapy, results of positioning accuracy in clinical practice have not been reported.

It was the purpose of this work, to investigate the use of implanted gold markers for position verification during radiotherapy of head-and-neck cancer, and particularly the toxicity and reliability of this marker-based position verification. For

Table 5.1: The original tumor site and TNM classification of the tumor, the prescribe dose and the CTC score, for radiation mucositis, direct after radiotherapy (t=0) and 8 weeks after radiotherapy (t=8).

Patient	Tumor site	TNM stage	Presr. Dose	CTC	
				t=0	t=8
1	unknown primary	$T_xN_{2c}M_0$	50	2	0
2	glottis larynx	$T_{2a}N_0M_0$	70	3	0
3	larynx	$T_{2a}N_0M_0$	70	3	0
4	tonsil	$T_3N_{2b}M_0$	66	3	1
5	nasopharynx	$T_1N_2M_x$	70	3	0
6	larynx	$T_1N_0M_0$	70	2	0
7	supraglottis larynx	$T_4N_0M_0$	66	2	0
8	oropharynx	$T_2N_xM_0$	69.5*	3	1
9	larynx	$T_0pN_{2b}M_0$	70	2	0
10	nasopharynx	$T_4N_2M_x$	-	-	-

*accelerated fractionation scheme

this purpose, markers were implanted in ten patients treated with conventional radiotherapy. Their position was monitored during the treatment of these patients using an a-Si flat panel imager.

5.2 Methods and materials

5.2.1 Patients

Ten patients with localized head-and-neck tumors (Table 5.1) received 2 fiducial markers (Nederveen *et al.*, 2001a). One patient refused radiotherapy after implantation. Nine patients received 3-D conformal radiotherapy. For one of those patients the treatment course was combined with chemotherapy. Patients were treated with isocentric multi-field techniques including 6 MV lateral wedged beams. Customized blocks or MLC were used to match the field shape to the target in beams-eye-view. A five-points thermoplastic mask (PR5, Sinmed Radiotherapy Products, Reeuwijk, The Netherlands) was used to immobilize the patient.

5.2.2 Marker implantation

The use of radiopaque markers for position verification during radiotherapy, has been investigated for treatment of the prostate in our institute (Dehnad *et al.*,

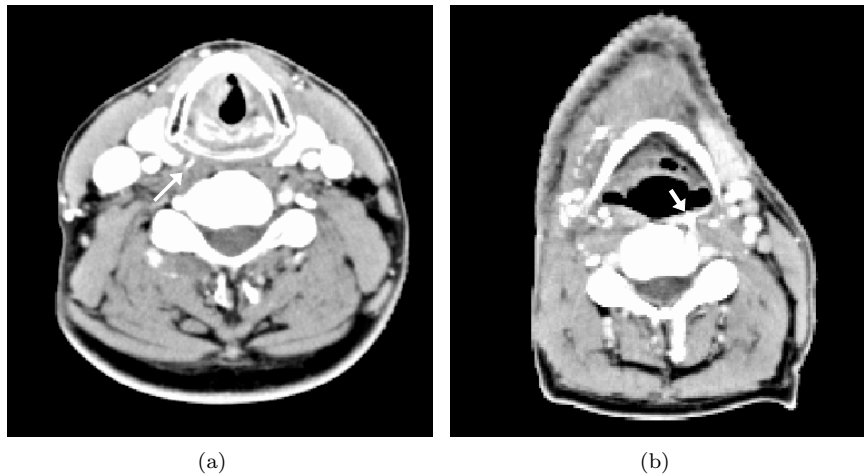


Figure 5.1: A transversal slice of CT scan of two patients with implanted gold markers. For one patient the marker is located in deep muscle compartments (a). For an other patient the marker is located superficially (b). In order to prevent artifacts, the transversal slices are shown imaging the tip of the markers.

2003). The radiopaque markers consist of a gold rod (1.0 mm diameter, 5 mm length). The same markers have been used for this study. The markers were implanted in all patients under general anesthesia while undergoing their work up panendoscopy. The implantation of the markers took approximately 5 min. An Iodine-implantation needle with a homemade stopper was used to implant the markers in the parapharyngeal region (Fig. 5.1). This stopper could be fixed to the needle at any point from its sharp end to define the insertion depth. The diagnostic CT scan was used as a guide for the implantation. The stopper was placed 5 to 8 mm from its sharp end. For one patient the markers were placed deeper, namely 40 mm. The patients did not receive prophylactic antibiotic.

5.2.3 Toxicity

All patients were asked to inform the physician as soon as they noticed the following symptoms: fever, chills, intractable throat pain and bleeding. The acute and late radiation related head-and-neck toxicity, radiation induced mucositis, were scored in each patient prospectively, using Common Toxicity Criteria (National Cancer Institute, 1999).

5.2.4 Portal imaging

The portal images of all treatments fields were made with an a-Si flat-panel imager (*iView GT*, Elekta Oncology Systems, Crawley, UK). The imaging area of the panel is $26 \times 26 \text{ cm}^2$ at the isocenter, with a spatial resolution of 0.25 mm. The imager is mounted on the gantry of a linac (SLi20, Elekta Oncology Systems, Crawley, UK).

For each patient, the beam setup contained lateral beams for the first part of the treatment (25 fractions). In order to compare the data of all patients, images were taken during these fractions. On average, images were taken during 19 fractions (range 10–25) for each patient. For patient 9, only 10 fraction were obtained. In total, images were recorded during 173 treatment fractions. For each gantry angle an image was taken of at least 100 MU, which was used for inter-fraction motions analysis. High frequency intrafraction motions (van Asselen *et al.*, 2003) are consequently not influencing the data.

When marker-based position verification is used during an IMRT treatment, the markers should be visible in images taken with a few monitor units. Images were also taken with a small number of MU (approximately 4 MU).

The marker location in the portal images were detected using software developed at our institution. This software is currently used for position verification during the treatment of the prostate and is capable of automatic detection of the markers (Nederveen *et al.*, 2001a; Dehnad *et al.*, 2003). It is, however, also possible to localize the markers manually. The reproducibility of the marker detection was approximately 0.2 mm (1 standard deviation), which was determined from repeated analysis.

5.2.5 Marker migration

In order to achieve a high accuracy in position verification, the position of the marker should not change relative to the surrounding tissue during radiotherapy. For that reason markers should better not be implanted inside the tumor, which might show regression during the treatment. This will result in displacement of the markers relative to the anatomy of the patient.

The inter-marker distance can be used as an indicator for marker migration. Since for all patients the lateral beams were used, the three-dimensional inter-marker distances could not be determined. Instead, the projected inter-marker distance is used to investigate the migration of the markers.

5.2.6 Rotations

The three dimensional coordinates of the markers could not be determined, since only lateral beams were used. Therefore rotations could not be detected. Rotations,

however, might cause changes in the projection of the inter-marker distance. In order to estimate the effect of rotations on the inter-marker distance we simulated rotations. After the patients underwent computer tomography (CT), the coordinates of the markers were determined. The influence of rotation on the projected inter-marker distance was determined using the spine as rotation axis.

5.2.7 Interfraction motion

The center of gravity of the position of both markers was determined for each fraction in the lateral fields for all patients. The center of gravity is used in further analysis of the setup errors. The displacements were calculated relative to the reference positions of the patients, which was the position of the markers in the patient during the localization procedure of the treatment. Although the number of patients is small for this feasibility study the mean systematic error (M), the standard deviation of the systematic errors (Σ) and the mean of the standard deviation of the random error (σ) were calculated.

To investigate the effect of position verification, an off-line position correction was performed using a shrinking action level protocol (Bel *et al.*, 1993). The running average of the displacements was therefore calculated over the last number of N_{max} fractions. A correction is applied when this average exceeds a certain action level. This action level shrinks when more fractions are delivered without corrections. After correction, the action level is set to the initial value (α). The corrections were performed for each direction separately. The correction parameters were $N_{max} = 4$ and $\alpha = 4$ mm.

In six patients, sufficient bony structures were visible in the portal images. For these patients, the correlation between the position of the markers and the bony structures was investigated using the portal images of 10 fractions per patient. The bony structures, as well as the marker location was therefore determined, using the iView-GT software.

5.3 Results

5.3.1 Marker detection

Using the a-Si flat-panel imager it was possible to obtain high quality portal images of the head-and-neck region during the treatment. In all images, the location of the markers could be determined. In order to test the visibility of the markers, images were taken with low monitor unit exposure. Even in images obtained with 4 MU, the markers were clearly visible (Fig. 5.2).



Figure 5.2: A portal image taken with approximately 4 monitor units. The location of the markers is indicated with two arrows.

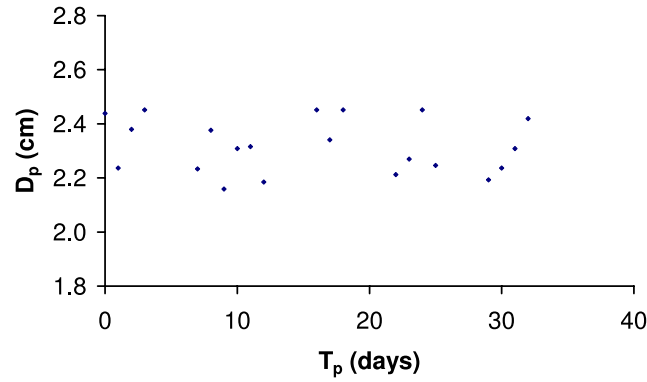
5.3.2 Toxicity

We observed no acute major complications such as pain, bleeding or infection by gold seed implantation. No rejection reaction by the seeds was observed and there was no loss of seeds. The acute head-and-neck toxicity grade (Table 5.1) did not differ from the expected aspects in head-and-neck tumors. At the follow up examination there was no sign of foreign body reaction at the implantation site.

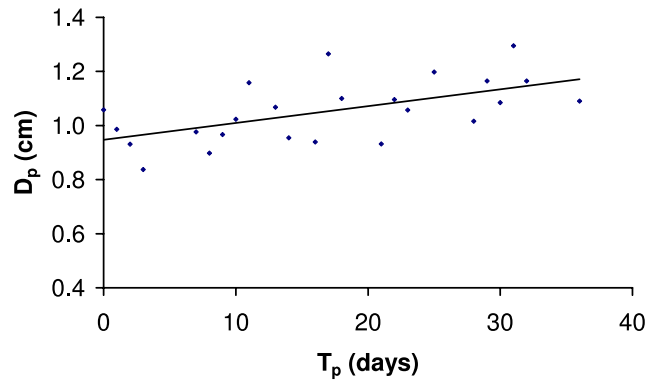
5.3.3 Marker migration

The projected inter-marker distances were calculated for each patient for all recorded fractions. This resulted in nine lists of distances, on average consisting of 19 distances (range 10–24). A relatively small variation was observed in the projected inter-marker distances (Fig. 5.3). The average standard deviation of the projected inter-marker distance was 0.8 mm.

A linear regression analysis was performed to investigate migration of the markers. The data of six patients did not show a significant change in the projected inter-marker distances (Fig. 5.3). For three patients, however, a correlation was determined with a correlation coefficient (r) of 0.58, 0.67, and 0.66 for patient 3, 4 and 5 respectively. In these cases the projected inter-marker distance increased during the treatment (Fig. 5.3 and Fig. 5.4). The magnitude of the increase was 0.06, 0.05 and 0.07 mm/day for patient 3, 4 and 5 respectively. For the overall



(a)



(b)

Figure 5.3: The observed projected inter-marker distance (D_p) during the treatment (T_p) of a patient without time trend in inter-marker distance (a) and a patient with a time trend (b).

treatment time of 30 days this would result in an increase of approximately 1.8 mm. The increase was mainly in the caudal-cranial direction. To evaluate the migration of the seeds, the parapharyngeal region was delineated in all CT scans. Migration occurred, when at least one of the markers was implanted superficially in the mucosa or pharyngeal constrictor muscle (Fig.5.5). No migration was determined for markers implanted in deeper muscle compartments, such as the longus capitis, longus colli and scalene group (Fig. 5.5).

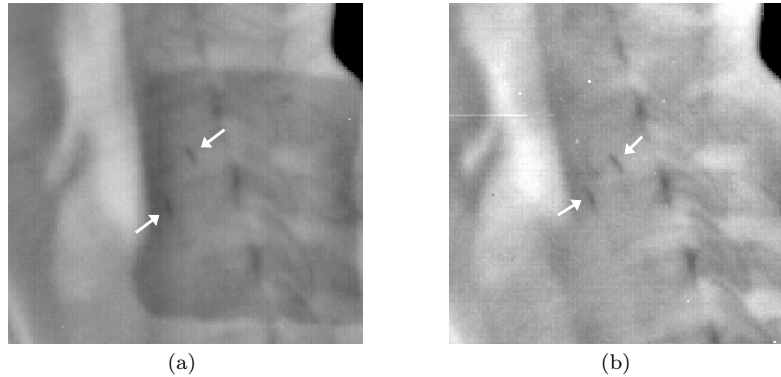


Figure 5.4: Two portal images of the same patient showing the situation with maximum projected inter marker distance (a) and minimum projected inter marker distance (b). The location of the markers is indicated with two arrows.

5.3.4 Rotation

The rotations were simulated using the coordinates determined from the CT-scan. For rotations of 5 degrees, with the spine as rotation axes, the projected inter-marker distance could change up to 2.6 mm. On average, however, a rotation of 5 degrees resulted in changes in inter-marker distances of 0.9 mm (range 0.01 - 2.60 mm).

5.3.5 Interfraction motion

For each marker, the displacement relative to the marker in the reference image was calculated. An example of the position of two markers relative to the reference image is shown in figure 5.6. In order to determine the interfraction motions, the center of gravity of both markers was calculated for each fraction and for all patients. The markers of patient 3, 4 and 5 were included, because the marker migration was relatively small and the center of gravity is less sensitive to time trends. The values of the mean systematic error (M), the standard deviation of all systematic errors (Σ) and the mean of the standard deviations of the random error (σ) are similar for both directions (Table 5.2). The systematic error of patient 7 was large, and amounted to 4.4 mm and 3.8 mm in the AP and CC direction, respectively.

Using the shrinking action level protocol for corrections of the patient position, the standard deviation of the systematic errors decreased substantially (Table 5.2). The average number of corrections was 0.7 in the anterior-posterior direction and

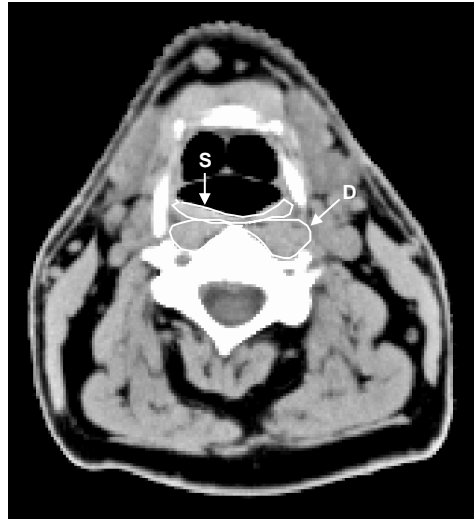


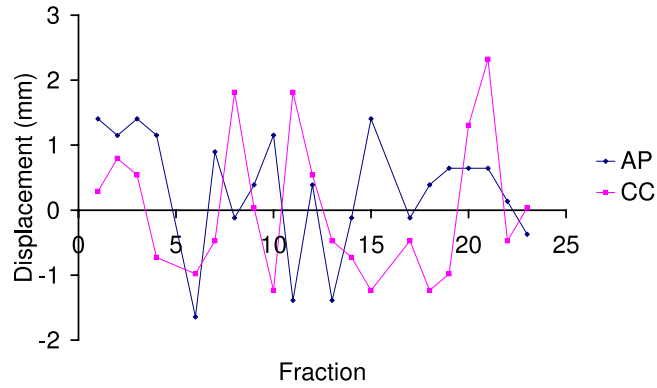
Figure 5.5: The location of the implanted markers was divided in two compartments, which are delineated in a CT image. The superficial compartment (S) containing the mucosa of pharyngeal constrictor muscle, and deeper muscle compartments (D), such as the longus capitis, longus colli and scalene group.

0.8 in the caudal-cranial direction per patient.

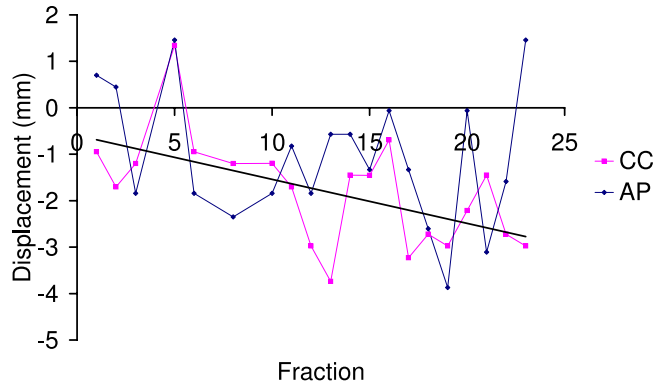
For six patients, the correlation between the location of the bony structures and the marker location was investigated. On average, the correlation coefficient was 0.81 (range 0.71–0.97) in the anterior-posterior direction for both markers. For the caudal-cranial the average correlation coefficient was 0.70 (range 0.24–0.95). Especially for patient 5, the correlation was poor. The same patient showed a time trend in the projected inter-marker distance.

5.4 Discussion

In this study, position verification using implanted gold markers was investigated for head-and-neck radiotherapy. Gold markers were implanted in the parapharyngeal region. No acute major complications were observed after implantation. The markers did not induce any additional toxicity. We therefore conclude that the implantation of markers for position verification during the treatment of head-and-neck cancer is a clinically safe procedure.



(a)



(b)

Figure 5.6: The displacements of a marker relative to the reference position for the caudal-cranial (CC) and the anterior-posterior (AP) direction for a fixed marker (b) and a marker showing migration (b).

The projected inter-marker distance differed from day to day, with a standard deviation of 0.8 mm, which is the result of detection accuracy, setup uncertainties and migration. Besides rotations, random displacements of the patient can also cause slight changes in the projected inter-marker distances. Small rotations of 5 degrees around the spine may have caused differences in inter-marker distances of approximately 1 mm. For six patients, no significant change in the projected inter-marker distance during the treatment was observed, indicating that

Table 5.2: The mean systematic error (M), the standard deviation of the systematic errors (Σ) and the mean of the standard deviations of the random error (σ) of 9 patients without corrections and using a shrinking action level (SAL) protocol for position corrections.

	No correction		SAL	
	AP (mm)	CC (mm)	AP (mm)	CC (mm)
M	-0.5	0.0	0.0	0.2
Σ	1.6	1.9	0.5	0.6
σ	1.4	1.1	1.5	1.5

the marker position did not change systematically relative to the surrounding patient anatomy. Another indication that the marker position did not change is that the determined random error was relatively small, on average 1.1 and 1.4 mm in the caudal-cranial and anterior-posterior direction, respectively. Three patients showed a small increase in the projected inter-marker distance during the treatment. For each of these three patients, at least one marker was implanted superficially in the pharyngeal mucosa or pharyngeal constrictor muscle. Radiation induced inflammation of the mucosa might be an explanation for this increase, since the epithelial component of the mucosa is prone to radiation induced inflammation. The correlation between this effect and the grade of mucositis was, however, not studied. Any swelling resulting from the acute reaction could increase the inter-marker distance. Therefore to avoid any chance of migration, markers should be implanted deep in the muscular compartment which is not prone to this phenomenon.

The random and systematic errors determined in this study were relatively small, an amounted to 1-2 mm. The number of patients is, however, small and data of more patients are needed to more accurately determine the setup errors. In a review of Hurkmans *et al.* (2001b) random and systematic errors of respectively 1.6-4.6 and 1.1-2.5 mm (1 standard deviation) were reported for patient with head-and-neck cancer. With the currently available equipment, a standard deviation of 2 mm for both random and systematic error can be considered good clinical practice (Hurkmans *et al.*, 2001b). Bel *et al.* (1995) used metal markers placed in a wax mold of the outer ear for position verification. These were only used during portal imaging in order to prevent radiation damage to the outer ear, approximately 8 fractions were imaged per patient. The treatments fields had to be adjusted to visualize the markers. The standard deviations, averaged over the three directions, were equal to 1.8 and 1.4 mm for the distributions of the systematic and random deviations, respectively (Bel *et al.*, 1995). The reported random and systematic errors are similar to our results.

The shrinking action level protocol (Maes *et al.*, 2002) used in this paper, was also applied by De Boer *et al.* (2001) to their positioning verification data determined for head-and-neck irradiation. Using a value of 2 for N_{max} and an α of 4 mm their observed systematic error reduced to 1 mm.

For some patients no bony structures are included in the treatment fields. In the presented study, bony structures were not visible in the portal images of three patients. For these treatment fields implanted markers could improve the treatment, since without them, position verification is hardly possible. For the treatment fields including bony structures, the correlation between the marker location and location of these bony structures was determined. In general the correlation was good, especially in the anterior-posterior direction. For one patient the correlation was poor. The same patient also showed a time trend in inter-marker distances, indicating that at least one marker is loosely attached to the surrounding anatomy. The markers and bony structures are not located at the same position in the patient. Projections of the markers and bony structures will be differently affected by small rotations or displacements of the patient. For bony structures this can result in small deformations compared to the projection on the reference image, which results in less accurate position verification. In further studies the lateral displacement should also be determined to exclude errors due to rotations.

The projection of the bony structures can be difficult to interpret when an arbitrary gantry angle is used, especially when the field size is relatively small. Extra fields could be added for position verification purposes. This will however result in an extra dose to the surrounding tissue, thereby creating a less conformal dose distribution. Another approach to solve the problem of small fields, might be that the portal images of each individual segments are added to obtain a larger area which can be used for positioning verification (Fielding *et al.*, 2002). The use of markers instead of bony structures, however, makes the matching procedure less complicated. Due to their high visibility and because the calculation of the three-dimensional coordinates is straightforward, the detection of markers in small segments for arbitrary gantry angles is relatively easy, and might therefore be useful when using, for example, IMRT. The positioning verification procedure will take little time, what makes it also suitable for on-line position verification.

5.5 Conclusion

The implantation of the gold markers did not result in increased toxicity for the patient and the markers could be easily detected in all portal images. When the gold seeds are not placed superficially, but in deeper muscular compartments such as the longus capitis, longus colli and scalene group, their location did not change

relative to the patient anatomy. The use of gold markers for position verification for head-and-neck tumors seems feasible.

Chapter 6

Intrafraction motions of the larynx during radiotherapy

This chapter has been published as

B. van Asselen, C.P.J. Raaijmakers, J.J.W. Lagendijk, C.H.J. Terhaard 2002 Intrafraction motions of the larynx during radiotherapy *International Journal of Radiation Oncology Biology Physics* **56** 384–390

Abstract

Purpose: To quantify the intrafraction motions of the larynx during radiotherapy of laryngeal cancer. Depending on the magnitude, duration and incidence, these motions may have clinical consequences for the choice of margins around the clinical target volume.

Methods and Materials: The intrafraction motions were analyzed for 10 patients, treated in 33 or 35 fractions. The intrafraction motions of the larynx were visualized using an a-Si flat panel imager. Images were obtained every 200 ms, resulting in a movie of images for each beam. In addition to visual analysis of all movies, the tip of the epiglottis was delineated and used as a landmark, the coordinates of which were followed in time.

Results: Movies were obtained during 79% of the total number of radiotherapy fractions. The total duration of swallowing was on average 0.45% (range 0.0 – 1.5) of the total irradiation time. Deviations of motions other than swallowing, ranged between 0.3 and 11.5 mm. Some of these motions were more sudden, and others were probably related to breathing, because the frequency of these motions was 8 – 20 per minute.

Conclusion: The incidence and total duration of swallowing is low. Therefore, it is not necessary to apply an internal margin to take into account these displacements. Other motions, however, occur more often. In 95% of the irradiation time the tip of the epiglottis moves within a range of 7.1 mm. A margin should be applied to the clinical target volume to take into account these motions.

6.1 Introduction

During the irradiation of laryngeal cancer, patients are usually immobilized using masks to reduce geometric uncertainties during treatment. These uncertainties are caused by setup errors and organ motion and are taken into account by applying, respectively, a setup margin and an internal margin (International Commission on Radiation Units and Measurements (ICRU), 1999) to the clinical target volume (CTV) on the basis of the magnitude of the deviations. The setup uncertainties for head-and-neck cancer have been determined in several studies (Hurkmans *et al.*, 2001b; De Boer *et al.*, 2001). Intrafraction organ motions are mainly studied for the prostate and organs within the thorax and upper abdomen (Nederveen *et al.*, 2002; Langen and Jones, 2001; Jaffray *et al.*, 1999). The larynx is also a rather mobile organ, and motion may occur from swallowing, breathing, or movement of the tongue. Using videofluoroscopy to study liquid bolus swallows, deviations of the larynx of 20–25 mm in the caudal-cranial direction and 3–8 mm in the anterior-posterior direction were reported (Dantas *et al.*, 1990; Jacob *et al.*, 1989; Leonard *et al.*, 2000). The duration of swallowing for normal subjects is approximately 1 s (Kendall *et al.*, 2000; Hamlet *et al.*, 1993). Although for head-and-neck cancer patients the swallowing function is worse compared with normal subjects (Pauloski *et al.*, 2000; Stenson *et al.*, 2000), the swallowing time is still small compared with the total irradiation time. Consequently, the incidence of swallowing is important. In addition to motion due to swallowing, other motion might occur during irradiation. Because both the larynx and the base of the tongue are attached to the hyoid bone, tongue movement may result in displacement of the larynx. Inspiration and expiration also causes displacement of the larynx. The displacement is small during normal breathing and large during large inspiratory effort. Depending on the magnitude, duration, and incidence, these motions contribute to the internal margin, which is applied to the CTV.

Only recently, have techniques become available that can be used to detect internal motion. Consequently no data are available about the intrafraction motion of the larynx. Using an a-Si flat panel imager (Nederveen *et al.*, 2002) it is, however, currently possible to visualize internal structures using a few monitor units (MU) and observe and quantify intrafraction motion.

It was the purpose of this work to quantify the magnitude, duration and incidence of laryngeal intrafraction motion during radiotherapy of laryngeal tumors. A better understanding of these motions may lead to optimized treatment margins.

6.2 Methods and materials

6.2.1 Patients

The intrafraction motion of the larynx was analyzed for 10 patients with varying stages of laryngeal cancer (Table 6.1). All patients were treated with two lateral 6-MV opposing wedged fields. For most patients, 70 Gy (2 Gy/fraction five times weekly) was prescribed at the isocenter. Three patients (Patients 5, 6 and 10; Table 6.1), received a dose of 66 Gy to the isocenter (2 Gy/fraction five times weekly). The treatment fields were reduced after 25 fractions.

Before the start of treatment, patients were instructed not to swallow during irradiation. A five-point thermoplastic mask (PR5, Sinmed Radiotherapy Products, Reeuwijk, The Netherlands) was used to immobilize the patient. The mask was fixated to the table at five positions, including positions near the shoulders.

Table 6.1: Original tumor site and TNM classification of tumor.

Patient.	Tumor site	TNM stage
1	Supra glottis	$T_1 N_x M_0$
2	glottis	$T_2 N_0 M_0$
3	glottis	$T_2 N_0 M_0$
	Supra glottis	$T_1 N_0 M_0$
4	Supra glottis	$T_2 N_0 M_0$
5	glottis	$T_{1a} N_0 M_0$
6	glottis	$T_{1b} N_0 M_0$
7	glottis	$T_2 N_0 M_0$
8	glottis	$T_2 N_0 M_0$
9	glottis	$T_2 N_0 M_0$
10	glottis	$T_{is} N_0 M_0$

6.2.2 Flat-panel imager

An a-Si flat-panel imager (RID 256-L, EG&G Heimann Optoelectronics, Wiesbaden, Germany) was used for imaging the larynx during delivery of radiation. The detector plate consists of 256×256 pixels, with a pixel pitch of $800 \mu\text{m}$, resulting in an imaging area of 20.48×20.48 cm. The imager was mounted on the gantry of the linear accelerator (SL25, Elekta Oncology Systems, Crawley, UK) with an in-house-made removable arm at a distance of 1.575 m from the focus of the beam. This results in an imaging area of 13×13 cm² at the isocenter and a spatial resolution of approximately 0.5 mm. For accurate measurements of the swallowing actions and other motions of the larynx, the panel operated with a frame time of 200 ms. Each frame was taken with 1 – 2 monitor units.

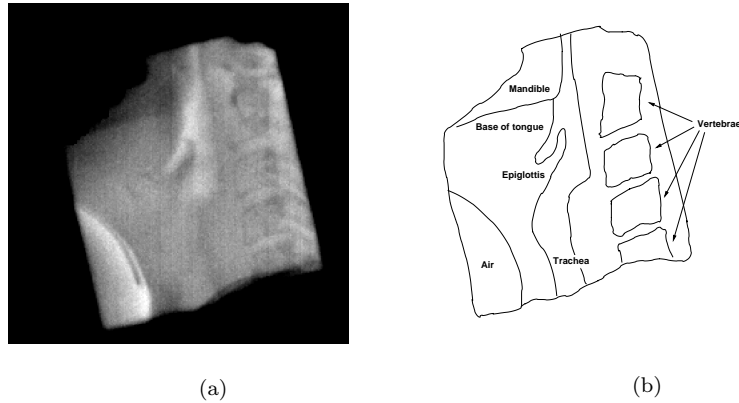


Figure 6.1: (a) Example of a single portal image taken with a frame time of 200 ms and (a) a schematic view of structures within portal image (a).

Between 25 and 30 fractions were imaged for each patient. In total, images were obtained during 272 of a total of 344 fractions, resulting in a >4.5-hour recorded irradiation time. It was not possible to obtain images for all fractions of patients, because the patients were not always treated on the linear accelerator on which the flat panel could be mounted. In each fraction, two movies were obtained. Each movie consisted of the consecutive frames (100 - 200 frames) obtained during the delivery of one treatment portal. Because of the high image quality it is possible to determine intra-fraction motions of several soft tissues, such as the epiglottis, base of tongue and arytenoid (Fig. 6.1). Because of the different size of the treatment fields for individual patients, not all soft tissues mentioned were incorporated within the treatment field for each patient.

6.2.3 Analysis of larynx motions

The incidence of swallowing was detected by visual inspection of all movies. To calculate the time of each swallowing action, a physician determined the start and end of the swallowing action. The structures are in the same positions at the start and end of the swallow, except for when the swallowing started before irradiation began or ended after irradiation stopped. In those cases, the start and end were the start and end points of the irradiation, respectively. The total time a patient was swallowing was a summation of the time of each swallowing action. By calculating the total recorded irradiation time of a patient, the percentage of time the patient was swallowing could be calculated. Furthermore, the incidence as a function of the treatment progress was determined. The treatment was therefore divided in

periods of five treatment fractions. For the 3 patients with 33 fractions, the last period included only three fractions.

To investigate the magnitude and duration of various motions, specific landmarks were delineated in each frame of a movie. The resulting list of consecutive coordinates of the landmark yielded two traces, one in the caudal-cranial direction and one in the anterior-posterior direction. The best defined landmark was the tip of the epiglottis (Fig. 6.1), for which the displacement could be determined in the anterior-posterior and the caudal-cranial direction. In the treatment fields of 6 of the 10 patients, the tip of the epiglottis was visible. For these patients, the tip of the epiglottis was delineated in 10 movies during the first 25 fractions. This analysis was done for movies containing no swallowing action to quantify the deviations of motion other than that caused by swallowing. The first 25 fractions were chosen, because the fields of the last 8-10 fractions were smaller and often did not include the complete epiglottis. For each fraction, the peak-to-peak value (i.e. the maximal displacement during one fraction) was calculated in both the anterior-posterior and the caudal-cranial direction (A_{100}). This value was also calculated for 95% of the points closest to the mean coordinate (A_{95}), that is, when 5 % of the points, with the largest deviation from the mean, were excluded. The magnitude of the motions for the other patients were determined by visual analysis.

6.3 Results

On average, movies were obtained during 79% of the total number of radiotherapy fractions for a patient. Bony anatomy and various soft tissues could be visualized in images of 1 – 2 monitor units (Fig. 6.1). In general, the quality of the images was good, and motion of the larynx could be visualized (Fig. 6.2). In addition to the swallowing actions, various other movements could be observed. There was a large discrepancy between the deviations and frequency of the larynx motion from patient to patient. For some patients, only small deviations were determined (<1 mm), and for others, large deviations were seen (≤ 11.5 mm). Also, large variations in the frequency of these deviations were observed.

The number of swallowing actions per patient, during the recorded irradiation time, ranged from 0 to 26 (Table 6.2). Eight patients, however, swallowed between 0 and 3 times. Not all swallowing actions were complete, some started before the beginning of irradiation and some ended after irradiation stopped. The time of a complete swallowing action differed (range 0.8 – 6.3 s). On average, the total duration of all swallowing actions was 0.45% (range 0.0 – 1.5 %) of the total irradiation time recorded for a patient (Table 6.2).

The incidence of swallowing was also determined as a function of the treatment progress. This analysis showed that most swallowing actions occurred during the first five fractions (Fig. 6.3).

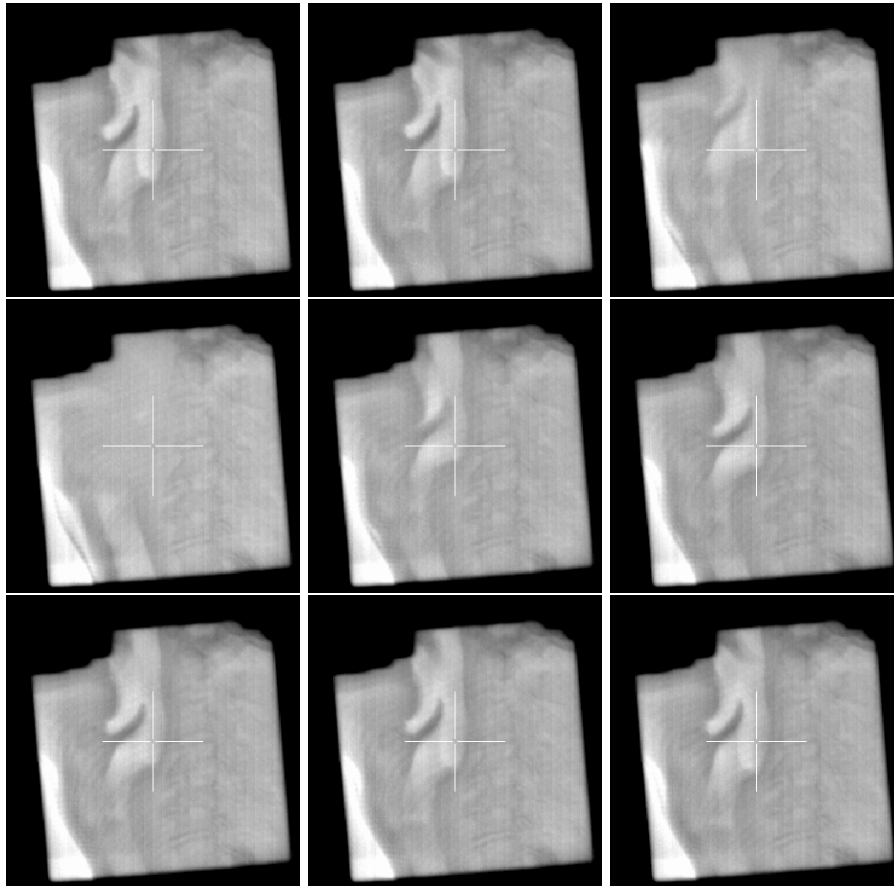


Figure 6.2: Example of a swallowing action. Each following line should be read from left to right. Images taken with a frame time of 0.2 s (1-2 monitor units). Every third image is shown, resulting in an interval time of 0.6 s between each image.

In figure 6.4, a trace with a swallowing action is shown. The maximal displacement during a swallowing action is difficult to determine, because at the point at which the deviations are the largest, it is difficult to distinguish between structures. At that phase, there is a lack of air between the base of tongue, epiglottis, arytenoid, and pharyngeal wall, resulting in less contrast in that area. During swallowing the displacements were >1 cm.

In 6 patients, the peak-to-peak values of the deviations of the tip of the epiglottis

Table 6.2: Total number of swallowing actions, (N_s), the total recorded irradiation time (T_{rec}), total time patient swallowed, (T_s) and ratio between the T_s and T_{rec} .

Patient	N_s^*	T_{rec} (s)	T_s (s)	$\frac{T_s}{T_{rec}} * 100$ (%)
1	1	1355.4	0.2	0.01
2	0	1727.6	-	0
3	3	1291.5	11.0	0.85
4	9	1517.6	22.6	1.49
5	3	1960.0	4.6	0.23
6	26	2154.6	28.4	1.32
7	0	1622.8	-	0
8	2	1416.2	6.0	0.42
9	0	1566.0	-	0
10	3	1710.6	3.4	0.20

* complete and incomplete swallowing actions

Table 6.3: Peak-to-peak value of deviations of tip of epiglottis averaged from 10 movies and range for cranial-caudal direction and anterior-posterior direction for 6 patients.

Pat	AP(mm)		CC(mm)	
	A ₉₅	A ₁₀₀	A ₉₅	A ₁₀₀
1	0.9(0.5 - 1.4)	1.8(0.7 - 5.4)	0.8(0.3 - 1.2)	1.2(0.5 - 2.5)
2	1.2(0.6 - 2.1)	1.9(0.9 - 3.1)	1.8(0.6 - 3.5)	2.2(0.8 - 4.3)
3	3.0(1.4 - 4.7)	3.6(2.2 - 5.1)	4.2(1.4 - 6.8)	5.1(1.9 - 7.6)
4	2.8(1.9 - 4.6)	3.6(2.5 - 5.6)	2.5(1.4 - 4.6)	3.0(1.9 - 5.1)
8	3.4(2.0 - 5.2)	4.7(3.6 - 6.3)	5.7(3.4 - 7.1)	8.1(6.3 - 11.5)
9	1.1(0.7 - 2.1)	1.5(1.0 - 2.5)	0.9(0.3 - 1.9)	1.2(0.7 - 2.3)

Abbreviations: AP = anterior-posterior; CC = cranial-caudal; A₉₅ = peak-to-peak value for 95% of points closest to the mean values; A₁₀₀ = maximal peak-to-peak value.

Data presented as mean, with range in parentheses.

for 10 radiotherapy fractions were calculated (Table 6.3). The range of the A₁₀₀ value was 0.7–6.3 mm for the anterior-posterior direction and 0.3–11.5 mm for the caudal-cranial direction. The A₉₅ value was on average 27% (range 0 - 75%) and 24% (range 0 - 67%) smaller than A₁₀₀ for the anterior-posterior and caudal-cranial directions, respectively. The magnitude of the deviations for patients 5 and

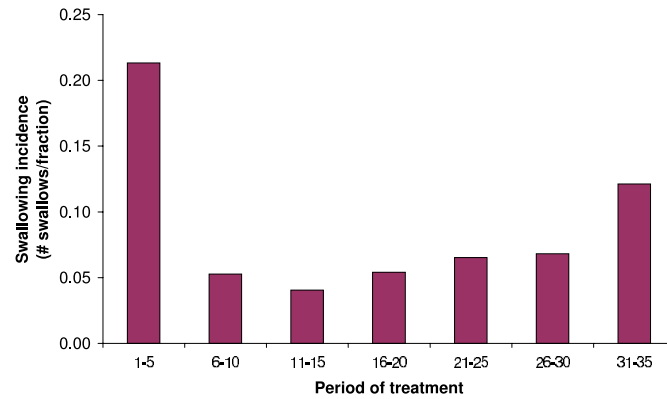
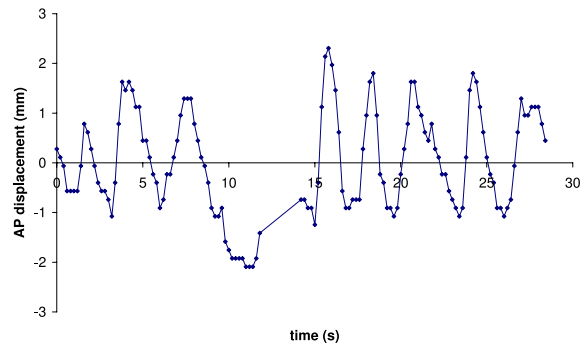


Figure 6.3: Incidence of total number of swallowing actions during the treatment. Treatment divided into periods of five fractions.

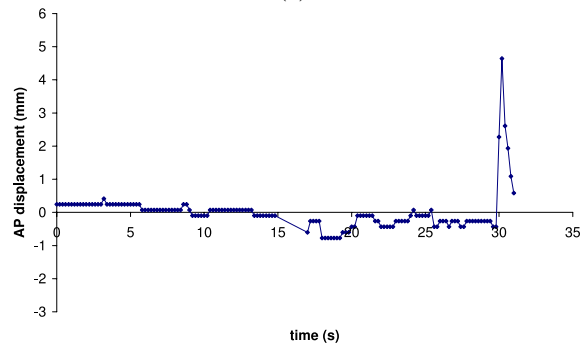
7 was approximately 2-3 mm and for patients 6 and 10 was approximately 5-8 mm. Some typical examples of traces of the tip of the epiglottis are shown in figure 6.4. Some movies showed a regular motion of the epiglottis, with a frequency between 8 and 20/min. For other patients, almost no motion was observed; however, an instant deviation could occur.

6.4 Discussion

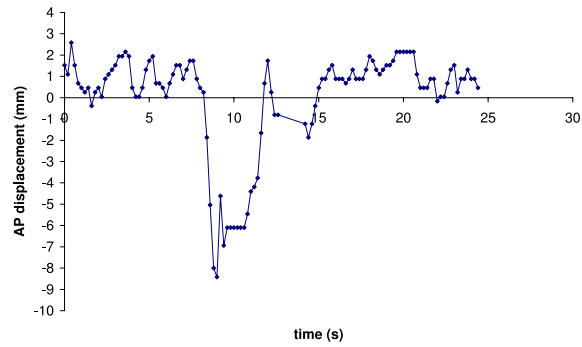
The maximal displacement of the larynx caused by swallowing is large (>20 mm) in the cranial-caudal direction (Dantas *et al.*, 1990), which could have implications for the dose distribution in the target. The incidence during irradiation is, however, low for most patients. On average, 0.45% of the irradiation time, a patient was swallowing, with a maximum of 1.5%. The effect on the dose distribution was even less, because during this period, the larynx is not always in its maximal position. Swallowing has therefore, a small effect on the dose distribution in the target volume. Also, because the effect is small, it may not be necessary to adjust the internal margin to take displacements due to swallowing into account. The treatment time for the technique used at our department was <1 minute; for longer treatment times, the swallowing incidence will increase (Hamlet *et al.*, 1993). In such cases, for example, when using intensity-modulated radiotherapy, the impact on the dose distribution might be larger. Hamlet *et al.* (1993) reported a swallowing incidence of 0.27 per irradiation interval for intervals of <2 minutes. In their study, a close-up view of the patient's throat with the console monitor



(a)



(b)



(c)

Figure 6.4: Three examples of deviation of tip of epiglottis: (a) frequent motion of tip of epiglottis, (b) sudden deviation at end of fraction, and (c) irregular motion with swallowing action.

video camera was used to visually identifying a swallowing action. They could not, therefore, measure the duration time of the swallowing actions. Patients were not instructed not to swallow but to breath normally in that study.

Although it is not necessary to take into account deviations due to swallowing, care should be taken when reducing the margins. Irradiating an inhomogeneous region, due to the trachea, with too-small fields might result in a lack of lateral electron equilibrium (Martens *et al.*, 2002).

The swallowing times in our study were longer than those reported in the literature (Kendall *et al.*, 2000; Hamlet *et al.*, 1993). The difference may have been caused by the definition of the duration of a swallowing action. In studies on timing events for normal swallowing, a bolus is followed in time; however, in our study, the displacement of the larynx was determined during swallowing without a bolus (saliva only). In our definition, all structures should be in similar position at the beginning and end of the swallowing. It has also been shown that the swallowing function for patients with head-and-neck cancer is worse compared with healthy subjects (Pauloski *et al.*, 2000; Stenson *et al.*, 2000). This may also explain the differences with swallowing times in normal subjects.

Most swallowing actions did occur within the first period of treatment (i.e. the first five fractions). This might have been because by the fact that most patients are nervous during the first few fractions. At the end of the treatment, during the last period, the incidence of swallowing seemed to increase. This might have been caused by thick saliva and/or radiation-induced mucositis.

The displacement of the tip of the epiglottis differed from patient to patient. The largest displacements were seen in the caudal-cranial direction (range 0.5 – 11.5 mm). In the anterior-posterior direction, the displacements were smaller (range 0.5 – 6.3 mm). Because most motions occur with a frequency of 8–20/min, these are probably associated with breathing. The nervousness of a patient might cause heavy breathing, and for large inspiratory effort, the excursion is large. The nervousness of a patient also might be the cause of the differences between patients, assuming a nervous patient shows more activity than a more relaxed patient. The differences between A_{100} and A_{95} differed for each patient. When the difference was large, this was probably caused by a sudden movement of the epiglottis (i.e., on average, the motion of the epiglottis is much smaller than the maximal peak-to-peak value would imply). For some patients, the A_{100} , as well as the A_{95} , is large. Therefore, the margins to the target volume should be adjusted to take into account these motions, because it is not known whether a patient will shown a lot of organ motion before the start of treatment. During 95% of the time, the deviations were within 7.1 mm and 5.3 mm in the caudal-cranial and anterior-posterior direction, respectively. To accomplish a full coverage during 95% of the time the margin to the CTV would than be approximately 3.5 mm in the caudal-cranial direction and 3 mm in the anterior-posterior direction, assuming that the image used for delineation is the average position. For 99% of the time, all deviations

were within 10.5 mm and 5.9 mm in the caudal-cranial and anterior-posterior direction, respectively.

6.5 Conclusion

Although the displacement of the larynx due to swallowing can be large, the incidence is low for most patients (on average 0.45% of the irradiation time). Therefore, there is no need to adjust the margins around the CTVs to take into account these displacements. Other motions occur with a magnitude smaller than that caused by swallowing. In the cranial-caudal direction, the tip of the epiglottis moves within a range of 7.1 mm 95 % of the time. These motions can occur often and a margin should therefore be applied to the CTV to take these motions into account.

Chapter 7

General discussion

7.1 Introduction

In this thesis intensity-modulated radiotherapy was applied to breast and head-and-neck cancer. In chapter 2 an IMRT technique was developed for irradiation of the breast. A highly conformal dose distribution with a single dose level to the target was obtained. A form of dose painting was achieved for the IMRT irradiation of oropharyngeal cancer. The aim of this treatment was to deliver three dose levels to the target volumes while sparing the normal tissues (chapter 3 and 4). For accurate delivery of the dose distribution, resulting in reduction of the margins needed for geometric uncertainties, the use of gold markers for position verification was investigated for head-and-neck irradiation. Beside interfraction motions, intrafraction motions were determined in the head-and-neck region. In the next section image-guided IMRT will be discussed in general. A more detailed discussion about the use of IMRT and its implications for breast cancer and oropharyngeal cancer are presented in sections 7.3 and 7.4 respectively.

7.2 Image-guided IMRT

Images providing anatomical and biological data should be available to obtain the ideal radiotherapy plan (Ling *et al.*, 2000). In this thesis CT images are used to visualize the patient anatomy. Using CT scans, electron density information is available, which is needed for accurate dose calculations. Targets volumes and surrounding organs at risk are delineated within the CT images. Accurate delineation of volumes of interest becomes a mayor issue when delivering highly conformal plans with IMRT. When the actual target is larger than the delineated target volume, this results in underdosage in the target and can result in a reduction in TCP. On the other hand, when the actual target is smaller than the delineated

target, this may have consequences for the dose to the surrounding tissues. The uncertainties in delineation should be taken into account during the planning process. In order to estimate the uncertainties and improve the delineation process, delineation studies are essential. The simultaneous use of different imaging modalities, such as CT, MRI, or PET, could improve the delineation process, because the advantages of each separated imaging modality can then be combined. The advantage of MRI is that it can be used to visualize soft tissue. Several studies reported the use of MRI for delineation of various cancer sites (Rasch *et al.*, 1997, 1999; Weltens *et al.*, 2001; Nishioka *et al.*, 2002; Parker *et al.*, 2003; Ten Haken *et al.*, 1992). PET has shown to be helpful in detecting lymph node metastases for lung cancer (Marom *et al.*, 1999; Gould *et al.*, 2002), for the head-and-neck cancer the use of PET for that purpose is still controversial (Nishioka *et al.*, 2002). PET can also be used to determine the boundaries of primary tumors when there are inflammatory changes around the tumor (Nishioka *et al.*, 2002). The combined use of these techniques should be investigated. Image fusion, the 3D matching of each image data set, is then of crucial importance.

Using the anatomical data of the CT, the three-dimensional dose distribution can be calculated by inverse planning based on dose constraints assigned to the delineated volumes (chapter 3 and 4), or directly by using the CT three-dimensional geometrical information (chapter 2). The use of biological data for treatment planning is still under development and is not used for treatment planning in this thesis. Instead, the clinical starting points, i.e. the prescribed dose to the targets and the tolerance dose of the organs at risk, were based on clinical studies applying homogeneous dose distributions. Tumor characteristics, such as tumor cell density and radiosensitivity, however, are not homogeneously distributed throughout the target. The use of image modalities such as PET, SPECT and MRI, providing functional information of the tumor, should therefore be investigated. Using this information it might be possible to improve the TCP by applying a heterogeneous dose distribution based on tumor characteristics.

During radiotherapy, the position of the target should be the same as during the imaging process needed for the treatment planning. In this thesis the use of EPIDs has shown to be a useful tool to determine inter- and intrafraction motions (chapter 5 and 6). Although gold markers can be used for position verification purposes, there is lack of anatomical information during radiotherapy. Due to radiotherapy, the shape and size of the anatomy might change. In order to improve the quality of the treatment, a replanning using the actual size and shape of the target volume and the surrounding normal tissue could be considered. Other techniques are then needed to visualize the position as well as the shape and size of the target volume. A possible way to visualize the target during radiotherapy is the combination of a linear accelerator and a CT scanner as developed in tomotherapy (Mackie *et al.*, 1999). Jaffray and Siewerdsen (2000) developed a cone beam CT scanner, by mounting an X-ray source in combination with a flat panel imager on the gantry

of a linear accelerator. By rotating the gantry a CT scan is acquired. A mobile ultrasound-based targeting system (BAT) has been used for daily verification of the position of the prostate (Lattanzi *et al.*, 2000). Pressure of the ultrasound probe can, however, cause a shift in the prostate location itself (Van den Heuvel *et al.*, 2002), resulting in less accurate position verification of the prostate. The above mentioned systems allow visualization of the soft tissues just before each treatment fraction. An other possible system is proposed by Lagendijk and Bakker (2000). The integration of a linear accelerator and a MRI imager should result in the imaging of soft tissues during radiotherapy.

7.3 Breast cancer

2-field IMRT

Using the three-dimensional geometry of the breast, an IMRT technique was developed (chapter 2). The technique was based on the division of the treatment field in segments with similar equivalent path length through the breast and aims to deliver a homogeneous dose distribution. Several other techniques have been developed based on radiological thickness and transit dosimetry information from EPIDs (Donovan *et al.*, 2000; Lo *et al.*, 2000). In a study of Kestin *et al.* (2000), segments were designed from isodose surfaces calculated from an open tangential beam. Using these techniques 80% to 90% of the dose is delivered by an open field and 3-8 additional fields are added to create a homogeneous dose distribution. Using a simple dose model Chui *et al.* (2002) presented a technique where the optimum intensity is obtained by equalizing the dose to the midpoint of pencil beam segments. Others groups used an inverse-planning algorithm, based on dose constraints assigned to delineated volumes, to optimize the dose homogeneity in the breast (Hong *et al.*, 1999; Chang *et al.*, 1999; Hurkmans *et al.*, 2002; Thilmann *et al.*, 2002). Due to the inhomogeneity of the lung, the missing tissue effect and oblique incidence, accurate dose calculation is rather difficult and advanced dose models are required. Dose models used for inverse planning are usually simple compared with models used for conventional three-dimensional planning, in order to achieve acceptable calculations times for the optimization process. This resulted in a significant discrepancy between the dose calculation performed with the 3D planning model and the inverse-planning model used at our department. The inverse-planning module is therefore not used for IMRT for breast cancer until more advanced dose models are incorporated in the inverse-planning module. Most mentioned studies used conventional beam arrangements, i.e. two tangential fields. Using a four-field technique Landau *et al.* (2001) showed increased dose homogeneity and significant improvement in heart sparing compared to conventional techniques. This resulted, however, also in increased dose to the contralateral

breast, resulting in an increased risk of radiation induced cancer in the contralateral breast (Boice *et al.*, 1992). A six-field arc technique resulted in poorer results than conventionally achieved. Ma *et al.* (2003) reported that 2-field IMRT could reduce dose to the lung, heart and contralateral breast compared to conventional techniques. Multiple beam angle IMRT resulted in low dose regions in the normal tissues. Furthermore, it was concluded that modulated-electron radiotherapy resulted in high conformal dose distributions. Irradiation with electrons can, however, cause a high skin dose. Li *et al.* (2000) showed for a combined electron and IMRT technique improvement over the conventionally used tangential fields with reduced dose to the ipsilateral lung and heart dose. A 9-field technique showed similar results for the target coverage, but resulted in increased dose to other normal structures. Thilmann *et al.* (2002) calculated IMRT plans for various combinations of beams and intensity levels using inverse planning. The optimum treatment plan for a left sided breast consisted of 12 beams using 7 intensity levels. The results were not compared with a 2-field technique, the heart and lung did, however, receive a substantial dose. Overall the two field IMRT techniques seem to have the most benefits. Due to the use of a simple beam geometry, the dose to surrounding normal tissue can easily be avoided, similar to the conventional tangential fields. Till now, the clinical implementation of three techniques have been reported (Lo *et al.*, 2000; Yarnold *et al.*, 2002; Vinici *et al.*, 2002). All techniques use a two-field approach and a relatively simple segmental IMRT technique to optimize the dose distribution (Donovan *et al.*, 2000; Kestin *et al.*, 2000; Lo *et al.*, 2000). Yarnold *et al.* (2002) reported that the early results of a randomized trail of standard radiotherapy versus IMRT suggest that reduction in unwanted dose inhomogeneity impacts on clinically observable late breast changes.

Position verification

The IMRT technique presented in chapter 2 delivers 88 % of the dose with an open field containing the entire breast. The technique is therefore relatively insensitive to organ motion and setup errors and no differences compared to conventional treatment must be taken into account. The same margin was therefore used as conventionally applied for geometric uncertainties. Using a similar segmental IMRT technique as presented in chapter 2, Hector *et al.* (2000) showed that, although the IMRT treatment was more susceptible to patient movement, it was still superior compared to the standard treatment when considering the dose outside 95-105%. Studying the effect of intrafraction motion for dynamic IMRT, George *et al.* (2003) found no statistically differences between the planned and expected dose distributions.

As reported by Fein *et al.* (1996) and Lirette *et al.* (1995) portal images can be used for position verification for breast irradiation. The effect of normal respiratory function was thereby smaller than the effect of interfraction motion. A similar tech-

nique can be applied for the IMRT technique due to the use of an open field with similar size as conventionally used. Position verification might reduce the margin and therefore reduce the dose to the heart and lung. An improved breast board may also result in better reproducibility of the patient, and reducing the inter-fraction motion. For further improvements of the reproducibility, active breathing control (Wong *et al.*, 1999) could be applied. Beside improving the reproducibility, the separation between the chest wall and the heart is increased during deep inspiration. Sixel *et al.* (2001) showed that the deep inspiration breath hold technique has the potential to reduce the irradiated heart volume, and could be considered for clinical introduction.

Target delineation

For analysis of the breast, the PTV and the lungs were delineated. Lead wires were used to visualize the conventional field borders on the CT scan. In contradiction with the use of the inverse planning software used in chapter 3 and 4, the delineation of the PTV and the lung is not necessary for treatment planning. Using the 2-field IMRT technique presented in chapter 2, only the conventional field borders are required. Therefore, the introduction of the technique will not require extra time for delineation. Using the conventional field borders, many patients have been successfully treated. To achieve a more conformal dose distribution, however, delineation might be useful. Using the MLC, the field can be shaped around the target in order to prevent dose the lung and heart. Inter- and intra-observer variation in the delineation of the breast on CT scans can be rather large (Hurkmans *et al.*, 2001a; Pitkänen *et al.*, 2001). Differences between the breast parenchyma and fatty tissue can be difficult to distinguish. Detailed delineation protocols are therefore necessary for delineation of the breast for clinical practice.

Extensions to 2-field IMRT

In literature, the planning studies aim at a homogeneous dose distribution in the whole breast, an extra dose to the tumor bed is thereby not included. A large number of patients, however, receive this extra boost dose. The extra fields used to deliver the boost dose can result in an extra dose to the lung and heart. Integration of the boost in the IMRT technique would therefore be useful. The complexity of the geometry thereby increases and a simple form of dose painting is performed with two dose levels. In order to achieve a conformal dose distribution with two dose levels, the use of extra non-opposing tangential fields is probably unavoidable. This will also result in some extra dose to surrounding normal tissues. It will be difficult to incorporate the boost in the technique presented in chapter 2, because it is based on the equivalent path length and tends to achieve a homogeneous dose distribution. The aim of an integrated boost technique is, however, two level

dose painting. An inverse planning system similar to that used in chapter 3 might be useful. This is, however, currently not possible for clinical practice due to the simple dose model used for inverse planning.

An other extension of the 2-field IMRT technique is the integration in the multiple field techniques used to irradiate the axillary, supraclavicular and internal mammary nodes for breast cancer patients with positive lymph nodes. The technique presented in chapter 2 can be integrated in the multiple field technique used at our department (Lagendijk and Hofman, 1992). It can also be use to improve the match line between the tangential fields and the parasternal field. These conventional fields might, however, also be improved in the future using conformal radiotherapy. The anatomical boundaries of the regional lymph node target volumes should therefore be investigated (Dijkema *et al.*, 2003). Cho *et al.* (2002) compared different radiotherapy techniques, including IMRT, for the irradiation of the breast and upper mammary nodes. IMRT showed the best target coverage. The lowest NTCP values for heart and lung were found for the IMRT technique and a technique using oblique electron fields. Remouchamps *et al.* (2003) reported that moderate deep inspiration breath hold significantly reduces heart and lung doses when deep tangential fields are used for locoregional irradiation of the breast. The dose homogeneity was improved using IMRT, while the dose to the heart was slightly reduced.

7.4 Head-and-neck cancer

Segmental IMRT technique for oropharyngeal cancer

A segmental IMRT technique was developed for the irradiation of oropharyngeal cancer. Beside the ability to reduce the dose to the normal tissues, such as brain, spinal cord and parotid gland, and creating highly conformal dose distributions, IMRT was used to apply a simple form of dose painting. The aim was to deliver three different dose levels: one to the CTV of the lymph nodes, one to the CTV of the primary tumor and one to the GTV of the primary tumor. The different dose levels were simultaneously delivered in 30 fractions, resulting in a simultaneous integrated boost strategy (Mohan *et al.*, 2000). Like Mohan *et al.* (2000), we used an isoeffect relationship based on the linear-quadratic model to design IMRT fractionation strategies. Care should be taken when designing a fractionation strategy when delivering multiple dose levels simultaneously. Low fraction doses result in long treatments. High fraction doses can result in short treatment duration but also in an increased risk of injury to the embedded normal tissue. Until late complications (Withers *et al.*, 1995c; Maciejewski *et al.*, 1989) of the IMRT fractionation strategies are evaluated, care should be taken when escalating the dose. For the clinical introduction we therefore started with an increase of 3

Gy to the GTV.

Due to the complex geometry of the volumes of interest, most groups used an inverse planning algorithm based on dose constraints to volumes of interests to develop an IMRT technique for oropharyngeal cancer. Studying the effect of the use of positioning margins for the parotid gland, Manning *et al.* (2001) used a dynamic IMRT technique and nine beams for the irradiation of two oropharyngeal tumors. Vineberg *et al.* (2002) reported that sparing of the parotid glands is possible without compromising target dose homogeneity for irradiation of oropharyngeal cancer. Using nine beams, their optimized fluence profiles were deliverable with either segmental or dynamic IMRT. It was, however, not clear whether the dose was calculated using the deliverable segments or using the optimized fluence. Only Wu *et al.* (2000) did show data, although not quantitative, that supported the choice of nine beams for the irradiation of three head-and-neck tumors, including an oropharyngeal case. Chao *et al.* (2000) used tomotherapy-based IMRT for the irradiation of oropharyngeal cancers.

For segmental IMRT, the total number of segments is an important factor, since the treatment time is closely related to the total number of segments. As presented in chapter 3, the dose homogeneity correlated with the total number of segments. For clinical introduction, approximately 100 segments were used. More segments will result in too long treatment times (> 25 min.). The total number of segments is determined by the number of beams and the number of segments per beam. Minimizing the number of beams without reduction of the quality of the treatment would be useful. This might be achieved by applying beam orientation optimization (Pugachev *et al.*, 2001). The saturation level, for dose homogeneity in the target volumes, might than be reached using fewer beams. It could, however, also result in more segments per beam to achieve the same dose homogeneity similar to the findings of chapter 3. Beam optimization might result in better sparing of organs at risk adjacent to the target volumes. Chapter 3 shows that the five-beam plans result in a lower dose to the parotid gland than other beam geometries. Although beam orientation optimization might improve the treatment, it is still hampered by long computing times needed for the optimization process (Pugachev *et al.*, 2001; Rowbottom *et al.*, 2001). Another way to achieve fewer segments is to optimize the sequencing process. Different segmentation methods can result in a different amount of segments (Potter *et al.*, 2002). In chapter 3 and 4 the optimized fluence is divided into equidistant levels. Another division of the optimized fluence might also result in fewer segments. If, for example, the minimum monitor units delivered by one beam is 50 % of the total, this 50 % could be delivered in one segment instead of five in case the fluence is divided in 10 levels. Another method to reduce the number of segments is profile smoothing.

For the dose calculations in chapter 3 and 4 a bixel resolution of $1 \text{ cm} \times 1 \text{ cm}$ is used. The use of a higher bixel resolution might improve the dose distribution. For a simple “C”-shaped target volume, Shepard *et al.* (1999) reported an increase in

dose homogeneity for higher bixel resolution. For the 3D irradiation of the prostate Kubo *et al.* (1999) showed more sparing of the rectum and bladder when using a micro-multileaf (1.7-3 mm leaf width) instead of a normal MLC with 10 mm leaf width. Beside the ability to improve the blocking of the surrounding normal tissue using a higher resolution, it might be easier to deliver a heterogeneous dose distribution using a higher resolution. A higher resolution can result in a better sampling of the target volume, resulting in more degrees of freedom to deliver a dose to an individual part of the target volume. In the direction of the leaf motion, the resolution can be easily adjusted by choosing a smaller leaf step size, in the opposite direction the resolution is limited by the leaf width. In order to achieve a higher spatial resolution micro-multileaf collimators have been constructed, with leaf widths projecting in the isocenter between 1.6 and 4.5 mm (Cosgrove *et al.*, 1999; Schlegel *et al.*, 1992). The disadvantage of these systems is the limited field size. Other attempts to increase the resolution are the use of two superimposing MLC fields with a small shift in isocenter (Galvin *et al.*, 1996) or a collimator rotation (Evans and Partridge, 2000; Otto and Clark, 2002; Alfredo and Siochi, 2000). Topolnjak *et al.* (2003) reported a design study for a six-bank multi-leaf collimator, which has a resolution comparable to the micro-multileaf collimators and a field size of at least 40 cm. Bortfeld *et al.* (2000) utilized the methods of sampling theory and the theory of linear systems in an effort to identify the optimum leaf width. For a 6-MV beam this resulted in a minimum leaf width of 1.5-1.8 mm. Although a high resolution of the fluence matrix may have some advantages, the disadvantage for segmental IMRT is that it can result in more segments.

Parotid gland

The parotid glands are located adjacent to the lymph node containing target volume. Therefore it is rather difficult to avoid irradiation to the parotid glands, without reduction of the TCP. To achieve the prescribed dose in the lymph nodes, a dose gradient outside the PTV, thus partially in the parotid glands, is necessary to allow dose build up. Reduction of parotid dose could result in lower dose regions in the lymph node containing region (chapter 4), i.e. moving the dose gradient into the lymph node containing region. It should be investigated whether these lower dose regions result in an increased risk regarding local failure. Furthermore, the margin taken into account for position verification will result in an increased dose to the parotid gland (chapter 4). Dose reduction can therefore also be achieved by accurate position verification. Using the data of the marker based position verification (chapter 5) as input for the recipe of Van Herk *et al.* (2000), a margin of approximately 3 mm is determined. When decreasing the margin from 6 mm to 3 mm for moderate sparing of the parotid glands, the mean dose to the parotid gland reduces by approximately 4 Gy corresponding with a decrease in NTCP for xerostomia from 44 % to 35 %.

In order to decrease the dose to the contralateral parotid gland, the cranial border to which the contralateral lateral lymph nodes are irradiated might be lowered (Eisbruch *et al.*, 1998). In a recent study of Braam *et al.* (2003), it was shown that for a groups of N+ patients metastasis of oropharyngeal cancer rarely appear high cranially on the contralateral side, indication that the probability for microscopic metastasis in that area in N0 patients must be small. Lowering the cranial border of the lymph node containing area from C1 to C2 level II results in a decrease in mean dose to the parotid gland of approximately 6 Gy (Astreimidou *et al.*, 2003). The NTCP did thereby decrease by approximately 12 %. These results are currently clinically used.

Delineation of volumes

In order to deliver highly conformal dose distributions with different dose levels, accurate delineation of all volumes involved is necessary. Recent articles have reviewed the normal anatomy of the neck (Wijers *et al.*, 1999; Nowak *et al.*, 1999; Gregoire *et al.*, 2000). These were mainly focused at the delineation of the lymph node regions or levels in the normal neck. Guidelines are provided for the delineation of the electively treated lymph nodes. For the target volumes, the delineation relies on historical information from surgical pathologic experiences. Few studies reported the delineation of oropharyngeal tumors. In a study of Nishioka *et al.* (2002) was reported that image fusion between ^{18}F FDG-PET and CT/MRI was useful in GTV and CTV determination for oropharyngeal cancer. Rasch *et al.* (1997) reported that MRI-derived GTVs were smaller and had less interobserver variation than the CT-derived GTVs for advanced head-and-neck cancer. A pilot study is started at our department to investigate the use of PET for target delineation of head-and-neck tumors.

Beside the target volumes, also organs at risk should be accurately delineated. The delineation of the brain and the spinal cord is relatively easy, because these organs are enclosed by bony structures. The parotid glands is delineated on CT scans, the use of MRI might be more accurate due to the ability of imaging soft tissues. There are however no delineation studies concerning these normal tissues.

Position verification

Due to the complex geometry and high fraction doses, accurate position verification is essential for head-and-neck tumors. High doses should be delivered to the targets, while the dose to the brain and spinal cord should be minimized. A low dose to the parotid gland is also important to improve the quality of life after radiotherapy. As shown in chapter 4 one way to achieve this aim is accurate patient positioning. Position verification of head-and-neck tumors is usually performed by

applying an EPID or a megavoltage film (Hurkmans *et al.*, 2001b). The position of bony structures is thereby measured relative to a reference position. In a review of Hurkmans *et al.* (2001b), a standard deviation of the systematic error of 1.6-4.6 mm and a random error of 1.1-2.5 mm (1 standard deviation) was reported for the head-and-neck region. In chapter 5 markers were used for position verification purposes. Markers are more easy to detect compared with bony structures, and the determination of the coordinates is straightforward. Regarding IMRT, marker-based positioning verification is especially useful due to the small fields used for segmental IMRT with non-conventional gantry angles. When the marker is implanted inside a relatively mobile organ like the prostate (Dehnad *et al.*, 2003), it can be used to remove the systematic errors, while using bony structures this is not possible.

Beside interfraction motions, intrafraction motions should be evaluated since these can contribute to the margins taken for setup uncertainties. In the head-and-neck region, intrafraction motion can be caused by organ motions, such as swallowing, breathing, or tongue motions (chapter 6). Due to the low incidence, swallowing has a minor influence on the dose distribution (chapter 6). Most organs in the head-and-neck region are, however, relative immobile and attached to bony structures. Intrafraction motion may also occur due to patient movements or relaxation of the muscles. This might become an issue for IMRT treatments with long treatment times and result in an unstable position relative to the start of the irradiation. The delivery of an IMRT treatment plan can take 20 minutes. Markers could be used to quantify the intrafraction motion, by taking multiple images during a single fraction. When the determined intrafraction motions are large during long treatments, it could be investigated whether marker-based position verification should be applied during the treatment. This could reduce the margin taken for geometric uncertainties.

7.5 Conclusion

Two different segmental IMRT techniques have been developed in this thesis for respectively irradiation of the breast and the oropharynx. Both techniques have been implemented clinically. Various other improvements can be applied as have been discussed in this chapter. Part of them, concerning position verification for head-and-neck cancer, have been investigated in this thesis.

Summary

In this thesis, intensity-modulated radiotherapy is applied to the irradiation of breast and oropharyngeal cancer. Furthermore, interfraction and intrafraction motions are studied for head-and-neck cancer to further improve the treatment. In the following paragraphs the results are summarized per chapter.

In chapter 2 an IMRT breast technique is developed taking into account the complex three-dimensional geometry of the breast. The aim was to achieve dose homogeneity throughout the entire breast. The IMRT technique was based on the division of the tangential fields in four multi-leaf collimator shaped segments. The shape of these segments was obtained from an equivalent path length map of the irradiated volume. Approximately 88% of the dose was delivered by two open fields covering the whole treated volume. In a planning study including 5 patients, the dose homogeneity improved for the IMRT technique was compared with the conventional technique. The dose homogeneity in the PTV was 9.0% (range 6.4–11.4%) for the conventional and 7.6% (range 6.5–10.3%) for the IMRT technique. The mean lung dose was reduced for the IMRT technique by approximately 10% compared with the conventional technique. Beside the improvements in dose homogeneity and reduction in lung dose, the IMRT technique creates the possibility to improve the field matching in the case of irradiation of the breast and lymph nodes using multiple fields. The new breast irradiation technique has recently been clinically introduced.

In chapter 3 a segmental intensity-modulated radiotherapy technique for the treatment of oropharyngeal cancer was developed. The aim was to deliver three different dose levels simultaneously: one to the lymph nodes (54 Gy), one to the CTV of the primary tumor (66 Gy) and one to the GTV of the primary tumor (69 Gy). The relation between the quality of a treatment plan and the number of beams in combination with the number of segments was investigated in order to obtain a clinically acceptable and deliverable plan. The dose distribution was therefore optimized using beam geometries consisting of 3, 5, 7 and 9 equiangular beams. The optimization procedure resulted in an optimized intensity map for each beam. The optimized intensity map was divided in equidistant levels (5, 7, 10 or 15), in

order to vary the number of segments. The dose homogeneity within the target volumes improved when the total number of segments increased and reached a saturation level at approximately 150 segments. Seven beams were sufficient to achieve the saturation level for dose homogeneity. The mean dose to the parotid glands depended on the beam geometry and tumor location and did not depend on the number of segments.

In chapter 4 the sparing of the parotid glands during the irradiation of oropharyngeal cancer was further investigated. For three different IMRT strategies the effect of reduction of positioning margins was investigated. Margins of 0, 3, 6 and 9 mm were therefore applied to the CTVs in order to obtain four planning target volumes. The analysis of the three IMRT strategies resulted in: (1) an optimal dose distribution in the PTV, (2) an optimal dose distribution in the PTV while sparing the parotid gland and (3) more parotid gland sparing but at the expense of the dose homogeneity in the PTV. The mean parotid dose increased linearly with increasing margin by approximately 1.3 Gy per mm. As a result, the normal tissue complication probability for xerostomia decreased when smaller margins were applied. Reducing the margin from 6 to 3 mm resulted in a relative NTCP reduction of approximately 20%, showing the benefit of accurate position verification.

In chapter 5 the reliability and toxicity of the use of implanted gold markers for position verification during the irradiation of head-and-neck cancer was investigated. The markers were visualized using an a-Si flat panel imager. Accurate position verification is needed to deliver the dose to the right spot, and results in smaller setup margins and therefore less dose to surrounding normal tissues (chapter 4). Ten patients with localized head-and-neck tumors received two gold markers in the parapharyngeal region. The acute and late radiation related toxicity were scored prospectively, using common toxicity criteria. The marker location was detected in portal images taken on average during 19 fractions. The inter-marker distance as well as the interfraction motion were determined for all patients. No acute major complications were observed. The gold seeds did not enhance the acute toxicity grade. The markers were visible in all images. A small time trend was observed in the inter-marker distance for three patients. For these patients at least one marker was located in the pharyngeal mucosa or pharyngeal constrictor muscle. Deep-seated gold markers did not show a time trend. The random error of the geometric uncertainties obtained without correction during radiotherapy was 1-2 mm. It was concluded that the use of implanted gold markers for position verification during radiotherapy of head-and-neck patients seems feasible. To avoid any chance of migration, markers should be placed in deep muscular compartments.

In chapter 6 the intrafraction motions of the larynx were investigated during radiotherapy. The larynx is a rather mobile organ in the head-and-neck region, and motion may occur due to swallowing, breathing, or movement of the tongue. De-

pending on the magnitude, duration and incidence, these motions may have clinical consequences for the choice of margins around the clinical target volume. The intrafraction motions of the larynx were visualized using an a-Si flat panel imager. Images were obtained every 200 ms, resulting in a movie of images for each beam. Movies were obtained during 79% of the total number of radiotherapy fractions. The total duration of swallowing was on average 0.45% (range 0.0 – 1.5%) of the total irradiation time. Deviations of motions other than swallowing ranged from 0.3 to 11.5 mm. Some of these motions were sudden, while others were probably related to breathing, because the frequency of these motions was 8 – 20 per minute. Due to the low incidence it is not necessary to apply an internal margin to take into account displacements due to swallowing. A margin should however be applied for other more frequent motions.

Two different segmental IMRT techniques have been developed in this thesis for respectively irradiation of the breast and the oropharynx. Both techniques have been implemented clinically. Various other improvements can be applied as have been discussed in chapter 7. Part of them, concerning position verification for head-and-neck cancer, have been investigated in this thesis.

Samenvatting

Radiotherapie is een behandelingsmethode voor patiënten met kanker waarbij gebruik wordt gemaakt van straling. De meest voorkomende vorm van radiotherapie is een behandeling met uitwendige stralingsbundels. De hoogenergetische straling zorgt voor schade aan het weefsel. Dit kan tot het gevolg hebben dat de cellen die worden bestraald sterven. Bij radiotherapie wordt daarom geprobeerd een hoge stralingsdosis te bereiken in de tumor om de kanker cellen te doden en tegelijkertijd een lage dosis in het gezonde weefsel te bereiken om daar zo min mogelijk schade te veroorzaken. Bij uitwendige bestraling zal echter altijd ook een deel gezond weefsel worden bestraald. Hierdoor ontstaat er een kans op complicaties. De dosis, die bij een behandeling wordt toegediend, hangt af van de eigenschappen van de tumor zoals de dichtheid en de stralingsgevoeligheid van de tumorcellen. In het ideale geval zijn alle eigenschappen van de tumor bekend en kan de dosisverdeling daarop worden aangepast.

Door de ontwikkelingen in de digitale beeldvormingstechnieken, zoals CT en MRI, kan beter worden bepaald waar de tumor en de risico-organen zich bevinden in het lichaam. Hierdoor is het mogelijk om een meer conformale dosisverdeling te verkrijgen. Dat wil zeggen dat het hoge dosis gebied zich voornamelijk in de tumor bevindt en dat het omringende weefsel zo min mogelijk dosis ontvangt. Een geavanceerde vorm van radiotherapie is intensiteitsgemoduleerde radiotherapie (IMRT). Door het variëren van de intensiteit binnen een stralingsbundel kan de dosisverdeling worden aangepast. Hierdoor is het mogelijk om zeer conformale dosisverdelingen te verkrijgen waarbij de dosis in de tumor homogeen is verdeeld. Het is ook mogelijk om de dosis binnen de tumor te variëren en aan te passen aan karakteristieken van de tumor. Er zijn beeldvormingstechnieken, zoals PET en functionele MRI, die biologische informatie over de tumor geven. Het gebruik van deze informatie voor radiotherapie moet echter nog verder worden ontwikkeld. Daarom wordt op dit moment volstaan met het verhogen van de dosis in de tumor om zo een beter behandelingsresultaat te bereiken.

Bij radiotherapie worden patiënten meestal in meerdere fracties bestraald, het is daarom belangrijk dat de tumor zich elke keer op dezelfde plek bevindt ten opzichte van het bestralingsveld. Er zal echter een onzekerheid in de positie van de

tumor zijn, bijvoorbeeld door positioneringsfouten of interne bewegingen van organen. Door deze positie onnauwkeurigheden kan een deel van de tumor buiten het bestralingsveld komen te liggen waardoor de voorgeschreven dosis niet wordt ontvangen. Om ervoor te zorgen dat de tumor altijd de gewenste dosis krijgt wordt een extra marge rondom de tumor bestraald. Dit resulteert echter wel in extra dosis in het gezonde weefsel. Het is daarom belangrijk om de marge zo veel mogelijk te reduceren. Daarvoor moet de positie van de tumor tijdens elke behandeling worden geverifieerd en eventueel worden gecorrigeerd.

In dit proefschrift is IMRT toegepast op de bestraling van borstkanker. Het doel daarbij is het bereiken van een homogene dosisverdeling. Daarnaast is een IMRT techniek ontwikkeld voor de bestraling van oropharynx tumoren. Deze bestralings-techniek is complexer dan die gebruikt wordt bij de bestraling van de borst, omdat er meerdere doelvolumina moeten worden bestraald en verschillende risico-organen (speekselklieren, hersenen, ruggenmerg) gespaard moeten worden. Bovendien krijgen de doelvolumina verschillende doses. Verder is een positieverificatie methode voor hoofd-hals tumoren bekeken, met als doel de nauwkeurigheid van de behandeling te vergroten. De orgaanbewegingen van de larynx zijn onderzocht gedurende de behandeling. Deze bewegingen kunnen bijdragen aan een extra marge die rond de tumor moet worden genomen. Een gedetailleerde beschrijving per hoofdstuk volgt in de volgende paragrafen.

In hoofdstuk 2 is een IMRT techniek ontwikkeld voor het bestralen van borst kanker. Het doel hiervan is een homogene dosisverdeling te bereiken in de hele borst. Bij deze techniek wordt het behandelingsveld opgedeeld in 4 segmenten om zo de intensiteit te modelleren. De grootte en vorm van deze segmenten wordt bepaald uit de radiologische dikte van het bestraalde volume. De meeste straling wordt gegeven door een groot open veld. De drie overige segmenten worden gebruikt om de dosisverdeling homogeen te maken. Vergeleken met de conventionele behandeling wordt met de IMRT techniek een meer homogene dosis in het doelvolumen bereikt. Bijkomend voordeel van de techniek is dat de gemiddelde dosis in de long is verlaagd met ongeveer 10 %. De IMRT techniek kan ook worden geïmplementeerd in de meer complexe borstbestralingen waarbij ook lymfeklieren worden meegenomen in het bestralingsveld. De techniek is inmiddels klinisch in gebruik genomen.

In hoofdstuk 3 wordt een IMRT techniek voor de behandeling van oropharynx kanker gepresenteerd. Bij deze techniek worden drie verschillende stralingsdoses gegeven: één aan de lymfe klieren, één aan het CTV van de primaire tumor en één aan het GTV van de primaire tumor. Tevens wordt er gezorgd voor een lage dosis in het ruggenmerg en de hersenen, en wordt geprobeerd de dosis in de speekselklieren te minimaliseren. De relatie tussen de kwaliteit van het behandelingsplan en het aantal bundels in combinatie met het aantal segmenten is onderzocht om een klinisch acceptabel plan te verkrijgen dat goed is af te stralen. De dosisver-

deling is daarom uitgerekend voor 4 bundelgeometriën, met respectievelijk 3, 5, 7, en 9 bundels. De optimalisatie resulteerde in een intensiteitverdeling voor elke bundel. Door deze intensiteitverdeling op te delen in een verschillend aantal intensiteitsniveaus (5, 7, 10 of 15), kan een verschillend aantal segmenten per bundel worden verkregen. De homogeniteit van de dosisverdeling in de doelvolumina blijkt hoofdzakelijk afhankelijk van het totaal aantal segmenten dat wordt gebruikt en verbetert niet meer wanneer meer dan 150 segmenten worden gebruikt. Tussen 100 en 150 segmenten verbetert de homogeniteit echter maar weinig. De bundelgeometrie met 7 bundels blijkt voldoende om een acceptabele dosisverdeling te bereiken. De dosis in de speekselklieren blijkt niet afhankelijk van het aantal segmenten, maar varieert wel per bundelgeometrie.

In hoofdstuk 4 wordt de sparing van de speekselklieren verder bestudeerd. Het effect van marges voor onnauwkeurigheden in de positie op de dosis in de speekselklieren wordt bestudeerd voor drie verschillende IMRT strategieën. De drie strategieën resulteerden in: (1) een optimale dosisverdeling in het PTV, (2) een optimale dosisverdeling in het PTV en sparing van de speekselklieren en (3) verder sparing van de speekselklieren maar ten koste van de dosisverdeling in het PTV. De dosis in de speekselklieren neemt lineair toe met ongeveer 1.3 Gy per mm marge. Een reductie in de marge van 6 mm naar 3 mm zou resulteren in een NTCP verlaging van 20%. De conclusie luidt dat betere positieverificatie kan resulteren in minder complicaties. De gegevens van deze studie en die beschreven in hoofdstuk 3 zijn gebruikt om een studie op te zetten waarin bestudeerd wordt of IMRT resulteert in een betere parotischfunctie dan de conventionele behandeling. Deze studie is in 2003 van start gegaan.

In hoofdstuk 5 wordt de toxiciteit en de betrouwbaarheid van geïmplanteerde goudmarkers bekeken voor positieverificatie van tumoren in het hoofd-hals gebied. Het gebruik van goudmarkers moet leiden tot een nauwkeurigere positie bepaling, wat nodig is om de dosis op de juiste plek af te geven. Door het verkleinen van onnauwkeurigheden in de positie van de patiënt kan de marge worden verkleind. Dit kan leiden tot minder dosis aan het omliggende gezonde weefsel. In tien patiënten zijn daarom twee markers geïmplanteed in het pharynx gebied. De acute en late schade is prospectief gemeten. De locatie van de markers is bepaald met behulp van beelden opgenomen met een "a-Si flat panel". Gemiddeld zijn er beelden opgenomen gedurende 19 fracties per patiënt. De interfractie bewegingen en de afstand tussen de markers is bepaald. De acute schade is niet vergroot door het gebruik van goudmarkers. De afstand tussen de markers is groter geworden gedurende de behandeling voor drie patiënten. Deze verandering is echter klein. Als er een vergroting in de afstand tussen de markers werd waargenomen, was altijd een marker oppervlakkig geïmplanteed in de mucosa of in de musculus constrictor pharyngis. Markers die dieper waren geïmplanteed, vertoonden geen verandering in de onderlinge afstand en zitten dus vast. De random onnauwkeurigheid in de positie

van de patiënt was, zonder correctie van de positie van de patiënt, 1-2 mm. Het gebruik van goudmarkers voor de positieverificatie lijkt haalbaar.

In hoofdstuk 6 worden de bewegingen van de larynx bestudeerd tijdens de bestraling met behulp van een a-Si detector. De larynx beweegt ten gevolge van slikken, tongbewegingen en ademen. Afhankelijk van hun incidentie, grootte en duur kunnen deze bewegingen consequenties hebben voor de marge die wordt aangehouden voor onnauwkeurigheden in de positie. Met behulp van een a-Si detector zijn filmpjes gemaakt gedurende de behandeling, waarbij elke 200 ms een doorlichtingsbeeld is opgenomen. De filmpjes zijn gemaakt gedurende 79% van de behandelingsduur. De incidentie van slikken blijkt laag, gemiddeld slikte een patiënt gedurende 0,45% van de behandelingsduur. Er zijn echter wel andere bewegingen met een grootte van 0,3 tot 11,5 mm waargenomen. Sommige bewegingen traden plotseling op, andere werden waarschijnlijk veroorzaakt door de ademhaling omdat de frequentie waarbij deze optraden 8-20 per minuut was. De incidentie van slikken was laag, daarom hoeft daar geen extra marge voor te worden genomen. Met de overige bewegingen moet echter wel rekening worden gehouden bij het bepalen van een marge voor positie onnauwkeurigheden.

In dit proefschrift wordt de ontwikkeling van twee IMRT technieken beschreven, voor respectievelijk radiotherapie voor borstkanker en oropharynxkanker. Beide technieken zijn klinisch geïmplementeerd. De beschreven technieken kunnen in de toekomst nog worden verbeterd zoals beschreven in hoofdstuk 7. Een deel hiervan is beschreven in dit proefschrift en betreft positieverificatie van het hoofd-hals gebied (hoofdstuk 5 and 6).

References

- Alasti H, Petric P, Catton C N and Warde P R 2001 Portal imaging for evaluation of daily on-line setup errors and off-line organ motion during conformal irradiation of carcinoma of the prostate *International Journal of Radiation Oncology, Biology and Physics* **49** 869–884
- Alfredo R and Siochi C 2000 Virtual micro-intensity modulated therapy *Medical Physics* **27** 2480–2492
- Astreinidou E, Dehnad H, Terhaard C H J and Raaijmakers C P J 2003 Level II lymph nodes and radiation-induced xerostomia *International Journal of Radiation Oncology, Biology and Physics* **in press**
- Bartelink H, Horiot J, Poortmans P, Struikmans H, Van den Bogaert W, Barillot I, Fourquet A, Borger J, Jager J, Hoogenraad W, Collette L and Pierart M 2001 Recurrence rates after treatment of breast cancer with standard radiotherapy with or without additional radiation *New England Journal of Medicine* **345** 1378–1388
- Bel A, Keus R, Vijlbrief R E and Lebesque J V 1995 Setup deviations in wedged pair irradiation of parotid gland and tonsillar tumors, measured with an electronic portal imaging device *Radiotherapy and Oncology* **37** 153–159
- Bel A, Van Herk M, Bartelink H and Lebesque J V 1993 A verification procedure to improve patient set-up accuracy using portal images *Radiotherapy and Oncology* **29** 253–260
- Boice J D, Harvey E B, Blettner M, Stovall M and Flannery J T 1992 Cancer in the contralateral breast after radiotherapy for breast cancer *New England Journal of Medicine* **326** 781–785
- Bortfeld T, Bürkelbach J, Boesecke R and Schlegel W 1990 Methods of image reconstruction from projections applied to conformation radiotherapy *Physics in Medicine and Biology* **35** 1423–1434
- Bortfeld T, Oelfke U and Nill S 2000 What is the optimum leaf width of a multileaf collimator? *Medical Physics* **27** 2494–2502
- Bortfeld T and Schlegel W 1993 Optimization of beam orientations in radiotherapy: some theoretical considerations. *Physics in Medicine and Biology* **38** 291–304
- Bortfeld T, Schlegel W and Rhein B 1993 Decomposition of pencil beam kernels for fast dose calculations in three-dimensional treatment planning *Medical Physics* **20** 311–318
- Braam P, Raaijmakers C P J and Terhaard C H J 2003 Location of cervical lymph node metastasis in oropharyngeal or hypopharyngeal carcinoma: implications for cranial field borders *International Journal of Radiation Oncology, Biology and Physics* **in press**
- Brenner D J 1993 Dose, volume, and tumor-control predictions in radiotherapy *International Journal of Radiation Oncology, Biology and Physics* **26** 171–179
- Buchholz T A, Gurgoze E, Bice W S and Prestidge B R 1997 Dosimetric analysis of intact breast irradiation in off-axis planes *International Journal of Radiation Oncology, Biology and Physics* **39** 261–267
- Butler E B, Teh B S, Grant W H, Uhl B M, Kuppersmith R B, Chiu J K, Donovan D T and Woo S Y 1999 Smart (simultaneous modulated accelerated radiation therapy) boost: a new accelerated fraction schedule for the treatment of head and neck cancer with intensity

- modulated radiotherapy *International Journal of Radiation Oncology, Biology and Physics* **45** 21–32
- Carruthers L J, Redpath A T and Kunkler I H 1999 The use of compensators to optimize the three dimensional dose distribution in radiotherapy of the intact breast *Radiotherapy and Oncology* **50** 291–300
- CaseBow M P 1984 Matching of adjacent radiation beams for isocentric radiotherapy *British Journal of Radiology* **57** 735–740
- Chang S X, Katharin M, Deschesne M S, Cullip T J, Parker S A and Earnhart J 1999 A comparison of different intensity modulation treatment techniques for tangential breast irradiation *International Journal of Radiation Oncology, Biology and Physics* **45** 1305–1314
- Chao K S, Majhail N, Huang C J, Simpson J R, Perez C A, Haughey B and Spector G 2001 Intensity-modulated radiation therapy reduces late salivary toxicity without compromising tumor control in patients with oropharyngeal carcinoma: a comparison with conventional techniques. *Radiotherapy and Oncology* **61** 275–280
- Chao K S C, Low D A, Perez C A and Purdy J A 2000 Intensity-modulated radiation therapy in head and neck cancers: The mallinckrodt experience *International Journal of Cancer* **90** 92–103
- Cheng C, Das I J and Stea B 1994 The effect of the number of computed tomographic slices on dose distributions and evaluation of treatment planning systems for radiation therapy of intact breast *International Journal of Radiation Oncology, Biology and Physics* **30** 183–195
- Cho B C J, Hurkmans C W, Damen E M F, Zijp L J and Mijnheer B J 2002 Intensity modulated versus nonintensity modulated radiotherapy in the treatment of the left breast and upper internal mammary lymph node chain: a comparative planning study *Radiotherapy and Oncology* **62** 127–136
- Chui C, Chan M F, Yorke E, Spirou S and Ling C C 2001 Delivery of intensity-modulated radiation therapy with conventional multileaf collimator: Comparison of dynamic and segmental methods *Medical Physics* **28** 2441–2449
- Chui C, Hong L, Hunt M and McCormick B 2002 A simplified intensity modulated radiation technique for the breast *Medical Physics* **29** 522–529
- Convery D J and Webb S 1998 Generation of discrete beam-intensity modulation by dynamic multileaf collimation under minimum leaf separation constraints *Physics in Medicine and Biology* **43** 2521–2538
- Cosgrove V P, Jahn U, Pfaender M, Bauer S, Budach V and Wurm R E 1999 Commissioning of micro multi-leaf collimator and planning system for stereotactic radiosurgery *Radiotherapy and Oncology* **50** 325–336
- Crook J M, Raymond Y, Salhani D, Yang H and Esche B 1995 Prostate motion during standard radiotherapy as assessed by fiducial markers *Radiotherapy and Oncology* **37** 35–42
- Dantas R O, Kern M K, Massey B T, Dodds W J, Kahrilas P J, Brasseur J G, Cook I J and Lang I M 1990 Effect of swallowed bolus variables on oral and pharyngeal phases of swallowing *Am. J. Physiol.* **258** G675–681
- Dawson L A, Anzai Y, Marsh L, Martel M K, Paulino A, Ship J A and Eisbruch A 2000a Patterns of local-regional recurrence following parotid sparing conformal and segmental intensity-modulated radiotherapy for head and neck cancer *International Journal of Radiation Oncology, Biology and Physics* **46** 1117–1126
- Dawson L A, Litzenberg D W, Brock K K, Sanda M, Sullivan M, Sandler H M and Balter J M 2000b A comparison of ventilatory prostate movement in four treatment positions *International Journal of Radiation Oncology, Biology and Physics* **48** 319–323
- De Boer H C J, van Sörnsen de Koste J R, Creutzberg C L, Visser A G, Levendag P C and Heijmen B J M 2001 Electronic portal image assisted reduction of systematic set-up errors in head and neck irradiation *Radiotherapy and Oncology* **61** 299–308
- De Graeff A, De Leeuw J R J, Ros W J G, Hordijk G J, Blijham G H and Winnubst J A M

- 1999 A prospective study on the quality of life of patients with cancer of the oral cavity or oropharynx treated with surgery with or without radiotherapy *Oral Oncology* **35** 27–32
- De Neve W, De Gersem W, Derycke S, De Meerleer G, Moerman M, Bate M, Van Duyse B, Vackaet L, De Deene Y, Mersseman B and De Waeter C 1999 Clinical delivery of intensity modulated conformal radiotherapy for relapsed or second-primary head and neck cancer using a multileaf collimator with dynamic control *Radiotherapy and Oncology* **50** 301–314
- Dehnad H, Nederveen A J, Van der Heide U A, Van Moorselaar R J A, Hofman P and Legendijk J J W 2003 Clinical feasibility study for the use of implanted gold seeds in the prostate as reliable positioning markers during megavoltage irradiation *Radiotherapy and Oncology* **in press**
- Dijkema I M, Hofman P, Raaijmakers C P J, Legendijk J J W, Battermann J J and Hillen B 2003 Loco-regional conformal radiotherapy of the breast: recommendations for delineation of the regional lymph node target volumes *Radiotherapy and Oncology* **submitted**
- Donovan E M, Johnson U, Shentall G, Evans P M, Neal A J and Yarnold J R 2000 Evaluation of compensation in breast radiotherapy: A planning study using multiple static fields *International Journal of Radiation Oncology, Biology and Physics* **46** 671–679
- Eisbruch A, Marsh L H, Martel M K, Ship J A, Ten Haken R K, Pu A T and Fraass B A and Lichter A S 1998 Comprehensive irradiation of head and neck cancer using conformal multisegmental fields: assessment of target coverage and noninvolved tissue sparing *International Journal of Radiation Oncology, Biology and Physics* **41** 559–568
- Eisbruch A, Ten Haken R K, Kim H M, Marsh L H and Ship J A 1999 Dose, volume, and function relationships in parotid salivary glands following conformal and intensity-modulated radiation of head and neck cancer *International Journal of Radiation Oncology, Biology and Physics* **45** 577–587
- Emami B, Lyman J, Brown A, Coi L, Goitein M, Munzenrider J E, Shank B, Solin L J and Wesson M 1991 Tolerance of normal tissue to therapeutic irradiation *International Journal of Radiation Oncology, Biology and Physics* **21** 109–122
- Evans P M, Donovan E M, Fenton N, Hansen V N, Moore I, Partridge M, Reise S, Suter B, Symonds-Taylor J R N and Yarnold 1998 Practical implementation of compensators in breast radiotherapy *Radiotherapy and Oncology* **49** 255–265
- Evans P M, Hansen V N, Mayles W P M, Swindell W, Torr M and Yarnold J R 1995 Design of compensators for breast radiotherapy using electronic portal imaging *Radiotherapy and Oncology* **37** 43–54
- Evans P M and Partridge M 2000 A method of improving the spatial resolution of treatments that involve a multileaf collimator *Physics in Medicine and Biology* **45** 609–622
- Fein D A, McGee K P, Schultheiss T E, Fowble B L and Hanks G E 1996 Intra- and interfractional reproducibility of tangential breast fields: a prospective on-line portal imaging study *International Journal of Radiation Oncology, Biology and Physics* **34** 733–740
- Fielding A L, Evans P M, Phil D and Clark C H 2002 The use of electronic portal imaging to verify patient position during intensity-modulated radiotherapy delivered by the dynamic mlc technique *International Journal of Radiation Oncology, Biology and Physics* **54** 1225–1234
- Fisher B, Redmond C, Poisson R, Margoese R, Wolmark N, Wickerham L, Fisher E, Deutsch M, Caplan R, Plich Y, Glass A, Shibata H, Lerner H, Terz J and Sidorovich L 1989 Eight-year results of a randomized clinical trial comparing total mastectomy and lumpectomy with or without irradiation in the treatment of breast cancer *New England Journal of Medicine* **320** 822–828
- Gall K P and Verhey L J 1993 Computer-assisted positioning of radiotherapy patients using implanted radiopaque fiducials *Medical Physics* **20** 1153–1159
- Galvin J M, Leavitt D D and Smith A A 1996 Field edge smoothing for multileaf collimators *International Journal of Radiation Oncology, Biology and Physics* **35** 89–98
- George R, Keall P J, Kini V R, Vedam S S, Siebers J V, Wu Q, Lauterbach M H, Arthur D W and

- Mohan R 2003 Quantifying the effect of intrafraction motion during breast IMRT planning and dose delivery *Medical Physics* **30** 552–562
- Gilbeau L, Octave-Prignot M, Loncol T, Renard L, Scalliet P and Grégoire V 2001 Comparison of set-up accuracy of three different thermoplastic masks for the treatment of brain and head and neck tumors *Radiotherapy and Oncology* **58** 155–162
- Gould M K, Maclean CC, Kuschner W G, Rydzak C E and Owens D K 2002 Accuracy of positron emission tomography for diagnosis of pulmonary nodules and mass lesions: a meta-analysis *Journal of the American Medical Association* **285** 914–924
- Gray J R, McCormick B, Cox L and Yahalom J 1991 Primary breast irradiation in large-breasted or heavy women: analysis of the cosmetic outcome *International Journal of Radiation Oncology, Biology and Physics* **21** 347–354
- Grégoire V, Coche E, Cosnard G, Hamoir M and Reyckler H 2000 Selection and delineation of lymph node target volumes in head and neck conformal radiotherapy: proposal for standardizing terminology and procedure based on the surgical experience *Radiotherapy and Oncology* **56** 135–150
- Gyenes G, Rutqvist L E, Liedberg A and Fornander T 1998 Long-term cardiac morbidity and mortality in a randomized trial of pre- and postoperative radiation therapy versus surgery alone in primary breast cancer *Radiotherapy and Oncology* **48** 185–190
- Hamlet S, Ezzell G and Aref A 1993 Larynx motion associated with swallowing during radiation therapy *International Journal of Radiation Oncology, Biology and Physics* **28** 467–470
- Hamlet S, Klien B, Aref A, Fontanesi J, Stachler R, Shamsa F, Jones L and Simpson M 1997 Mastication and swallowing in patients with postirradiation xerostomia *International Journal of Radiation Oncology, Biology and Physics* **37** 789–796
- Hector C L, Webb S and Evans P M 2000 The dosimetric consequences of inter-fractional patient movement on conventional and intensity-modulated breast radiotherapy treatments *Radiotherapy and Oncology* **54** 57–64
- Hong L, Hunt M, Chui C, Spirou S, Forster K, Lee H, Yahalom J, Kutcher G J and McCormick B 1999 Intensity-modulated tangential beam irradiation of the intact breast *International Journal of Radiation Oncology, Biology and Physics* **44** 1155–1164
- Huguenin P U, Taussky D, Moe K, Meister A, Baumert B, Lutolf U M and Glanzmann C 1999 Quality of life in patients cured from carcinoma of the head and neck by radiotherapy: the importance of the target volume *International Journal of Radiation Oncology, Biology and Physics* **45** 47–52
- Hunt M A, Zelefsky M J, Wolden S, Chui C, LoSasso T, Rosenzweig K, Chong L, Spirou S, Fromme L, Lumley M, Amols H A, Ling C C and Leibel S A 2001 Treatment planning and delivery of intensity-modulated radiation therapy for nasopharynx cancer *International Journal of Radiation Oncology, Biology and Physics* **49** 623–632
- Hurkmans C W, Borger J H, Pieters B R, Russell N S, Jansen E P M and Mijnheer B J 2001a Variability in target volume delineation on CT scans of the breast *International Journal of Radiation Oncology, Biology and Physics* **50** 1366–1372
- Hurkmans C W, Cho B C J, Damen E, Zijp L and Minheer B J 2002 Reduction of cardiac and lung complication probabilities after breast irradiation using conformal radiotherapy with or without intensity modulation *Radiotherapy and Oncology* **62** 163–171
- Hurkmans C W, Remeijer P, Lebesque J V and Mijnheer B J 2001b Set-up verification using portal imaging: review of current clinical practice *Radiotherapy and Oncology* **58** 105–120
- ICRU Report No. 50 1993 *Prescribing, recording and reporting photon beam therapy* (ICRU Bethesda Maryland)
- ICRU Report No. 62 1999 *Prescribing, recording and reporting photon beam therapy* (Bethesda, MD:ICRU Publications)
- IMRT Collaborative Working Group 2001 Intensity-modulated radiotherapy: Current status and issues of interest *International Journal of Radiation Oncology, Biology and Physics* **51** 880–914

- International Commission on Radiation Units and Measurements (ICRU) 1999 *Prescribing, recording and reporting photon beam therapy*, ICRU Report No. 62 (Bethesda, MD:ICRU Publications)
- Jacob P, Kahrilas P J, Logemann J A, Shah V and Ha T 1989 Upper esophageal sphincter opening and modulation during swallowing *Gastroenterology* **97** 1469–1478
- Jaffray D A and Siewerdsen J H 2000 Cone-beam computed tomography with a flat-panel imager: initial performance characterization *Medical Physics* **27** 1311–1323
- Jaffray D A, Yan D and Wong J W 1999 Managing geometric uncertainty in conformal intensity-modulated radiation therapy *Seminars in Radiation Oncology* **9** 4–19
- Keller-Reichenbecher M, Bortfeld T, Levegrün S, Stein J, Preiser K and Schlegel W 1999 Intensity modulation with "step and shoot" technique using a commercial mlc: a planning study *International Journal of Radiation Oncology, Biology and Physics* **45** 1315–1324
- Kendall K A, McKenzie S, Leonard R J, Gonçalves M I and Wlaker A 2000 Timing events in normal swallowing: A videofluoroscopic study *Dysphagia* **15** 74–83
- Kestin L L, Sharpe M B, Frazier R C, Vicini F A, Yan Di, Matter R C, Martinez A A and Wong J W 2000 Intensity modulation to improve dose uniformity with tangential breast radiotherapy: initial clinical experience *International Journal of Radiation Oncology, Biology and Physics* **48** 1559–1568
- Knöös T, Nilsson M and Ahlgren 1986 A method for conversion of hounsfield number to electron density and prediction of macroscopic pair production crosssections *Radiotherapy and Oncology* **5** 337–345
- Kubo H D, Wilder R B and Pappas C T E 1999 Impact of collimator leaf width on stereotactic radiosurgery and 3D conformal radiotherapy treatment plans *International Journal of Radiation Oncology, Biology and Physics* **44** 937–945
- Kwa S L S, Lebesque J V, Theuws J C M, Marks L B, Munley M T, Bentel G, Oetzel D, Spahn U, Graham M V, Drzymala R E, Purdy J A, Lic hter A S, Martel M K and Ten Haken R K 1998 Radiation pneumonitis as a function of mean lung dose: an analysis of pooled data of 540 patients *International Journal of Radiation Oncology, Biology and Physics* **42** 1–9
- Legendijk J J W and Bakker C J G 2000 MRI guided radiotherapy: a MRI based linear accelerator in *ESTRO-2000: Abstracts* Istanbul European Society for Therapeutic Radiation Oncology
- Legendijk J J W and Hofman P 1992 A standardized multifield irradiation technique for breast tumours using asymmetrical collimators and beam angulation *British Journal of Radiology* **65** 56–62
- Landau D, Adams E J, Webb S and Ross G 2001 Cardiac avoidance in breast radiotherapy: a comparison of simple shielding techniques with intensity-modulated radiotherapy *Radiotherapy and Oncology* **60** 247–255
- Langen K M and Jones D T L 2001 Organ motion and its management *International Journal of Radiation Oncology, Biology and Physics* **50** 265–278
- Lattanzi J, McNeely S, Donnelly S, Palacio E, Schultheiss T E and E Hanks G 2000 Ultrasound-based stereotactic guidance in prostate cancer-quantification of organ motion and set-up errors in external beam radiation therapy *Comput. Aided Surg.* **5** 289–295
- Lebesque J V 1986 Field matching in breast irradiation: An exact solution to a geometrical problem *Radiotherapy and Oncology* **5** 47–57
- Leonard R J, Kendall K A, McKenzie S, Gonçalves M I and Walker A 2000 Structural displacement in normal swallowing: A videofluoroscopic study *Dysphagia* **15** 146–152
- Li J G, Williams S S, Goffinet D R, Boyer A L and Xing L 2000 Breast-conserving radiation therapy using combined electron and intensity-modulated radiotherapy technique *Radiotherapy and Oncology* **56** 65–71
- Ling C C, Humm J, Larson S, Amols H, Fuks Z, Leibel s and Koutcher J A 2000 Towards multidimensional radiotherapy (MD-CRT): biological imaging and biological conformality *International Journal of Radiation Oncology, Biology and Physics* **47** 551–560

- Lirette A, Pouliot J, Aubin M and Larochelle M 1995 The role of electronic portal imaging in tangential breast irradiation: a prospective study *Radiotherapy and Oncology* **37** 241–245
- Litzenberg D, Dawson L, Sandler H, Sanda M G, McShan D L, Ten Haken R K, Lam K L, Brock K K and M Balter J 2002 Daily prostate targeting using implanted radiopaque markers *International Journal of Radiation Oncology, Biology and Physics* **52** 699–703
- Lo Y C, Yasuda G, Fitzgerald T J and Urie M M 2000 Intensity modulation for breast treatment using static multi-leaf collimators *International Journal of Radiation Oncology, Biology and Physics* **46** 187–194
- Lyman J T 1985 Complication probability as assessed from dose-volume histograms *Radiat Res* **104** S13–19
- Ma C M, Ding M, Li J S, Lee M C, Pawlicki T and Deng J 2003 A comparative dosimetric study on tangential photon beams, intensity modulated radiation therapy (IMRT) and modulated electron radiotherapy (MERT) for breast cancer treatment *Physics in Medicine and Biology* **48** 909–924
- Maciejewski B, Withers H R, Taylor J M G and Hliniak A 1989 Dose fraction and regeneration in radiotherapy for cancer of the oral cavity and oropharynx: tumor dose-response and repopulation *International Journal of Radiation Oncology, Biology and Physics* **16** 831–843
- Mackie T R, Balog J, Ruchala K, Shepard D, Aldridge S, Fitchard R E, Reckwerdt P, Oliveira G, McNut T and Mehta M 1999 Tomotherapy *Seminars in Radiation Oncology* **9** 108–117
- Maes A, Weltens C, Flamen P, Lambin P, Bogaerts R, Liu X, Baetens J, Hermans R and Van den Bogaert W 2002 Preservation of parotid function with uncomplicated conformal radiotherapy *Radiotherapy and Oncology* **63** 203–211
- Mandel I D 1987 The functions of salvia *J Dent Res* **66** 623–627
- Manning M A, Wu Q, Cardinale R M, Mohan R, Lauve A D, Kavanagh B D, Morris M M and Schmidt-Ullrich R K 2001 The effect of setup uncertainty on normal tissue sparing with imrt for head-and-neck cancer *International Journal of Radiation Oncology, Biology and Physics* **51** 1400–1409
- Marom E M, McAdams H P, Erasmus J J, Goodman P C, Culhane D K, Coleman W E, Herndon J E and Patz E F 1999 Staging non-small cell lung cancer with whole-body PET *Radiology* **212** 803–809
- Martens C, Reynaert N, De Wagter C, Nilsson P, Coghe M, Palmans H, Thierens H and De Neve W 2002 Underdosage of the upper-airway mucosa for small fields as used in intensity-modulated radiation therapy: A comparison between radiochromic film measurements, monte carlo simulations, and collapsed cone convolution calculations *Medical Physics* **29** 1528–1535
- Mohan R, Wang X, Jackson A, Bortfeld T, Boyer A L, Kutcher G J, Leibel S A, Fuks Z and C Ling C 1995 The potential and limitations of the inverse radiotherapy technique *Radiotherapy and Oncology* **32** 232–248
- Mohan R, Wu Q, Manning M and Schmidt-Ullrich R 2000 Radiobiological considerations in the design of fractionation strategies for intensity-modulated radiation therapy of head and neck cancers *International Journal of Radiation Oncology, Biology and Physics* **46** 619–630
- Moody A M, Mayles W P M, Bliss J M, A'Hern R P, Owen J R, Regan J, Broad B and Yarnold J R 1994 The influence of breast size on late radiation effects and association with radiotherapy dose inhomogeneity *Radiotherapy and Oncology* **33** 106–112
- Morris AD, Morris RD, Wilson JF, White J, Steinberg S, Okunieff P, Arriagada R, Le MG, Blichert-Toft M and van Dongen JA 1997 Breast-conserving therapy vs mastectomy in early-stage breast cancer: a meta-analysis of 10-year survival *Cancer J Sci Am* **3** 6–12
- Murphy M J, Adler J R, Bodduluri M, Dooley J, Forster K, Hai J, Le Q, Luxton G, Martin D and Poen J 2000 Image-guided radiosurgery for the spine and pancreas *Computer Aided Surgery* **5** 278–288
- National Cancer Institute 1999 Common Toxicity Criteria Version 2.0
- Neal A J, Torr M, Helyer S and Yarnold J R 1995 Correlation of breast heterogeneity with

- breast size using 3D CT planning and dose-volume histograms *Radiotherapy and Oncology* **34** 210–218
- Nederveen A J, Lagendijk J J W and Hofman P 2000 Detection of fiducial gold markers for automatic on-line megavoltage position verification using a marker extraction kernel (MEK) *International Journal of Radiation Oncology, Biology and Physics* **47** 1435–1442
- Nederveen A J, Lagendijk J J W and Hofman P 2001a Feasibility of automatic marker detection with an a-Si flat-panel imager *Physics in Medicine and Biology* **46** 1219–1230
- Nederveen A J, Van der Heide U A, Dehnad H, Van Moorselaar R J A, Hofman P and Lagendijk J J W 2002 Measurements and clinical consequences of prostate motion during a radiotherapy fraction *International Journal of Radiation Oncology, Biology and Physics* **53** 206–214
- Nederveen A J, Van der Heide U A, Hofman P, Welleweerd H and Lagendijk J J W 2001b Partial boosting of prostate tumours *Radiotherapy and Oncology* **61** 117–126
- Nishioka T, Shiga T, Shirato H, Tsukamoto E, Tsuchiya K, Kato T, Ohmori K, Yamazaki A, Aoyama H, Hashimoto S, Chang T and Miyasaka K 2002 Image fusion between ^{18}F FDG-pet and ct/mri for radiotherapy planning of oropharyngeal and nasopharyngeal carcinomas *International Journal of Radiation Oncology, Biology and Physics* **53** 1051–1057
- Nowak P J C M, Wijers O B, Lagerwaard F J and Levendag P C 1999 A three-dimensional ct-based target definition for elective irradiation of the neck *International Journal of Radiation Oncology, Biology and Physics* **45** 33–39
- Otto K and Clark B G 2002 Enhancement of IMRT delivery through MLC rotation *Physics in Medicine and Biology* **47** 3997–4017
- Parker C C, Damyanovich, Haycocks T, Haider M, Bayley A and Catton C N 2003 Magnetic resonance imaging in the radiation treatment planning of localized prostate cancer using intraprostatic fiducial markers for computed tomography co-registration *Radiotherapy and Oncology* **66** 217–224
- Pauloski B R, Rademaker A W, Logemann J A, Stein D, Beery Q, Newman L, Hanchett C, Tusan S and MacCracken E 2000 Pretreatment swallowing function in patients with head and neck cancer *Head Neck* **22** 474–482
- Pigott K, Dische S and Saunders M I 1995 Where exactly does failure occur after radiation in head and neck cancer? *Radiotherapy and Oncology* **37** 17–19
- Pitkänen M, Holli K, Ojala A and Laippala P 2001 Quality assurance in radiotherapy of breast cancer *Acta Oncologica* **40** 50–55
- Potter L D, Chang S X, Cullip T J and Siochi A C 2002 A quality and efficiency analysis of the IMFASTTM segmentation algorithm in head and neck "step & shoot" imrt treatments *Medical Physics* **29** 275–283
- Pugachev A, Li J G, Boyer A L, Hancock S L, Le Q, Donaldson S S and Xing L 2001 Role of beam orientation optimization in intensity-modulated radiation therapy *International Journal of Radiation Oncology, Biology and Physics* **50** 551–560
- Que W 1999 Comparison of algorithms for multileaf collimator field segmentation *Medical Physics* **26** 2390–2396
- Rasch C, Barillot I, Remeijer P, Touw A, Van Herk M and Lebesque J V 1999 Definition of the prostate in CT and MRI: a multi-observer study *International Journal of Radiation Oncology, Biology and Physics* **43** 57–66
- Rasch C, Keus R, Pameijer F A, Koops W, de Ru V, Muller S, Touw A, Bartelink H, van Herk M and Lebesque J V 1997 The potential impact of CT-MRI matching on tumor volume delineation in advanced head and neck cancer *International Journal of Radiation Oncology, Biology and Physics* **39** 841–848
- Remouchamps V M, Letts N, Vicini F A, Sharpe M B, Kestin L L, Chen P Y, Martinez A A and Wong J W 2003 Initial clinical experience with moderate deep-inspiration breath hold using an active breathing control device in the treatment of patients with left-sided breast cancer using external beam radiation therapy *International Journal of Radiation Oncology, Biology and Physics* **56** 704–715

- Roesink J M, Moerland M A, Battermann J J, Hordijk G J and Terhaard C H J 2001 Quantitative dose-volume response analysis of changes in parotid gland function after radiotherapy in the head-and-neck region *International Journal of Radiation Oncology, Biology and Physics* **51** 938–946
- Roesink J M, Terhaard C H J, Moerland M A, van Iersel F and Battermann J J 2000 CT-based parotid gland location: implications for preservation of parotid function *Radiotherapy and Oncology* **55** 131–133
- Rowbottom C G, Nutting C M and Webb S 2001 Beam-orientation optimization of intensity-modulated radiotherapy: clinical application to parotid gland tumors *Radiotherapy and Oncology* **59** 169–177
- Rowbottom C G, Webb S and Oldham M 1999 Is it possible to optimize a radiotherapy treatment plan? *International Journal of Radiation Oncology, Biology and Physics* **43** 698–699
- Rubin P 2001 *Clinical Oncology A Multidisciplinary Approach for Physicians and Students* (W.B. Saunders Company) 8th edn.
- Schlegel W S, Pastyr O, Bortfeld T, Becker G, Schad L, Gademann G and Lorenz W 1992 Computer systems and mechanical tools for stereotactically guided conformation therapy with linear accelerators *International Journal of Radiation Oncology, Biology and Physics* **24** 781–787
- Schneider U, Pedroni E and Lomax A 1996 The calibration of CT Hounsfield units for radiotherapy treatment planning *Physics in Medicine and Biology* **41** 111–124
- Shepard D M, Olivera G, Angelos L, Sauer O and Reckwerdt P 1999 A simple model for examining issues in radiotherapy optimization *Medical Physics* **26** 1212–1221
- Shirato H, Shimizu S, Kitamura K, Nishioka T, Kagei K, Hashimoto S, Aoyama H, Kunieda T, Shinohara N, Dosak-Akita H and Miyasaka K 2000 Four-dimensional treatment planning and fluoroscopic real-time tumor tracking radiotherapy for moving tumor *International Journal of Radiation Oncology, Biology and Physics* **48** 435–442
- Sixel K E, Aznar M C and Ung Y C 2001 Deep inspiration breath hold to reduce irradiated heart volume in breast cancer patients *International Journal of Radiation Oncology, Biology and Physics* **49** 199–204
- Söderström S and Brahme A 1995 Which is the most suitable number of photon beam portals in coplanar radiation therapy *International Journal of Radiation Oncology, Biology and Physics* **33** 151–159
- Solin L J, Chu J C H, Sontag M R, Brewster L, Cheng E, Doppke K, Drzymala R E, Hunt M, Kuske R, Manolis J M, McCormick B and Munzenrider J E 1991 Three-dimensional photon treatment planning of the intact breast *International Journal of Radiation Oncology, Biology and Physics* **21** 193–203
- Sontag M and Cunningham J R 1978 The equivalent tissue-air ratio method for making absorbed dose calculations in a heterogeneous medium *Radiology* **129** 787–794
- Stein J, Mohan R, Wang X, Bortfeld T, Wu Q, Preiser K, Ling C C and Schlegel W 1997 Number and orientations of beams in intensity-modulated radiation treatments *Medical Physics* **24** 149–159
- Stenson K M, MacCracken E, List M, Haraf D J, Brockstein B, Weichselbaum R and Vokes E E 2000 Swallowing function in patients with head and neck cancer prior to treatment *Arch Otolaryngol Head Neck Surg* **126** 371–377
- Stroom J C, de Boer J C J, Huizenga H and Visser A G 1999 Inclusion of geometrical uncertainties in radiotherapy treatment planning by means of coverage probability *International Journal of Radiation Oncology, Biology and Physics* **43** 905–919
- Ten Haken R K, Thornton A F, Sandler H M, LaVigne M L, Quint D J, Fraass B A, Kessler M L and McShan D L 1992 A quantitative assesment of the addition of MRI to CT-based, 3-D treatment planning of brain tumors *Radiotherapy and Oncology* **25** 121–133
- Thilmann C, Zabel A, Nill S, Rhein B, Hoes A, Haering P, Milker-Zabel S, Harms W, Schlegel W,

- Wannenmacher M and Debus J 2002 Intensity-modulated radiotherapy of the female breast *Medical Dosimetry* **27** 79–90
- Topolnjak R, van der Heide U A, Raaijmakers B W, Kotte A N T J, Welleweerd J and Lagendijk J J W 2003 Six-bank multi-leaf system for IMRT *European journal of medical physics* **XIX** 59
- Tyburski L L, Kestin L, Yan D, Vicini F, Sharpe M and Wong J 1999 An efficient method to improve dose uniformity for tangential breast radiotherapy using multiple mlc segments *International Journal of Radiation Oncology, Biology and Physics* **45** 423–424
- van Asselen B, Dehnad H, Raaijmakers C P J, Roesink J M, Lagendijk J J W and Terhaard C H J 2002 The dose to the parotid glands with IMRT for oropharyngeal tumors: the effect of reduction of positioning margins *Radiotherapy and Oncology* **64** 197–204
- van Asselen B, Raaijmakers C P J, Lagendijk J J W and Terhaard C H J 2003 Intra-fraction motions of the larynx during radiotherapy *International Journal of Radiation Oncology, Biology and Physics* **56** 384–390
- Van den Heuvel F, Wang Y, Litrupp P and Forman J D 2002 Evaluation of ultrasound prostate alignment using implanted gold markers and electronic portal imaging in *Proc. of the 7th international workshop on electronic portal imaging* pp. 76–77 Vancouver, BC, Canada
- van Dieren E B, Nowak P J C M, Wijers O B, Sörensen de Koste J R, van der Est H, Binnekamp D P, Heijmen B J M and Levendag P C 2000 Beam intensity modulation using tissue compensators or dynamic multileaf collimation in three-dimensional conformal radiotherapy of primary cancers of the oropharynx and larynx, including the elective neck *International Journal of Radiation Oncology, Biology and Physics* **47** 1299–1309
- van Dongen JA, Bartelink H, Fentiman IS, Lerut T, Mignolet F, Olthuis G, van der Schueren E, Sylvester R, Tong D, Winter J and van Zijl K 1992 Factors influencing local relapse and survival and results of salvage treatment after breast-conserving therapy in operable breast cancer: EORTC trial 10801, breast conservation compared with mastectomy in tnm stage i and ii breast cancer *European journal of Cancer* **28A** 801–805
- Van Herk M, Remeijer P, Rasch C and Lebesque J V 2000 The probability of correct target dosage: dose-population histograms for deriving treatment margins in radiotherapy *International Journal of Radiation Oncology, Biology and Physics* **47** 1121–1135
- van Tienhoven G, Lanson J H, Crabeels D, Heukelom S and Mijneer B J 1991 Accuracy in tangential breast treatment set-up: a portal imaging study *Radiotherapy and Oncology* **22** 317–322
- Vigneault E, Pouliot J, Laverdière J, Roy J and Dorion M 1997 Electronic portal imaging device detection of radioopaque markers for the evaluation of prostate position during megavoltage irradiation: a clinical study *International Journal of Radiation Oncology, Biology and Physics* **37** 205–212
- Vineberg K A, Eisbruch A, Coselmon M M, McShan D L, Kessler M L and Fraass B A 2002 Is uniform target dose possible in imrt plans in the head and neck? *International Journal of Radiation Oncology, Biology and Physics* **52** 1159–1172
- Vinici F A, Sharpe M, Kestin L, Martinez A, Mitchell C K, Wallace M F, Matter R and Wong J 2002 Optimizing breast cancer treatment efficacy with intensity-modulated radiotherapy *International Journal of Radiation Oncology, Biology and Physics* **54** 1336–1344
- Vissink A, Panders A K, 's Gravenmade E J and Vermey A 1988 The causes and consequences of hyposalivation *Ear Nose Throat* **67** 166–176
- Vrieling C, Collette L, Fourquet A, Hoogenraad W J, Horiot J, Jager J J, Pierart M, Poortmans P M, Struikmans H, Maat B, Van Limbergen E and Bartelink H 2000 The influence of patient, tumor and treatment factors on the cosmetic results after breast-conserving therapy in the EORTC 'boost vs. no boost' trial *Radiotherapy and Oncology* **55** 219–232
- Webb S 1993 *The physics of three-dimensional radiation therapy* Medical Science Series (Bristol, UK: IOP Publishing Ltd)

- Webb S 1997 *The physics of conformal radiotherapy* Medical Science Series (Bristol, UK: IOP Publishing Ltd)
- Webb S 2001 *Intensity-modulated radiation therapy* Medical Science Series (Bristol, UK: IOP Publishing Ltd)
- Weltens C, Menten J, Feron M, Bellon E, Demaerel P, Maes F, Van den Bogaert W and van der Schueren E 2001 Interobserver variations in gross tumor volume delineation of brain tumors on computed tomography and impact of magnetic resonance imaging *Radiotherapy and Oncology* **60** 49–59
- Wijers O B, Levendag P C, Tan T, van Dieren E B, van Sörnsen de Koste J, van der Est H, Senan S and Nowak P J C M 1999 A simplified ct-based definition of the lymph node levels in the node negative neck *Radiotherapy and Oncology* **52** 35–42
- Withers H R, Peters L J and Taylor J M G 1995a Dose-response relationship for radiation therapy of subclinical disease *International Journal of Radiation Oncology, Biology and Physics* **31** 353–359
- Withers H R, Peters L J, Taylor J M G, Owen J B, Morrison W H, Schultheiss T E, Keane T, O'Sullivan B, van Dyk J, Gupta N, Wang C C, Jones C U, Doppke K P, Myint S, Thompson M, Parsons J T, Mendenhall W M, Dische S, Aird E G A, Henk J M, Bidmead M A M, Svoboda V, Chon Y, Hanlon A L, Peters T L and Hanks G E 1995b Local control of carcinoma of the tonsil by radiation therapy: an analysis of patterns of fractionation in nine institutions *International Journal of Radiation Oncology, Biology and Physics* **33** 549–562
- Withers H R, Peters L J, Taylor J M G, Owen J B, Morrison W H, Schultheiss T E, Keane T, O'Sullivan B, van Dyk J, Gupta N, Wang C C, Jones C U, Doppke K P, Myint S, Thompson M, Parsons J T, Mendenhall W M, Dische S, Aird E G A, Henk J M, Bidmead M A M, Svoboda V, Chon Y, Hanlon A L, Peters T L and Hanks G E 1995c Late normal tissue sequelae from radiation therapy for carcinoma of the tonsil: patterns of fractionation study of radiobiology *International Journal of Radiation Oncology, Biology and Physics* **33** 563–568
- Wong J W, Sharpe M B, Jaffray D A, Kini V R, Robertson J H, Stromberg J S and Martinez A A 1999 The use of active breathing control (abc) to reduce margin for breathing motion *International Journal of Radiation Oncology, Biology and Physics* **44** 911–919
- Wright W E 1987 Management of oral sequela *J Dent Res* **66** 699–702
- Wu Q, Manning M, Schmidt-Ullrich R and Mohan R 2000 The potential for sparing of parotids and escalation of biologically effective dose with intensity -modulated radiation treatments of head and neck cancers: a treatment design study *International Journal of Radiation Oncology, Biology and Physics* **46** 195–205
- Yarnold J R, Donovan E, Bleackly N, Reise S, Regan J, Denholm E, Patel S, Ross G, Tait D and Evans P 2002 Randomised trial of standard 2D radiotherapy versus 3D intensity modulated radiotherapy (IMRT) in patients prescribed breast radiotherapy *Radiotherapy and Oncology* **64** S15
- Zelevsky M J, Fuks Z, Happersett L, Lee H J, Ling C C, Burman C M, Hunt M, Wolfe T, Venkatraman E S, Jackson A, Skwarchuk and Leibel S A 2000 Clinical experience with intensity modulated radiation therapy (IMRT) in prostate cancer *Radiotherapy and Oncology* **55** 241–249

Publications

- van Asselen B, Raaijmakers C P J, Hofman P and Lagendijk J J W 2001 An improved breast irradiation technique using three-dimensional geometrical information and intensity modulation *Radiotherapy and Oncology* **58** 341–347
- van Asselen B, Dehnad H, Raaijmakers C P J, Roesink J M, Lagendijk J J W and Terhaard C H J 2002 The dose to the parotid glands with IMRT for oropharyngeal tumors: the effect of reduction of positioning margins *Radiotherapy and Oncology* **64** 197–204
- van Asselen B, Raaijmakers C P J, Lagendijk J J W and Terhaard C H J 2003 Intra-fraction motions of the larynx during radiotherapy *International Journal of Radiation Oncology, Biology and Physics* **56** 384–390
- van Asselen B, Dehnad H, Terhaard C H J, Lagendijk J J W and Raaijmakers C P J 2003 Segmental IMRT for oropharyngeal cancer in a clinical setting *Radiotherapy and Oncology* (Accepted)
- van Asselen B, Dehnad H, Raaijmakers C P J, Lagendijk J J W and Terhaard C H J 2003 Implanted gold markers for positioning verification during irradiation of head-and-neck cancers: a feasibility study *International Journal of Radiation Oncology, Biology and Physics* (Submitted)
- Roosendaal S J, van Asselen B, Elsenaar J W, Vredenberg A M and Habraken F H P M 1999 The oxidation state of Fe(100) after initial oxidation in O₂ *Surface Science* **442** 329–337

Dankwoord

Nu we aan het einde zijn gekomen van dit proefschrift wil ik een aantal mensen persoonlijk bedanken zonder wie dit proefschrift niet tot stand was gekomen. Alle collega's die ik niet persoonlijk zal noemen, bedankt voor de prettige werksfeer op de afdeling. Tevens wil ik hierbij mijn vrienden en familie bedanken. Door jullie was het leven buiten het werk interessant en vol uitdagingen, maar bovendien vaak erg gezellig. Hetgeen zeker heeft bijgedragen aan de totstandkoming van dit proefschrift!

Als co-promotor was Niels Raaijmakers mijn dagelijks begeleider, bij wie ik dan ook vaak kwam binnen vallen. Wanneer ik zelf wat minder tevreden was met mijn eigen resultaten, ging ik meestal toch weer positief bij Niels weg. De met potlood volgekladderde blaadjes van mijn artikelen, of eerste pogingen daartoe, zal ik ook niet snel vergeten. Wat betreft mijn project was mijn promotor Jan Lagendijk iets meer op de achtergrond aanwezig, en hield de grote lijnen in de gaten. Verder kon je door zijn grote enthousiasme voor wetenschap nauwelijks om hem heen. Naast de begeleiding vanuit de fysica groep, ben ik voor het KNO onderzoek begeleid door Chris Terhaard, die tevens mijn co-promotor was. Mede door zijn enthousiasme is de IMRT snel geïntroduceerd in de kliniek. Tevens was het prettig dat er iemand op de afdeling was met een nog chaotischer bureau dan dat van mijzelf. Pieter Hofman was de eerste arts met wie ik heb samengewerkt en hij heeft mij begeleid bij het borstonderzoek. Hij heeft me geïntroduceerd in de klinische kant van de radiotherapie.

Bij mijn onderzoek heb ik vooral samengewerkt met Homan Dehnad, die als arts aan hetzelfde project werkte. Naast wetenschappelijke discussies hebben we vele andere interessante discussies gehad, waaronder vele politieke. Wat ik vooral zal missen is het volgende: "Meneer Brams, mag ik *een* vraag stellen?". Aart Nederveen was een jaar eerder begonnen als AIO, toen ik nog student was. Aart en ik hebben veel tooltjes met elkaar uitgewisseld en Aart heeft me geholpen bij het leren gebruiken van de flatpanel. We hebben zelfs op het punt gestaan samen een onderzoek op te zetten. Dit laatste project is helaas niet doorgegaan. Met de komst van Eleftheria Astreinidou en Pètra Braam werd het aantal promovendi op

het KNO gebied uitgebreid. Er onstond dan ook een echte KNO groep, samen met Niels, Chris, Homan, Judith en Rien. Dit was niet alleen bevorderlijk voor het onderzoek maar bovendien ook vaak erg gezellig. Ulke van der Heide is een tijd lang mijn kamergenoot geweest, het was vaak verfrissend om zijn kijk op een probleem te horen. Samen zijn we nog bezig geweest met het resolutieprobleem, tot op heden zijn er echter geen bevredigende resultaten geboekt.

Het programmeren in C++ heb ik geleerd van Alexis Kotte, al heb ik het generiek programmeren zo nu en dan niet geheel overgenomen van de meester zelf. Ik kon bij hem bovendien altijd terecht met andere computer gerelateerde vragen. Ook bij Jeroen van de Kamer, Gijsbert Bol, Kees Imhof en Ric Exterkate ben ik regelmatig langs geweest met computerproblemen. Gijsbert heeft tevens gezorgd voor het opschonen van alle data op mijn `local_scratch`. Jeroen heeft verder een belangrijke bijdrage geleverd aan de klinische implementatie van de borst IMRT techniek, waardoor er nu ook patiënten met deze techniek worden behandeld. Theo van Soest heeft me wegwijs gemaakt in de Plato omgeving, waardoor ik mijn data met de researchtools kon analyseren. André Wopereis heeft mij regelmatig geholpen bij het opzoeken van data opgenomen met de flatpanel of bij het terugvinden van oude doorlichtingsfoto's.

Ook wil ik de laboranten bedanken die mij geholpen hebben bij het maken van de larynx filmpjes en de plaatjes van de marker patiënten. Mede dankzij hen was ik in staat op een efficiënte manier alle data te verzamelen.

Martijn Ketelaars wil ik nog bedanken voor het briljante idee een blower in onze kamer te zetten waardoor het, ondanks het zuurstof tekort nog aardig uit te houden was op onze kamer.

Tot slot mijn ouders, Otto en Corrie, en natuurlijk Lonneke, bedankt voor jullie onvoorwaardelijke steun.

Bram, Augustus 2003

Curriculum vitae

Bram van Asselen werd geboren op 4 mei 1975 te Vinkeveen. In 1993 behaalde hij het VWO-diploma aan het Alkwin Kollege in Uithoorn. Hierna begon hij aan de studie natuurkunde aan de Universiteit Utrecht, waar hij in 1999 slaagde voor het doctoraal examen experimentele natuurkunde. In het laatste jaar van zijn studie was hij reeds werkzaam op de afdeling radiotherapie van het Universitair Medisch Centrum Utrecht en deed hij onderzoek naar de bestraling van borst kanker. In 1999 is hij begonnen aan een promotieonderzoek binnen de afdeling radiotherapie van het Universitair Medisch Centrum Utrecht.